GEORGIA DOT RESEARCH PROJECT 16-19

FINAL REPORT

DEVELOPMENT OF MEPDG INPUT DATABASE FOR ASPHALT MIXTURES

OFFICE OF PERFORMANCE-BASED MANAGEMENT AND RESEARCH
15 KENNEDY DRIVE
FOREST PARK, GA 30297-2534

1. Report No.: FHWA-GA-19-1619	2. Government Accession No.:	3. Recipient's Catalog No.:
4. Title and Subtitle: Development of MEPDG Input Database for Asphalt Mixtures		5. Report Date: April 2019 6. Performing Organization Code:
7. Author(s): S. Sonny Kim, Ph.D., P.E., F.ASCE, J. Robert A. Etheridge, M.S., Mi G. Chorzepa, Ph.D., P.E., Y. Richard Kim, Ph.D., P.E., F.ASCE,		8. Performing Organization Report No.: 16-19
9. Performing Organization Name and Address: University of Georgia, College of Engineering Driftmier Engineering Center, Athens, GA 30602 Phone: (706) 542-9804, Email: kims@uga.edu		10. Work Unit No.: 11. Contract or Grant No.: PI# 0015117
12. Sponsoring Agency Name and Address: Georgia Department of Transportation Office of Performance-Based Management and Research 15 Kennedy Drive, Forest Park, GA 30297-2534		13. Type of Report and Period Covered: Final; July 2016 – April 2019 14. Sponsoring Agency Code:

15. Supplementary Notes:
Prepared in cooperation with the U.S. Department of Transportation, Federal Highway Administration.

16. Abstract:
Fatigue cracking is one of the most critical distresses involved in flexible pavement failure. For state departments of transportation, the accurate prediction of flexible pavement service life in terms of potential fatigue cracking is crucial for pavement design, maintenance, and rehabilitation. Therefore, it is imperative to understand the asphalt mixture characteristics that contribute to fatigue cracking.

The Georgia Department of Transportation (GDOT) is interested in learning more about the material characteristics of Georgia-sourced asphalt material and how different mixtures can affect the predicted fatigue life. This interest includes investigating different asphalt mixtures to see how the growth of damage and fatigue cracking performance change over time.

This research study investigates predictions of the fatigue cracking performance of Georgia asphalt mixtures using three fatigue test methods: (1) overlay test, (2) Illinois flexibility index test (I-FIT), and (3) cyclic direct tension based on the simplified viscoelastic continuum damage (S-VECD) model. The results from these fatigue test methods were further used to examine the material characteristics that make up the asphalt material influence on the performance of the pavement. This report summarizes the effects of asphalt material characteristics such as asphalt binder type, nominal maximum aggregate size (NMAS), reclaimed asphalt pavement (RAP) percentage, and asphalt binder content on asphalt fatigue cracking resisting performance.

Further, this report provides a database of dynamic modulus (|E*|) for 19 different asphalt mixtures from across the state of Georgia that can be used in the Mechanistic–Empirical Pavement Design Guide (MEPDG) for pavement design and performance analysis. Long-term aging and dynamic shear rheometer (DSR) test results of two binders (PG 64-22 and PG 76-22) from the state of Georgia are also present in this report for MEPDG Level 2 inputs.

17. Keywords: Dynamic Modulus, S-VECD, SCB, Overlay Test Fracture, Fatigue Cracking	18. Distribution Statement:		
19. Security Classif. (of this report): Unclassified	20. Security Classification (of this page): Unclassified	21. No. of Pages: 124	22. Price:

Form DOT 1700.7 (8-69)

GDOT Research Project No. 16-19

Final Report

DEVELOPMENT OF MEPDG INPUT DATABASE FOR ASPHALT MIXTURES

By

S. Sonny Kim, Ph.D., P.E., F.ASCE
Associate Professor

Robert A. Etheridge
Graduate Research Assistant

Mi G. Chorzepa, Ph.D., P.E.
Associate Professor
Civil Engineering, College of Engineering
University of Georgia

Y. Richard Kim, Ph.D., P.E., F.ASCE
Jimmy D. Clark Distinguished University Professor
Alumni Association Distinguished Graduate Professor
Department of Civil, Construction, and Environmental Engineering
North Carolina State University

Contract with

Georgia Department of Transportation
In cooperation with
U.S. Department of Transportation
Federal Highway Administration

April 2019

TABLE OF CONTENTS

Page

LIST OF TABLES

Table **Page**

LIST OF FIGURES

EXECUTIVE SUMMARY

Fatigue cracking is one of the critical distresses in asphalt concrete pavement. This distress is a result of repeated loading from traffic that reduces the pavement performance and structural life. Pavement failure that results from these distresses is costly to state departments of transportation that maintain and repair these issues. Letting these cracks go unrepaired will only quicken deterioration through the presence of moisture and freeze/thaw cycles, leading to more costly repairs. To mitigate fatigue cracking, the underlying properties of asphalt concrete (AC) mixtures that contribute to crack propagation must be well understood.

One fundamental property of asphalt concrete is dynamic modulus. It defines the stiffness characteristics as a function of loading frequency and temperature. In order for Georgia's Department of Transportation (GDOT) to implement the Mechanistic–Empirical Pavement Design Guide (MEPDG), level 1 inputs of dynamic modulus consisting of laboratory testing must be conducted. This will allow for GDOT to use the predictive capabilities of MEPDG to predict pavement performance and the amount of fatigue cracking over the pavement's design life.

This research project built a database of dynamic modulus values for 19 different asphalt mixtures from across the state of Georgia to be used in the MEPDG for pavement design and performance analysis. It also investigated three different fatigue tests that could possibly be implemented by GDOT as a way to rank asphalt mixtures in their ability to resist fatigue cracking. These different tests were further used to examine the material characteristics that make up the asphalt material's influence on the performance of the pavement. A number of characteristics were investigated, such as asphalt binder type,

nominal maximum aggregate size (NMAS), reclaimed asphalt pavement (RAP) percentage, and asphalt binder content. Quality control was conducted on all asphalt materials that the lab received, including theoretical maximum specific gravity, bulk specific gravity, gradation, and air voids.

After conducting numerous dynamic modulus and fatigue tests, the following conclusions and recommendations were made:

Dynamic Modulus

- Generally, Superpave (Superior Performing Asphalt Pavements) mixtures with higher PG binder and increased RAP content (up to 30% RAP) result in higher dynamic modulus.
- Dynamic modulus values for NMAS between 25 mm and 19 mm were not significantly different. The same was true for 12.5 mm and 9.5 mm mixtures.
- Values for dynamic modulus were significantly different between 12.5 mm and 19 mm, as well as 12.5 mm and 25 mm.
- Binder type influenced dynamic modulus values, with the stiffer PG 76-22 binder being significantly different from both PG 64-22 and PG 67-22. However, there was not a notable difference between PG 64-22 and PG 67-22.
- RAP content had a great effect on dynamic modulus between 15% and 30% RAP contents.

Fatigue Test Method Comparisons

- For the fatigue tests, the semicircular bed (SCB) test and cyclic direct tension test with simplified viscoelastic continuum damage (S-VECD) model provide consistent test results that could be used in identifying AC cracking potential. The advantage of the SCB test over the S-VECD test is simple sample fabrication, ease of operation, and quick testing time. The cyclic direct tension test with the S-VECD model provides more theoretically sound in-depth information to better understand AC mixture behavior. On the other hand, the cyclic direct tension test with the S-VECD model requires intensive training to complete a successful test compared to the SCB test. This concern could be overcome through lab training and a workshop at the University of Georgia upon GDOT's request.

- It is apparent from the results that the overlay test (OT) is the least favorable method to predict fatigue performance of asphalt mixtures. The issues of reliability and repeatability give concern for its use.
- With a larger database of dynamic modulus values created, the MEPDG can be implemented for design of flexible roadways. The implementation of the MEPDG would be most successful with training of staff and personnel regarding the inputs needed for the MEPDG. Having a firm background about these inputs and their significance will help GDOT use the MEPDG successfully in their design–build projects. For successful MEPDG implementation, calibration of AASHTOWare Pavement ME and an accurate calibration coefficient for AC pavement is essential.
- Future studies to predict AC fatigue cracking should focus on the investigation of cracking performance using field-cored specimens and comparison of pavement condition surveys.
- The cyclic direct tension test method has a capability to estimate the calibration coefficients for fatigue cracking in Pavement ME based on S-VECD analyses.

Based on laboratory test results using field-cored specimens with different NMAS (i.e., 12.5 mm, 19 mm, and 25 mm), the calibration coefficients in Pavement ME can be obtained. Also, Sapp criteria in the S-VECD model can be developed to select the appropriate mixture for field construction according to the design traffic.

- Finally, it is recommended that the flexibility index (FI) criteria are developed based on the SCB test method using field-cored specimens to accurately assess cracking performance.

ACKNOWLEDGMENTS

This project was conducted in cooperation with the Georgia Department of Transportation. The authors gratefully acknowledge the contributions of many individuals to the successful completion of this research project. This especially includes Mr. Binh Bui, Ms. Sheila Hines, Dr. Peter Wu, and Mr. Ian Rish, who have helped and advised the research team toward successful completion of the study.

SI CONVERSION FACTORS

SI* (MODERN METRIC) CONVERSION FACTORS				
APPROXIMATE CONVERSIONS TO SI UNITS				
Symbol	**When You Know**	**Multiply By**	**To Find**	**Symbol**
		LENGTH		
in	inches	25.4	millimeters	mm
ft	feet	0.305	meters	m
yd	yards	0.914	meters	m
mi	miles	1.61	kilometers	km
		AREA		
in^2	square inches	645.2	square millimeters	mm^2
ft^2	square feet	0.093	square meters	m^2
yd^2	square yard	0.836	square meters	m^2
ac	acres	0.405	hectares	ha
mi^2	square miles	2.59	square kilometers	km^2
		VOLUME		
fl oz	fluid ounces	29.57	milliliters	mL
gal	gallons	3.785	liters	L
ft^3	cubic feet	0.028	cubic meters	m^3
yd^3	cubic yards	0.765	cubic meters	m^3
		NOTE: volumes greater than 1000 L shall be shown in m^3		
		MASS		
oz	ounces	28.35	grams	g
lb	pounds	0.454	kilograms	kg
T	short tons (2000 lb)	0.907	megagrams (or "metric ton")	Mg (or "t")
		TEMPERATURE (exact degrees)		
^oF	Fahrenheit	5 (F-32)/9 or (F-32)/1.8	Celsius	^oC
		ILLUMINATION		
fc	foot-candles	10.76	lux	lx
fl	foot-Lamberts	3.426	candela/m^2	cd/m^2
		FORCE and PRESSURE or STRESS		
lbf	poundforce	4.45	newtons	N
lbf/in^2	poundforce per square inch	6.89	kilopascals	kPa
APPROXIMATE CONVERSIONS FROM SI UNITS				
Symbol	**When You Know**	**Multiply By**	**To Find**	**Symbol**
		LENGTH		
mm	millimeters	0.039	inches	in
m	meters	3.28	feet	ft
m	meters	1.09	yards	yd
km	kilometers	0.621	miles	mi
		AREA		
mm^2	square millimeters	0.0016	square inches	in^2
m^2	square meters	10.764	square feet	ft^2
m^2	square meters	1.195	square yards	yd^2
ha	hectares	2.47	acres	ac
km^2	square kilometers	0.386	square miles	mi^2
		VOLUME		
mL	milliliters	0.034	fluid ounces	fl oz
L	liters	0.264	gallons	gal
m^3	cubic meters	35.314	cubic feet	ft^3
m^3	cubic meters	1.307	cubic yards	yd^3
		MASS		
g	grams	0.035	ounces	oz
kg	kilograms	2.202	pounds	lb
Mg (or "t")	megagrams (or "metric ton")	1.103	short tons (2000 lb)	T
		TEMPERATURE (exact degrees)		
^oC	Celsius	1.8C+32	Fahrenheit	^oF
		ILLUMINATION		
lx	lux	0.0929	foot-candles	fc
cd/m^2	candela/m^2	0.2919	foot-Lamberts	fl
		FORCE and PRESSURE or STRESS		
N	newtons	0.225	poundforce	lbf
kPa	kilopascals	0.145	poundforce per square inch	lbf/in^2

*SI is the symbol for the International System of Units. Appropriate rounding should be made to comply with Section 4 of ASTM E380. (Revised March 2003)

1. INTRODUCTION

1.1 Problem Statement

Developed under National Cooperative Highway Research Program (NCHRP) 1-37A, the Mechanistic–Empirical Pavement Design Guide (MEPDG) provides three hierarchical levels of design inputs (i.e., levels 1, 2, and 3) to allow the designer to select the quality and the level of details of design inputs according to the level of importance of the project. Typically, level 1 offers the highest design reliability but requires the highest level of accuracy and laboratory dynamic modulus (|E*|) testing to run the MEPDG software for flexible pavement designs. The |E*| is considered one of the fundamental asphalt mix properties and is obtained from a series of complex modulus tests at different temperature and loading frequency conditions. Several State highway agencies (SHAs) have already created or are in the process of creating an |E*| database for the calibration and implementation of the MEPDG.

Georgia Department of Transportation (GDOT) has made a continued commitment to the performance enhancement of pavement and has proactively calibrated and implemented the MEPDG methodology for the design of flexible pavement structures. There already exists an |E*| database for some hot mix asphalt (HMA) mixes that are conventionally used in the state of Georgia through GDOT RP 12-07 and GDOT RP 14-12. Although the GDOT material input library includes |E*| for 25 mm, 19 mm, and 12.5 mm Superpave mixes with PG 64-22 and PG 67-22, the library is based on only two sources of aggregate. Further, an |E*| library for polymer-modified asphalt (PMA) mixtures has not been developed yet even though the PMA mixtures are being used for high-volume traffic roads in Georgia.

1.2 Study Objectives

The primary objectives of the proposed research are to: (1) extend the |E*| database for different aggregate sources with PG 64-22, PG 67-22, and PG 76-22 PMA; (2) recommend to GDOT a fatigue test method that provides better fatigue cracking prediction; and (3) identify the effects of nominal maximum aggregate size (NMAS), aggregate source, binder type, and other mix characteristics on the |E*|, and the long-term pavement performance to propose guidelines for the choice of input data.

This study uses the asphalt mixture performance tester (AMPT) to expand the GDOT material input database. Three fatigue test methods—the cyclic direct tension test based on the simplified-viscoelastic continuum damage (S-VECD) model, the semicircular bend (SCB) test, and the modified overlay test (OT)—are used to the determine cracking potential of asphalt concrete (AC) mixtures.

This study presents the fatigue index parameters from those fatigue test methods for different asphalt mixtures that are commonly used in Georgia. The relations among fatigue index parameters from each test method and AC mixture properties such as NMAS, reclaimed asphalt pavement (RAP) content, asphalt binder type, and asphalt binder content were also investigated to: (1) determine how these properties affect fatigue cracking potential of AC mixtures; and (2) compare fatigue test methods for usefulness as a test method and better fatigue cracking prediction.

Finally, this report presents the pavement performance analyses using AASHTOWare Pavement ME and FlexPAVE™ to rank the mixes on their ability to resist cracking.

2. LITERATURE REVIEW

2.1 Mixture Characteristics

In order to determine how mixture characteristics impact asphalt pavement behavior, the research team performed tests to determine those properties. This section details those laboratory tests that were performed to obtain the physical properties of the different asphalt mixtures.

2.1.1 Bulk Specific Gravity and Theoretical Maximum Specific Gravity

The bulk specific gravity (G_{mb}) test determines the specific gravity of compacted hot mix asphalt by determining the ratio of a specimen's weight to the weight of an equal volume of water (PI, 2011). The test is performed according to AASHTO Standard T 166 – "Bulk Specific Gravity of Compacted Asphalt Mixtures using Saturated Surface-Dry Specimens" (AASHTO T 166, 2015). The test measures a specimen's weight under three different conditions: dry, saturated surface dry (SSD), and submerged in water. After a specimen's dry weight is recorded, it is placed in a water bath for 4 minutes. At the end of the 4 minutes, the submerged weight is recorded and then the specimen is rolled on top of damp towels to remove any excess water on the surface while leaving the voids saturated. The SSD weight is recorded and the three different masses are used to calculate the bulk specific gravity using Eq. (1):

$$\text{Bulk Specific Gravity } (G_{mb}) = \frac{A}{B - C} \tag{1}$$

Where,

A = mass of specimen in air (g)

B = mass of SSD in air (g)

C = mass of specimen in water (g)

The theoretical maximum specific gravity (G_{mm}) of an HMA mixture is the specific gravity of a sample excluding air voids (PI 2011). This test is performed on a sample of loose HMA by weighing the sample and then determining the volume by calculating the volume of water the sample displaces. The test is performed according to AASHTO T209 – "Theoretical Maximum Specific Gravity and Density of Hot Mix Asphalt (HMA)" (AASHTO T209, 2016). A loose mixture, which is a broken-up sample with fine aggregates separated into particles smaller than 0.25 inch, is weight and dry mass recorded. The sample is then placed into a rigid container and filled with water enough to cover the sample by about 1 inch. The container is sealed and a vacuum of 25–30 mm Hg is applied for 15 minutes. The container is periodically struck with a hammer to release trapped air bubbles. After 15 minutes, the vacuum is released and the container is submerged in water for 10 minutes and then the submerged weight is recorded. The recorded weights are used to determine G_{mm} using Eq. (2):

$$\text{Theoretical Maximum Specific Gravity } (G_{mm}) = \frac{\text{A}}{\text{A-C}} \quad (2)$$

Where,

A = mass of dry sample in air

C = mass of water displaced by the sample

2.1.2 Air Voids

Air voids in HMA pavement have a significant effect on its long-term performance. Studies on the effects high percentages of air voids have on HMA have concluded that tensile strength, static and resilient moduli, stability, and fatigue life are reduced. (Kennedy et al. 1984, Pell and Taylor 1969, Epps and Monismith 1969, Linden et al. 1989, Finn et al. 1973). For these reasons, it is important in this study to create specimens with consistent air voids of 7 ± 0.5% for super gyratory compacted (SGC) specimens. The percent air voids was chosen based on the target air voids described in the procedures for each test, and 7 ± 0.5% satisfied all four tests. Percent air voids of a compacted HMA specimen can be determined from G_{mb} and G_{mm} using Eq. (3):

$$\text{Air Voids (Va)} = \left(1 - \frac{G_m}{G_{mm}}\right) \times 100 \quad (3)$$

2.1.3 Binder Content

Binder content affects asphalt mixture performance related to stiffness, strength, durability, fatigue life, raveling, rutting, and moisture damage (PI 2011). In order to determine binder content of HMA, the ignition test is commonly used. The ignition test is performed in accordance with AASHTO T 308, "Determining the Asphalt Binder Content of HMA by the Ignition Method." A sample of loose mix asphalt is placed into a mesh basket and into a forced air furnace. For this study, an NCAT Asphalt Content Furnace was used to determine binder content. The furnace heats the basket containing the loose mix to a temperature of 1000°F. The internal scale measures the weight of the asphalt as the binder burns off. The weight before ignition and after ignition is used to determine the binder content, and a correction factor is applied to account for the loss of aggregate mass.

2.1.4 Gradation

Performance of pavement is greatly influenced by particle size distribution or gradation of aggregate. Gradation is an important aggregate characteristic that determines properties such as stiffness, stability, durability, permeability, workability, fatigue resistance, frictional resistance, and moisture susceptibility (Roberts et al. 1996). A maximum density gradation is a common reference in determining the desired gradation. To determine the maximum density gradation, a standard gradation graph known as the 0.45 power curve was introduced by the Federal Highway Administration (FHWA), which plots sieve sizes raised to the 0.45 power to percent passing of a sieve analysis. The maximum density line in this graph is a straight diagonal line from zero to the maximum aggregate size of the mixture being considered. The maximum aggregate size is considered to be one sieve larger than the nominal maximum aggregate size, while the NMAS is one sieve size larger than the first sieve to retain more than 10 percent of the material (Roberts et al. 1996). Typical HMA mix designs are considered dense graded which have a gradation near the 0.45 power curve but not exactly on it because there needs to be adequate volume for the binder to occupy. Figure 2.1 shows a 0.45 power curve.

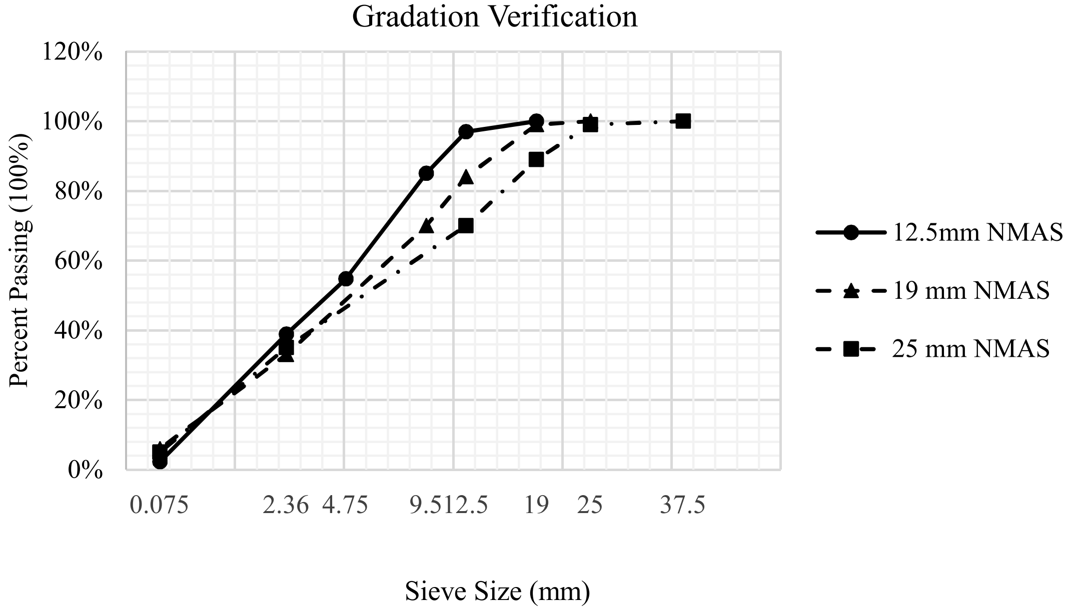

FIGURE 2.1

0.45 Power Curve for 12.5, 19, and 25 mm NMAS Asphalt Mixtures

2.2 Fracture Mechanics

Fatigue cracking is one of the critical distresses in asphalt concrete pavement. This distress is a result of repeated loading from traffic that reduces the performance and life cycle of roads. Pavement failure that results from these distresses are costly to state departments of transportation that maintain and repair these issues. Letting these cracks go unrepaired will quicken deterioration through the presence of moisture and freeze/thaw cycles, leading to more costly repairs. To mitigate fatigue cracking, the underlying properties of AC mixtures that contribute to crack propagation must be well understood. Fracture mechanics can be used to determine the properties of AC mixes that provide better cracking resistance.

To address the issues related to fatigue cracking, fracture mechanics–based tests were developed. These include a variety of tests, such as the single-edge notch beam (SEB) test, disk-shaped compaction test (DCT), semicircular bend test, and modified overlay test. While reliable, the SEB test suffers due to fabrication of a rectangular specimen (Wagoner et al. 2005). DCT, initially more favorable than the SCB test due to its potential crack surface being larger than SCB, can result in erroneous results if the crack propagation deviates from a straight path. The geometry is also much harder to create than an SCB specimen. The SCB test was chosen due to the research that indicates its success with identifying mixes that have fracture resistance properties and its repeatability (Wu et al. 2005, Li and Marasteanu 2009, Im et al. 2014)

Linear elastic fracture mechanics (LEFM) was developed to describe crack growth and fracture within a material under essentially linear elastic conditions (Irwin 1948). LEFM was first used in the fracture mechanics of metals. With the introduction of fracture mechanics to geological materials, the research and influence of rock mechanics fracture covered a huge field of studies. This led to the development of the SCB test by Chong and Kuruppa (1984) for rock fracture tests. The concept was then applied to asphalt, which acts at a quasi-brittle material especially at low temperatures. The underlying principle is that if energy stored near the crack tip exceeds the crack resistance of the material, then cracking initiates in the vicinity of the crack. Plastic deformation in the material creates a crack inelastic zone around the crack tip. If the inelastic region at the crack tip grows too large, then the elastic stress analysis will be inaccurate. The stress field at the crack tip is defined by the stress intensity factor, K. This factor depends on the mode of loading. The three principle modes are tensile mode, sliding mode, and tearing mode, which are called Mode I, Mode II, and Mode III, respectively. A combination of one or more modes is called mixed mode. This study focuses on Mode I. In Mode I, the crack initiation occurs when the stress intensity factor reaches its critical value, K_{IC}, which is known as fracture toughness. The stress intensity factor can be written as Eq. (4) (Lim et al. 1993):

$$K_1 = Y_1 \sigma_o \sqrt{\pi a} \tag{4}$$

Where,

a = notch depth

σ_o = applied stress

Y_1 = normalized Mode I stress intensity factor

Stress is given by Eq. (5):

$$\sigma_o = \frac{P}{2rt} \tag{5}$$

Where,

P = applied load

r = radius

t = thickness

Lim et al. (1993) developed expressions for Y_1 for different specimen geometry based on span length divided by the radius. For example, when $\frac{s}{r}$ = 0.8, Y_1 can be expressed as Eq. (6):

$$Y_{1\{0.8\}} = 4.782 - 1.219(a/r) + 0.063\exp(7.045(a/r)) \tag{6}$$

Stress intensity factor has been used to study fracture behavior on asphalt mixtures below subzero temperatures (Biligiri 2012, Khalid and Monney 2009). However, LEFM may not be applicable to mixtures that are above subzero temperatures. At higher temperatures, asphalt exhibits a viscoelastic response that creates a large inelastic zone around the crack tip, which leads to inaccuracies. An alternate to the LEFM approach is elastic plastic fracture mechanics (EPFM), which has been used to measure fracture resistance based on the energy of fracture.

2.3 Dynamic Modulus

Dynamic modulus, $|E^*|$, is a fundamental property of asphalt concrete that defines the stiffness characteristics as a function of loading frequency and temperature. Dynamic modulus is used as a property input in the Mechanistic–Empirical Pavement Design Guide developed by NCHRP Project 1-37A (ARA 2004). Using the principles of time–temperature superposition, a master curve can be created to predict the behavior of asphalt under a given loading condition and temperature. $|E^*|$ is an important linear viscoelastic property that can be used in pavement models based on viscoelasticity. The dynamic modulus tests were performed according to AASHTO T 342 at three temperatures of 4ºC, 20ºC, and 40ºC (39.2ºF, 68ºF, and 104ºF) and six frequencies 25, 10, 5, 1, 0.5, and 0.1 Hz.

2.3.1 Complex Modulus

Complex modulus, E^*, is a stress–strain ratio of linear viscoelastic materials under sinusoidal loading. The complex modulus contains a storage or elastic component (E') and a loss or viscous component (E'') and can be written as Eq. (7):

$$E^* = E' + iE'' \qquad (7)$$

Taking the absolute value of this complex number gives the dynamic modulus. It is equal to the amplitude of the sinusoidal stress, σ_0, divided by the maximum recoverable strain, ε_0, as in Eq. (8):

$$|E^*| = \frac{\sigma_0}{\varepsilon_0} \tag{8}$$

Due to the responses being time-dependent, the strain occurs after the load is applied in a time lag, which is defined as the phase angle, ϕ, and determined from Eq. (9):

$$\phi = 2\pi f \Delta t \tag{9}$$

Where,

f = loading frequency in Hz

Δt = time delay between the stress and strain cycles

For perfectly elastic materials the phase angle would be equal to 0, and it would be equal to 1 for perfectly viscous materials. Figure 2.2 shows the time lag between the stress and strain for a uniaxial sinusoidal compressive stress test.

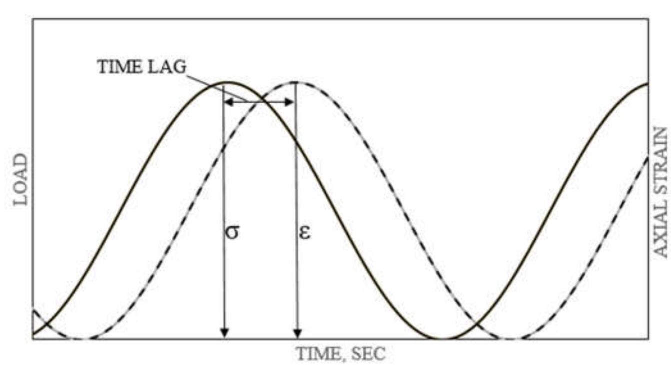

FIGURE 2.2

Stress and Strain Curves from Sinusoidal Loading

2.3.2 Master Curve Development

In asphalt mixtures, dynamic modulus values vary with temperature and loading frequency. Due to this variation, it is difficult to compare test results. The master curve was introduced to give better comparison between test results (AASHTO R84-17). The master curve is based upon the thermorheological attributes of asphalt, which allow the time–temperature superposition (t–Ts) principle to be applied. This principle allows the same modulus value to be inferred at either low temperatures and long loading times or high temperatures and short loading times. Using a time–temperature shift factor, dynamic modulus results from each temperature at each loading frequency can be shifted graphically along the frequency domain to create the master curve. Figure 2.3 shows the results of a dynamic modulus test and how the data can be shifted.

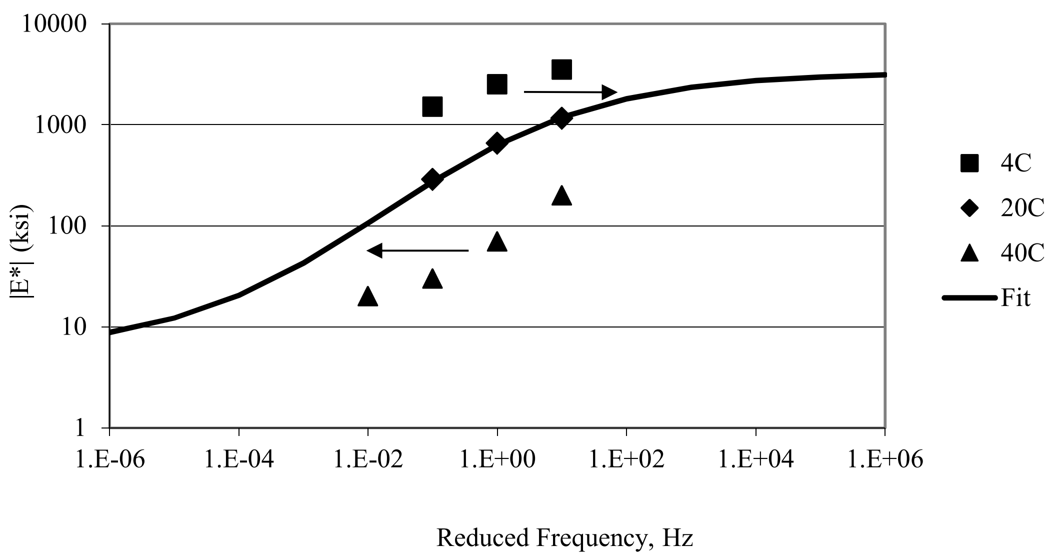

FIGURE 2.3

Results of Dynamic Modulus Test Before Shifting

The master curve can be defined mathematically with a sigmoidal function as Eq. (10):

$$\text{Log } |E^{*}| = \delta + \frac{}{1+e^{\beta+\gamma(\log t_r)}} \tag{10}$$

Where,

t_r = reduced time of loading at reference temperature

δ = minimum value of E^*

$\delta + \alpha$ = maximum value of E^*

β and γ = parameters describing the shape of the sigmoidal function

The shift factor can be shown as Eq. (11).

$$a(T) = \frac{t}{t_r} \tag{11}$$

Where,

a(T) = shift factor as a function of temperature

t = time of loading at desired temperature

t_r = reduced time of loading at reference temperature

T = temperature of interest

While the shift factor as a function of temperature is defined by a linear relationship, a second order polynomial fit is more accurate leading a(T) to be commonly described by the quadratic Eq. (12):

$$\text{Log } a(T) = aT^2 + bT + c \tag{12}$$

Where,

T = temperature of interest

a, b, c = regression coefficients

The resulting master curve from Figure 2.4 can be used to estimate |E*| at temperatures and frequencies that available equipment cannot mechanically test.

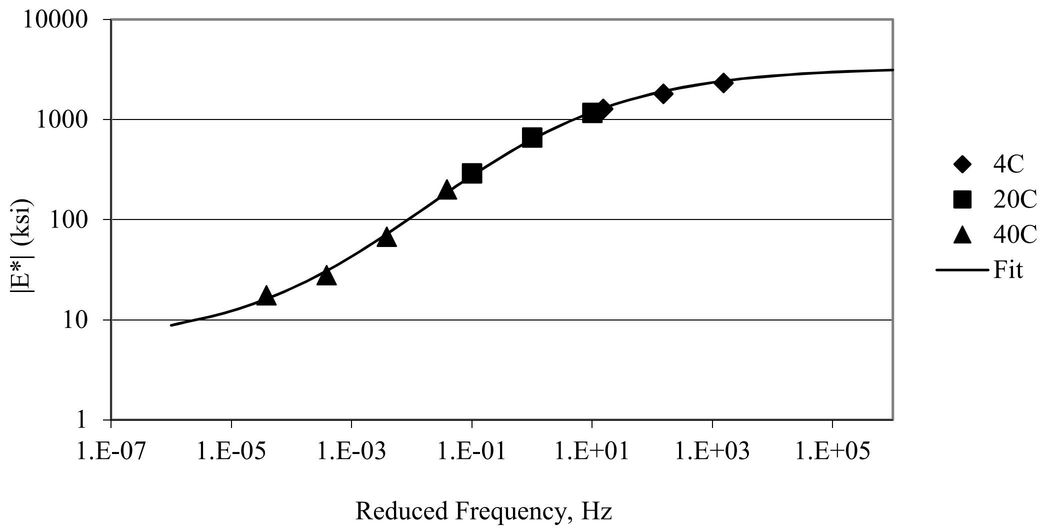

FIGURE 2.4

Master Curve with Shifted Dynamic Modulus Values

2.3.3 Predictive Models

The MEPDG provides three levels of input design. Level 1 is the highest level and requires regional material characterization of $|E^*|$ from laboratory testing. Levels 2 and 3 determine $|E^*|$ through predictive models. These models are based on simpler material properties and volumetric properties. The predictive models are briefly described in the following subsections.

2.3.4 Original Witczak Equation

The original Witczak equation, developed as part of NCHRP 1-37A, used data from 205 mixtures to create Eq. (13):

$$\text{Log}_{10} |E^*| = -1.249937 + 0.02923\, p_{200} - 0.001767 (p_{200})^2 - 0.002841\, p_4 - 0.05809 V_a$$

$$- 0.082208 \frac{V_{beff}}{V_{eff} + V_a} + \frac{\left(3.871977 - 0.0021 p_4 + 0.003958 p_{3/8} \cdot 0.000017 (p_{3/8})^2 + 0.00547\right)}{\left(1 + e^{(-0.603313 - 0.313351 \log f - 0.393532 \log \eta)}\right)} \quad (13)$$

Where,

$|E^*|$ = dynamic modulus

p_{200} = percent passing #200 sieve

p_4 = percent retained on #4 sieve

$p_{3/8}$ = percent retained on ⅜ inch sieve

$p_{3/4}$ = percent retained on ¾ inch sieve

V_a = percent of air voids

V_{beff} = percent of effective asphalt content

f = loading frequency (Hz)

η = binder viscosity at temperature of interest (10^6 poise)

This Witczak equation based on nonlinear regression analysis is an option for Level 2 analysis. There are limitations to the Witczak equation (Bari 2005). It relies on other models to change the binder shear modulus $|G^*|$ into binder viscosity. There is also a need for improved sensitivity to volumetric properties such as voids in mineral aggregate (VMA), voids filled with asphalt (VFA), asphalt content, and air void (AV).

2.3.5 Modified Witczak Equation

Under NCHRP Project 1-40D, Witczak reformulated Eq. (13) to include binder $|G^*|_b$ in the model as Eq. (14):

$$\text{Log}_{10} |E^*| = -0.349 + 0.754(|G^*|_b^{-0.0052})(6.65 - 0.032p_{200} - 0.027(p_{200})^2 + 0.011p_4$$

$$+ 0.006p_{3/8} - 0.00014(p_{3/8})^2 - 0.0014(p_{3/8})^2 - 0.08V_a - 1.06\left(\frac{V_{beff}}{V_{beff} + V_a}\right))$$

$$+ \frac{2.558 + 0.032V_a + 0.713\frac{V_{beff}}{V_{eff} + V_a} + 0.0124p_{3/8} - 0.0001(p_{3/8})^2 + 0.0098p_{3/4}}{1+\exp(-0.7814 - 0.5785\log|G^*|_b + 0.8834\log\delta_b)} \quad (14)$$

Where,

$|G^*|_b$ = dynamic shear modulus of asphalt binder

δ_b = binder phase angle associated with $|G^*|_b$

The NCHRP 1-40D model is based on nonlinear regression similar to NCHRP 1-37A, and it used 346 mixtures. This G*-based model is used in Level 2 analysis in the MEPDG.

2.3.6 Hirsch Model

Another model used to estimate $|E^*|$ is the Hirsch model suggested by Christensen et al. (2003) that incorporates the binder modulus, VMA, and VFA as Eq. (15), Eq. (16), and Eq. (17):

$$|E^*| = P_c(4,200,00(1-\frac{VMA}{100}) + 3|G^*|_b\left(\frac{VFA*VMA}{10,000}\right) + \frac{(1-P_c)}{\frac{(1-\frac{VMA}{100})}{4,200,000} + \frac{VMA}{3|G^*|\ (VFA)}} \quad (15)$$

$$\Phi = -21(\log P_c)^2 - 55\log P_c \quad (16)$$

$$P_c = \frac{(20+3|G^*|\ (\frac{VFA}{VMA})^{.58}}{650+3|G^*|\ (\frac{VFA}{VMA})^{.58}} \quad (17)$$

Where,

P_c = the aggregate contact volume

This model lacks a strong dependence on volumetric parameters, but the use of the empirical phase angle equation is beneficial when converting $|E^*|$ to the relaxation modulus or creep compliance.

2.3.7 Effects of AC Materials Characteristics on $|E^*|$

The continued effort by GDOT to update the $|E^*|$ database relies on laboratory testing to provide the highest design input level. The dynamic testing done in this study to extend the database for GDOT investigated the properties of AC mixtures and the effect on the resulting dynamic modulus. A number of studies have been conducted to evaluate dynamic modulus test results and the effect of different factors on dynamic modulus and phase angle. Factors including aggregate, asphalt content, and RAP percentage had influence on the response (Flintsch et al. 2007, Cross and Jakatimath 2007). Binder was also determined to affect dynamic modulus, with a softer binder providing a lower modulus (Clyne et al. 2003). Studies completed show that a stiff asphalt binder, low asphalt content, and air voids contribute significantly to increase dynamic modulus values (Shu and Huang 2008). Polymer-modified binders have been shown to increase dynamic modulus values (Zhu et al. 2011).

2.4 Fatigue Cracking Tests for Asphalt Mixtures

2.4.1 Cyclic Direct Tension Test with Simplified Viscoelastic Continuum Damage Model (S-VECD)

Materials that show time-dependent behavior, such as viscoelastic materials, are affected by current input and past input history. The stress–strain relationship of linear viscoelastic materials is expressed with two convolution integrals, Eq. (18) and Eq. (19):

$$\sigma = \int_0^t E(t-\tau)\frac{d\varepsilon}{d\tau}d\tau \tag{18}$$

$$\varepsilon = \int_0^t D(t-\tau)\frac{d\sigma}{d\tau}d\tau \tag{19}$$

Where,

$E(t)$ = relaxation modulus

D(t) = creep compliance

τ = integration variable

Complex modulus that is composed of two parts—the storage modulus and the loss modulus—is a parameter of linear viscoelastic behavior. AC stiffness is dependent on loading rate and temperature, which would cause the need to test stiffness over a large range of frequencies and temperatures. Due to the impracticality of performing a large number of tests, researchers are able to take advantage of the time–temperature superposition principle, which greatly reduces the amount of testing needed. Tests at different frequencies and temperatures can be shifted to a reference temperature, with the resulting shifted frequency called *reduced frequency*. These shifted frequencies form a master curve over which a dynamic modulus value can be obtained over a range of temperatures and frequencies. Materials that are capable of forming a master curve are called thermorheologically simple materials. Linear viscoelastic theory allows for relaxation modulus and creep compliance to be converted from the complex modulus in the frequency domain. All three functions are considered unit response functions. Relaxation modulus is a stress response due to a unit step strain input, and creep compliance is a strain response due to a unit step stress input. Schapery (1984) suggested that the stress and strain terms in viscoelastic materials are defined as pseudo variables in the form of convolution integrals. Physical stress or strain in elastic solutions can be replaced by pseudo stress or strain. Eq. (20) presents the pseudo strain, ε^R, that can be calculated based on the correspondence principle:

$$\varepsilon^R = \frac{1}{E_R}\int_0^t E(t-\tau)\frac{d\varepsilon}{d\tau}d\tau \tag{20}$$

Where,

ε^R = pseudo strain

ε = the measured strain

E(t) = the linear viscoelastic relaxation modulus

E_R = the reference modulus (typically taken as 1)

Pseudo strain equals the stress response of linear viscoelastic material due to a certain strain input. This property allows for the time effect in a stress–pseudo strain plot that forms nonlinear behavior to be removed. Removing the time effect proves that damage does not actually occur. Continuous damage ignores microscale behaviors and characterizes material using macroscale observations. To assess the structural integrity, an instantaneous secant modulus can be employed; however, damage is more difficult to quantify. A theory to address this is Schapery's work potential theory based on thermodynamics principles. The theory quantifies damage by an internal state variable, S, that accounts for microstructural changes in the material. Eq. (21), Eq. (22), and Eq. (23) summarize the damage evolution law:

$$W^R = f(\varepsilon^R, S); \tag{21}$$

$$\sigma = \frac{\partial W^R}{\partial \varepsilon^R} \tag{22}$$

$$\frac{dS}{dt} = \left(\frac{\partial W^R}{\partial \varepsilon^R}\right) \tag{23}$$

Where,

W^R = pseudo strain energy density function

α = the damage growth rate

Based on this theory, cyclic fatigue tests are conducted in accordance with AASHTO TP107 entitled, "Standard Method of Test for Determining the Damage Characteristic Curve and Failure Criterion Using the Asphalt Mixture Performance Tester (AMPT) Cyclic Fatigue Test". By applying a cyclic fatigue test using the AMPT shown in Figure 2.5, the S-VECD model shows the fatigue damage growth as the modulus changes based on the pseudo strain energy input history (Kim and Little 1990, Daniel and Kim 2002, Chehab et al. 2003, Underwood et al. 2010).

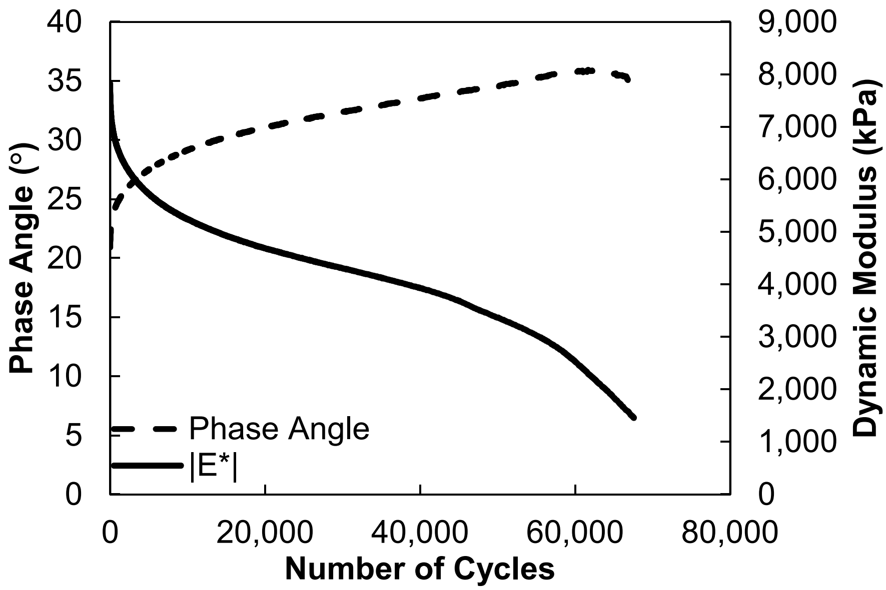

FIGURE 2.5

Results from a Cyclic Direct Tension Fatigue Test

The relationship between the internal state variable representing damage, S, and the pseudo stiffness, C, is the primary interest of the model. A damage characteristic curve can be formed between C and S where the pseudo stiffness value starts at 1, indicating the material is intact and decreases as damage accumulates. The function can be fitted as a power function represented by Eq. (24), where C_{11} and C_{12} are model coefficients:

$$C = 1 - C_{11}S^{C_{12}} \tag{24}$$

This relationship is independent of mode of loading, temperature, and load amplitude, making it a fundamental material property. A study was performed to investigate how air voids and binder content affect damage characteristic curves, and it concluded that higher air voids increase damage accumulation and higher binder content decreases damage accumulation (Zeiada et al. 2013). Another study looked at RAP content and showed that an increase of RAP decreases fatigue performance (Sabouri et al. 2015).

In this study, this model is compared to other fatigue tests to determine which provides the best information about cracking resistance. The damage characteristic curve is useful to represent how damage grows, but failure criterion is needed to determine failure.

The D^R failure criterion is used to predict material failure in the S-VECD model. The D^R failure criterion is based on observation that the average reduction in pseudo stiffness up to failure is independent of the mode of loading, temperature, and load amplitude (Wang and Kim 2017). D^R is defined by the slope of the linear relationship between the sum of 1−C to failure and the number of cycles to failure, N_f, in Eq. (25):

$$D^R = \frac{\int_0^{N_f}(1-c)dN}{N_f} = \frac{sum(1-c)}{N_f} \tag{25}$$

Wang and Kim (2017) reported that D^R changes with mixture characteristics, such as a higher RAP content lowering D^R and polymer-modified binders having a higher D^R value. While good trends have been recognized with D^R, this value alone cannot compare the fatigue performance of different asphalt mixtures. To index mixtures for fatigue performance, a cracking index property was developed, called the apparent damage capacity (S_{app}). The S_{app} was developed by Wang and Kim (2017) based on concepts of the S-VECD model and the D^R failure criterion. It can be defined as the corresponding S value on the damage characteristic curve when C is equal to ($1-D^R$). S_{app} is expressed in Eq. (26):

$$S_{app} = \frac{1}{10000} \times \left(\frac{1}{C_{11}} \times D^R\right)^{\frac{1}{C_{12}}} \tag{26}$$

The value of $1/_{10000}$ is a normalization factor used to make the S_{app} value in the range of 0–40 if the unit of stress is kPa. Using the S_{app} parameter, the predictions of fatigue performances on Georgia-sourced asphalt mixtures were investigated.

2.4.2 Semicircle Bend Test

The AAHSTO TP105 standard for the SCB test is based on the calculation of fracture energy, G_f, which is the energy required to create a unit surface area of a crack and is less dependent on linear elasticity and homogeneity (Marasteanu 2004). Figure 2.6 shows the results from a typical SCB test.

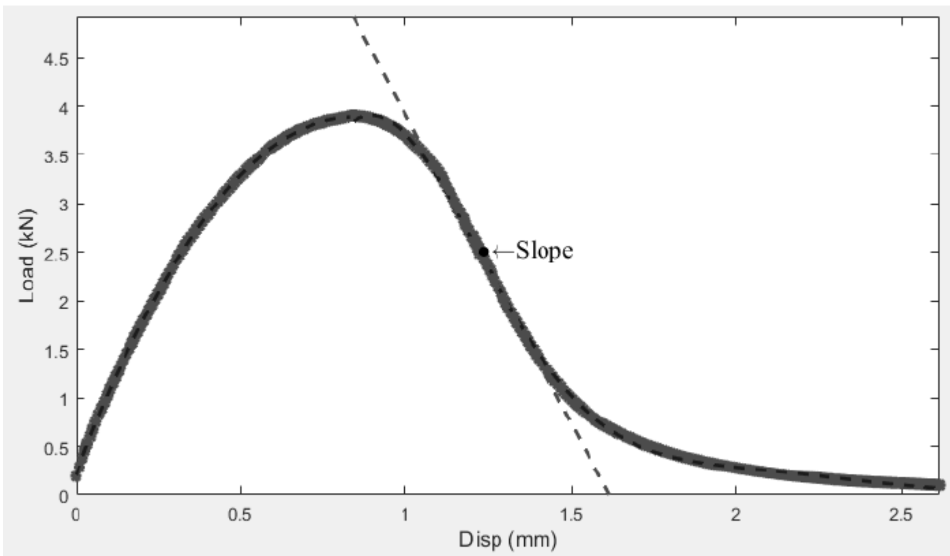

FIGURE 2.6

Load vs. Load Line Displacement Curve for a Typical SCB Test

Fracture energy is obtained using the work of fracture, W_f, which is the total area under the load line displacement curve as in Eq. (27):

$$G_f = \frac{W_f}{Area_{lig}} \tag{27}$$

In Eq. (28), W_f is the work of fracture and calculated by finding the area underneath the load line displacement curve. $Area_{lig}$ is the ligament area calculated as in Eq. (28):

$$Area_{lig} = t(r-a) \tag{28}$$

Where,

t =thickness

r = radius

a = notch length

This test has been used to characterize the low temperature cracking resistance in AC mixtures. More recently, a new procedure has been developed by the University of Illinois to characterize fracture cracking at intermediate temperature. This test procedure (AASHTO TP124) is able to screen AC mixtures for their ability to resist fatigue cracking by creating a new index parameter to better discriminate AC mixture performance, called the flexibility index (FI). This procedure uses fracture mechanic principles to distinguish between AC mix characteristics. The Illinois Flexibility Index Test (I-FIT) uses fracture energy and post-peak slope to determine the FI. This new parameter is meant to identify brittle mixtures that are prone to cracking. I-FIT has shown consistent and repeatable trends and is able to determine with greater distinction between fracture properties than fracture energy alone (Ling et al. 2017; Ozer, Al-Qadi, Lambros et al. 2016; Ozer, Al-Qadi, Singhvi et al. 2016). The FI is more sensitive to changes within mix designs compared to fracture energy (Ling et al. 2017). Mixture characteristics such as reclaimed asphalt pavement have been shown to impact fracture resistance with great significance and that the use of RAP can increase the amount of cracking in pavement (Ling et al. 2017; Ozer, Al-Qadi, Lambros et al. 2016; Ozer, Al Qadi, Singhvi et al. 2016; Norouzi et al. 2017; Cascione et al. 2015). The hardened and stiffer binders within RAP are prone to cracking and are shown to decrease FI (Ling et al. 2017, Ozer et al. 2016). In Georgia, 25%–30% RAP is widely used in surface mixes. This increase in RAP usage as a sustainable practice could have future impacts on the cost to GDOT to maintain roads. Aging of asphalt mixtures was shown to greatly affect FI and its resistance to cracking (Ling et al. 2017, Kim et al. 2012). Since this study was not investigating the effect of aging on asphalt, precautions were taken to ensure the material was not aged.

Performance grade (PG) of binder has also been shown to greatly affect FI, as a stiffer binder has significant variation to a softer binder (Ling et al. 2017, Ozer et al. 2016). The use of modified binders is to provide better resistance to rutting, thermal cracking, and fatigue damage. Previous studies have proven that polymer-modified asphalt binder can improve permanent deformation from rutting and fatigue cracking resistance (Sargand and Kim 2001, Bahia 2011). The expected trend from the I-FIT test resulting from the modified binder would be an increase in fracture energy and FI. However, in one study on the sensitivity of the I-FIT procedure, a peculiar result occurred during the testing of polymer-modified asphalt binder mixtures. The study results suggested that the modified binder affected FI negatively, resulting in lower FI for the asphalt with modified binder (Ling et al. 2017). This trend is the opposite of what was expected and was noted as such in the study. This could be an important finding to improve the test method because the study suggests that the procedure cannot adequately characterize polymer- modified asphalt binders.

Several studies have focused on the sensitivity analyses of testing variables, including loading rate, specimen thickness, and testing temperature (Ling et al. 2017). These study showed sensitivities of the testing variables (Ling et al. 2017). Further, an investigation was done on the variables of the SCB test to determine its reliability and repeatability (Nsengiyumva 2016). The study evaluated the number of specimens needed for sufficient sample representation, specimen thickness, notch length, loading rate, and testing temperature. Their key findings are summarized as follows:

- A reasonable number of SCB tests is six to evaluate representative fracture behavior of asphalt concrete with a 95% level of confidence.
- A thickness of SCB specimen in the range of 40 mm to 60 mm provides consistent fracture energies.
- Notch depth from 5 mm to 40 mm presents consistent fracture energy.
- Although it is known that loading rate affects fracture energy, the loading rates in their study did not find significant difference, as the loading rate was low (0.1 to 10 mm/min).
- Mixtures with 25% and 30% RAP content are not significant for fracture energy or FI since this was due in part to the different binder types controlling the response, as the change in RAP content was only 5%.

2.4.3 Modified Overlay Test

The overlay test (TxDOT Tex-248-F) was first designed in the 1970s by Germann and Lytton (1979) and consisted of two steel plates with one fixed and the other moveable in the horizontal direction. The test was developed to simulate cracks that formed in the old pavement beneath an overlay and the reflective cracking caused to the overlay pavement. The original overlay test was upgraded by Zhou and Scullion (2005) to ease the fabrication of specimens and be compatible with field cores in order to evaluate the reflective cracking resistance. Testing is performed at room temperature with a loading rate of one cycle per 10 seconds with a maximum displacement of 0.025 inch. These loading rates do not actually represent field conditions; however, the purpose of the test is to be an accelerated crack resistance test. The results of the test can be interpreted in two ways: (1) the reflective cracking life of an asphalt mixture, and (2) the fracture parameters of the mixture. The reflective cracking life of an asphalt mixture is defined as the number of cycles needed to propagate a crack through a specimen under a defined test condition. The plot formed by the load and displacement versus time results in three distinct phases, as shown in Figure 2.7.

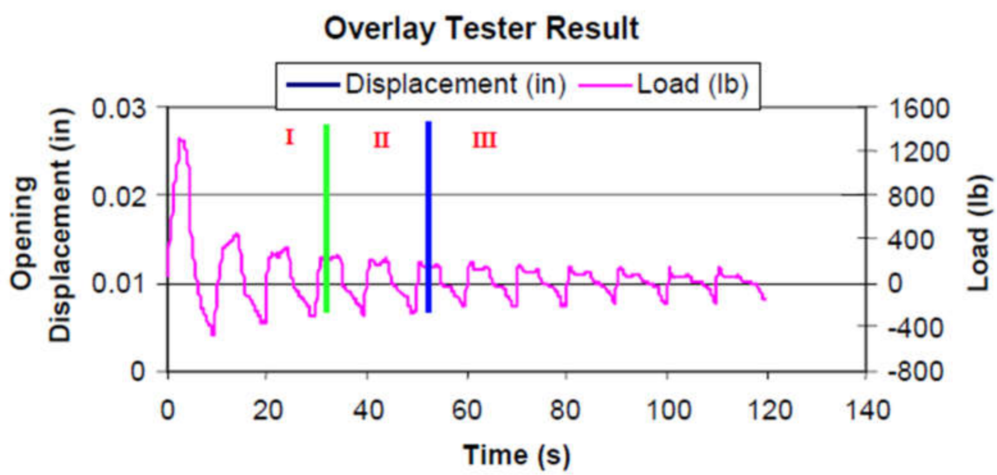

FIGURE 2.7

Overlay Test Result, Zhou and Scullion (2005)

Phase I is the crack initiation and steady propagation. The load reaches a maximum value before the displacement reaches a maximum, indicating a crack initiation at the bottom. The load then decreases rapidly as the crack propagates, but the load and displacement reach maximums at the same time, indicating a steady and slow propagating crack at the top surface. Phase II is the late-stage crack propagation represented as a saddle-shaped load, which indicates the crack has partially gone through the entire cross section of the specimen. The first peak load is associated with minor adhesion, which rapidly decreases after breaking the weak adhesion bonds. Continuing the cyclic loading will break the specimen and starts the beginning of phase III. Phase III has the crack propagated completely through the specimen. The reflective life cracking of the asphalt mixture can then be defined as the onset of phase II.

While the OT has been validated for reflective cracking, which is driven by crack propagation, the interest of this study is on fatigue cracking which centers on crack initiation and crack propagation. Work presented by Zhou and Scullion (2005) summarizes how crack initiation is related to crack propagation, which gives theory and then validation for the usefulness of the OT to be used for fatigue cracking. While the OT mainly characterizes crack propagation, the validated results from that study conclude that the OT can be used as a performance test for fatigue cracking. Previous studies show factors that affect the reflective cracking life on the OT include RAP percent, NMAS, binder content, and polymer-modified binders. An increase in asphalt content improved reflective cracking life of asphalt (Zhou and Scullion 2005). In the same study, binder grade PG 64-22 and PG 76-22 were investigated, and it was determined that the polymer-modified binder decreased reflective cracking life. Several studies investigated the effect of RAP on the OT and concluded that an increase in RAP decreases the reflective cracking life. Finally, a study looked at the NMAS and concluded that the smaller 9.5 mm NMAS compared to 12.5 mm NMAS increased reflective cracking life.

While some studies have shown good results from the OT, others have had challenges due to repeatability and variability issues (Walubita et al. 2012, Walubita et al. 2013). Issues with the OT came from a number of different sources. Walubita et al. (2012) discussed that one of the reasons for the large variability was not adhering to test specifications and procedures. Other factors the study found that contributed to the variability of results was a function of sample fabrication and test setup. A consistent gluing method was also found to be crucial to improving variability (Garcia and Miramontes 2015). Recently, researchers have suggested an alternative way to interpret data from the OT, which resulted in the crack progression rate during the crack propagation phase (Garcia et al. 2017). The crack propagation can be quantified by fitting a power equation (29) to the load reduction curve. Figure 2.8 shows a typical load reduction curve.

$$y = ax^{\beta} \tag{29}$$

Where,

a = 1

β = crack progression rate

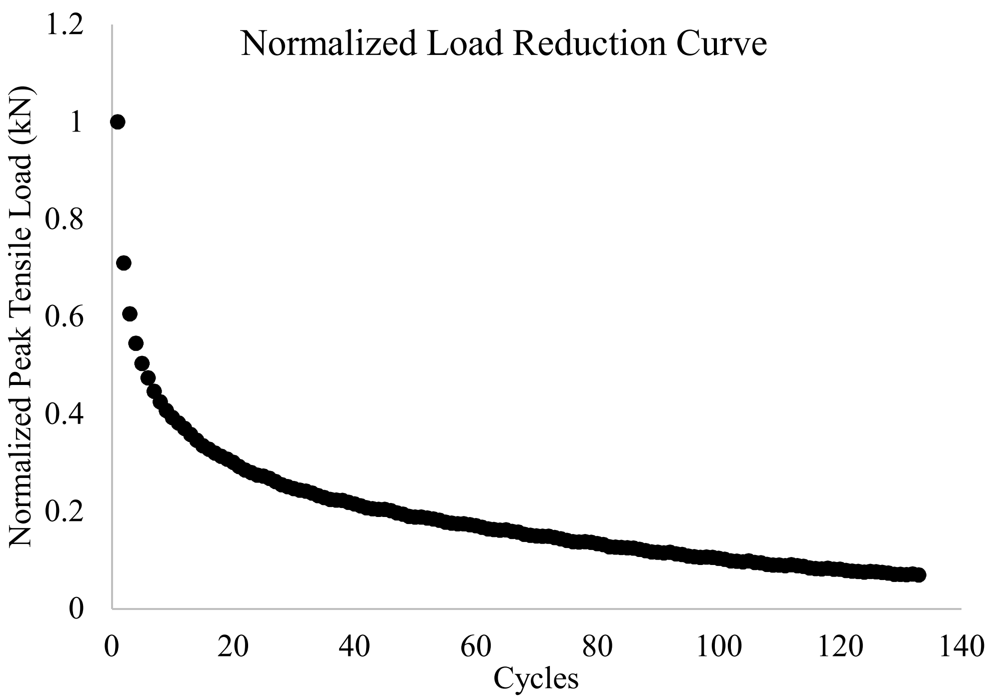

FIGURE 2.8

Typical Load Reduction Curve for Overlay Test

The crack progression rate was shown to follow a trend in which a lower value for β indicated better cracking resistance. Even with the studies that have been performed to help improve the repeatability and variability of the OT, concerns still remain regarding it reliably predicting fatigue cracking.

2.5 Summary of Test and Comparison Chart

Table 2.1 compares the test procedure, loading mode, outcomes, and factors affecting test from literature reviews.

TABLE 2.1

Comparison of Test Summary

Test Procedure	Loading Mode	Load Control	Dimension, AV, Test Temperature	Outcome	Factors Affecting Test from Literature Review
SVECD (AASHTO TP107)	**Fingerprint** Cyclical compression **Fatigue** Cyclical tension	**Fingerprint** Strain 50–75 micro strain **Fatigue** Strain Low micro strain Mid micro strain High micro strain	38 mm diam., 110 mm height AV: 7.0 ± 0.5% Based on PG T= ((Hi Temp+Low Temp)/2) − 3	Relationship between damage and the pseudo secant modulus to create the Damage Characteristic Curve	• Increased RAP decreases fatigue resistance • Increased binder content increases fatigue resistance • Increased air voids decreases fatigue resistance
SCB (AASHTO TP124)	Monotonic	Displacement 50 mm/min (1.97 in/min)	150 mm ± 1 mm diam., 50 mm ± 1 mm thick, cut in half (form two semi-circles) AV: 7.0 ± 0.5% 25°C (77°F)	Fracture Energy (G), Flexibility Index (FI) for damage resistance	• Increased RAP decreases fracture energy and FI • Aging decreases FI • Polymer-modified binder decreases FI
TXOverlay (TxDOT Tex-248-F)	Cyclical tension	Displacement 0.025 in (0.06 cm)	150 mm ± 2 mm diam., 38 mm height, 76 ± 0.5 mm width AV: 7.0 ± 0.5% 25°C (77°F)	Susceptibility to fatigue or reflective cracking	• Increased RAP percent decreases reflective cracking life (RCL) • NMAS of 9.5 mm increases RCL compared to 12.5 mm • Increased binder content increases RCL • PM binder decreases RCL
DM (AASHTO T342)	Cyclical compression	Strain 50–75 micro strain	38 mm diam., 110 mm height AV: 7.0 ± 0.5% 4°C, 20°C, 40°C (39.2°F, 68°F, 104°F)	Dynamic modulus (E*) and phase angle, master curve	• Increased RAP percent increases DM • PM binder increases DM • Increased air voids decreases DM

3. MATERIAL AND QUALITY CONTROL

The materials for this study were obtained from four hot mix asphalt production plants from different aggregates sources within the state of Georgia. Table 3.1 summarizes the materials used in this study.

TABLE 3.1
Plant Produced Mixture Properties

Specimen_ID	NMAS (mm)	Binder Grade	RAP (%)	Binder (%)	G_{mm}	Air Void (%)	VMA (%)	VFA (%)	Effective Binder (%)	Test Performed
A 19_64_N1	19	PG 64-22	25	4.6	2.545	5.5	14.7	68.8	10.1	$\|E^*\|$
A 25_64_N1	25	PG 64-22	25	4.3	2.542	5.5	15.0	65.1	9.8	$\|E^*\|$
A 12.5_67_N	12.5	PG 67-22	30	5.52	2.466	6.3	18.0	65.3	11.8	$\|E^*\|$, OT
A 12.5_76_N	12.5	PG 76-22	30	5.41	2.549	5.7	18.4	68.7	12.6	$\|E^*\|$, SVECD, SCB
A 19_64_N2	19	PG 64-22	30	5.25	2.501	5.5	17.1	68.0	11.6	$\|E^*\|$, SVECD
A 25_64_N2	25	PG 64-22	30	5.20	2.513	5.5	16.7	67.3	11.2	$\|E^*\|$
B 9.5_64_M1	9.5	PG 64-22	30	5.90	2.447	6.5	19.3	65.2	12.6	$\|E^*\|$, OT
B 9.5_64_M2	9.5	PG 64-22	30	5.60	2.498	6.4	18.1	64.3	11.6	$\|E^*\|$, SVECD
C 9.5_67_M	9.5	PG 67-22	30	5.63	2.494	5.5	17.8	72.9	12.9	$\|E^*\|$, SCB, OT
A 12.5_64_M2	12.5	PG 64-22	30	5.40	2.468	5.6	17.7	68.7	12.2	$\|E^*\|$, SVECD, SCB, OT
A 12.5_64_M1	12.5	PG 64-22	30	5.50	2.459	5.5	17.7	70.7	12.5	$\|E^*\|$, SVECD, SCB
B 12.5_64_M	12.5	PG 64-22	30	5.50	2.463	5.6	18.0	69.2	12.5	$\|E^*\|$
C 12.5_67_M	12.5	PG 67-22	30	5.68	2.526	5.8	17.3	66.3	11.5	$\|E^*\|$, SVECD, OT
C 12.5_76_M	12.5	PG 76-22	15	5.10	2.477	5.5	16.8	68.6	11.5	$\|E^*\|$, OT
B 19_64_M	19	PG 64-22	30	4.70	2.529	5.5	15.8	66.3	10.5	$\|E^*\|$, SVECD
B 25_64_M	25	PG 64-22	30	4.40	2.554	5.9	15.3	61.4	9.4	$\|E^*\|$
B 9.5_67_S	9.5	PG 67-22	25	5.84	2.454	5.6	18.4	69.4	12.8	$\|E^*\|$, SCB, OT
B 12.5_67_S	12.5	PG 67-22	25	5.40	2.468	6.0	18.1	66.8	12.1	$\|E^*\|$, SVECD, SCB
D 12.5_76_S	12.5	PG 76-22	25	5.37	2.483	5.6	17.5	68.1	11.9	$\|E^*\|$. SVECD, SCB OT

Note: Specimen ID labeled as X ##_##_X denotes Plant Source, NMAS, Binder Type, and Location.

For this study and the procurement of materials, the state was divided into three separate regions (i.e., North Georgia, Middle Georgia, and South Georgia) to differentiate the aggregate sources shown in Figure 3.1. The North Georgia region was subdivided into 1A and 1B due to 1A having limestone aggregates. The regions were divided based on soil support value (SSV) and climate differences. Plant A had material sourced from North and Middle Georgia. Plant B was sourced from Middle and South Georgia. Plant C was sourced from Middle Georgia, and Plant D was sourced from South Georgia. All of the mixtures except for A 19_64_N1 and A 25_64_N1 had granite aggregates, while those two had limestone aggregates. Three different binder types were used, which are PG 64-22, PG 67-22, and PG 76-22. All three binder types were used to create 12.5 mm NMAS mixtures. PG 64-22 and PG 67-22 were used to create three 9.5 mm NMAS mixtures. PG 64-22 was used for a 19 mm mixture and a 25 mmm mixture. Five mixtures had a RAP content of 25% and thirteen mixtures had a RAP content of 30% and one had a RAP content of 15%. Testing took place on the mixture available at the time. This is the reason that not all the mixtures presented in Table 3.1 were used in each test. More information can be found about relating selected mixtures and binders to MEPDG inputs in Appendix A and Appendix B, respectively.

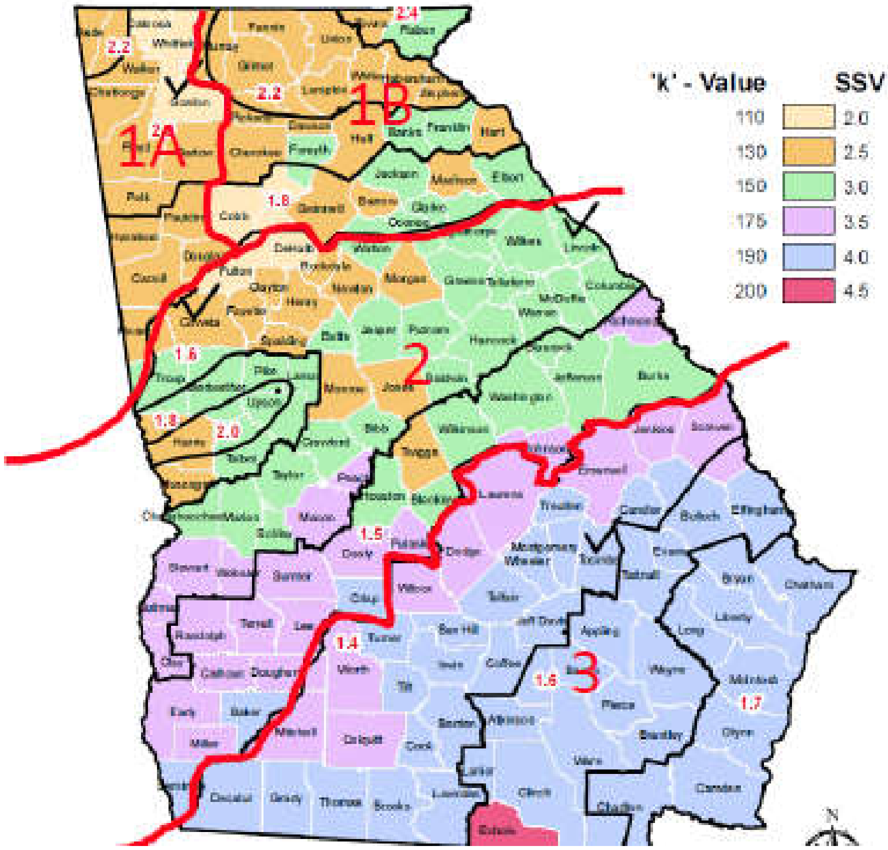

FIGURE 3.1

Regional Separation of Plant Produced Mixtures

4. DYNAMIC MODULUS

4.1 Specimen Fabrication

Developed under NCHRP Project 9-29, the asphalt mixture performance tester is used in this study to measure dynamic modulus. AASHTO TP 79 (now AASHTO T378) was developed from the research performed in NCHRP Project 9-19 specifically for measuring dynamic modulus in an AMPT. The procedure for dynamic modulus testing in AASHTP TP 79 requires a specimen size of 100 mm in diameter by 150 mm in height. However, these dimensions are often impossible to obtain from field cores. In order to solve this problem, research was done to develop a test procedure and determine dynamic modulus from specimen sizes of 38 mm by 150 mm using an indirect tension test (Kim et al. 2004). Further research was performed to develop small-specimen dynamic modulus testing through uniaxial compression, and the results concluded that small and large specimens provided equivalent results (Kutay et al. 2009). Li and Gibson (2013) and Bowers et al. (2015) concluded that a specimen height of 110 mm provided the most consistent data. Lee et al. (2017) performed S-VECD tests using mixtures with an NMAS range from 9.5 mm to 25 mm, different binder types and gradations, and concluded the equivalence of the small specimen results with the large specimens. This study used small specimen geometry in accordance with NCHRP IDEA Project 181 (Castorena 2017).

All mixtures were compacted in a super gyratory compactor to a height of 178 mm and 150 mm in diameter. Small specimens were cored vertically from the inner 100 mm diameter of the large specimens. This provided 4 small specimens of 38 mm diameters from each 150 mm diameter specimen. The ends of the 38 mm specimens were sawed off to a height of 110 mm. The target air void of the compacted specimen was 7 ± 0.5%. Cores taken from the compacted specimen had their air voids measured, and the three with the most similar air voids were used.

4.2 Experimental Procedure

The uniaxial compression test was performed in the AMPT at temperatures of 4°C, 20°C, and 40°C. The loading frequency at each temperature was 25, 10, 5, 1, 0.5, and 0.1 Hz. Each specimen had mounting studs glued to the specimen with a gage length of 70 mm. Linear variable differential transformers (LVDT) were mounted to the specimen and a polytetrafluoroethylene sheet was used to reduce friction between the specimen and the loading platen shown in Figure 4.1. The allowed strain range was between 50 and 75 microstrains.

FIGURE 4.1

Dynamic Modulus Test Setup

4.3 Results and Analysis

Results from the test were used to create dynamic modulus master curves of each mixture. Data collected from dynamic modulus testing were used to form the master curves plotted in Figure 4.2. The data presented are the average for the three replicates.

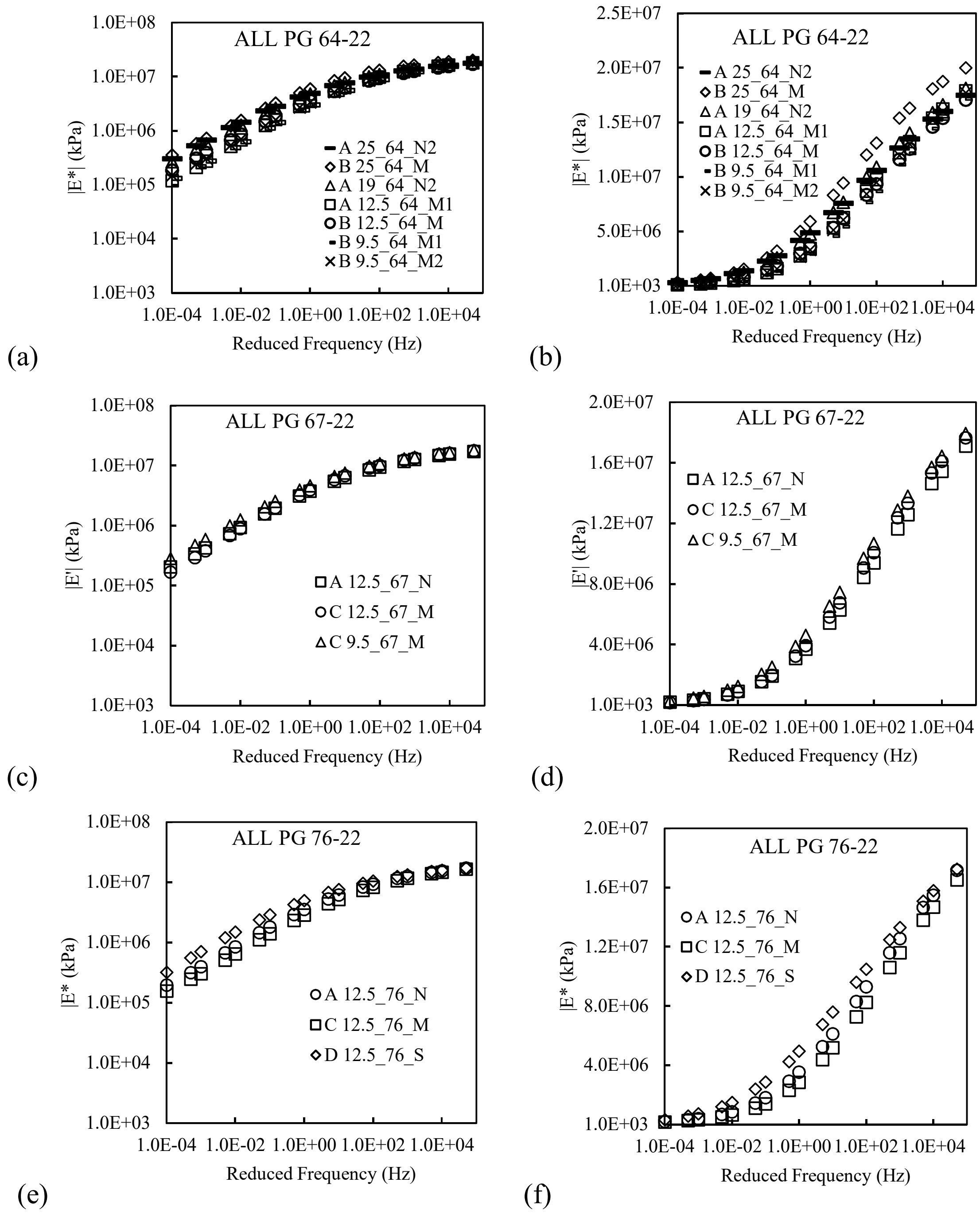

FIGURE 4.2

Dynamic Modulus |E| Results for Mixture with Different NMAS, Binder Types, RAP, and Aggregate Source*

Statistical analysis was performed using an unequal variance *t*-test for the mixtures. The *t*-test was performed for all three temperatures at three different frequencies (i.e., 25, 5, and 0.5 Hz) to compare the difference in NMAS, binder type, and RAP content. The null hypothesis is that the dynamic moduli for different NMAS, binder grade, or RAP content are the same. The P-value was calculated and compared to the critical value of 0.05 to reject or accept the null hypothesis. A value greater than 0.05 indicates that the dynamic values are statistically the same.

4.4 NMAS

P-values are summarized in Table 4.1 for different NMAS. In this comparison, the only difference between the mixtures is the NMAS. The binder type and RAP content are the same for each mixture.

TABLE 4.1
Dynamic Modulus Comparison Against NMAS

25 mm vs 19 mm				
Temperature	4°C	20°C	40°C	Total
P-Value < 0.05	50%	50%	50%	50%
P-Value > 0.05	50%	50%	50%	50%
25 mm vs 12.5 mm				
Temperature	4°C	20°C	40°C	Total
P-Value < 0.05	50%	75%	75%	67%
P-Value > 0.05	50%	75%	25%	33%
19 mm vs 12.5 mm				
Temperature	4°C	20°C	40°C	Total
P-Value < 0.05	83%	83%	50%	72%
P-Value > 0.05	17%	17%	50%	28%
12.5 mm vs 9.5 mm				
Temperature	4°C	20°C	40°C	Total
P-Value < 0.05	17%	58%	0%	25%
P-Value > 0.05	83%	42%	100%	75%

For NMAS of 25 mm and 19 mm, this table shows that there was not statistical difference between dynamic modulus values. The same is true for the 12.5 mm and 9.5 mm NMAS. However, the NMAS of 25 mm and 19 mm compared to the 12.5 mm showed that the larger NMAS influenced the dynamic modulus.

4.5 Binder Type

Table 4.2 summarizes the P-values between different binder types. These binder types were compared against mixtures that had the same NMAS and RAP content.

TABLE 4.2
Dynamic Modulus Comparison Against Binder Type

PG 64-22 vs PG 76-22				
Temperature	4°C	20°C	40°C	Total
P-Value < 0.05	58%	92%	50%	67%
P-Value > 0.05	42%	8%	50%	33%
PG 64-22 vs PG 67-22				
Temperature	4°C	20°C	40°C	Total
P-Value < 0.05	42%	0%	25%	22%
P-Value > 0.05	58%	100%	75%	78%
PG 67-22 vs PG 76-22				
Temperature	4°C	20°C	40°C	Total
P-Value < 0.05	50%	92%	100%	81%
P-Value > 0.05	50%	8%	0%	19%

For binder types PG 64-22 and PG 67-22, the P-value was greater than 0.05 for 78% of the frequencies at all temperatures, meaning that there is no statistical difference between the PG 64-22 and PG 67-22 mixtures. However, the total amount of P-values that are below 0.05 when comparing PG 64-22 and PG 76-22 would suggest that there is a significant difference between the two binders. The same is true for PG 67-22 and PG 76-22. PG 76-22 is a stiffer binder, which is the reason for the higher moduli values.

4.6 RAP Content

RAP content was compared between a mixture that had 15% RAP and mixtures that had 30% RAP but the same NMAS and binder type. The results are shown in Table 4.3.

TABLE 4.3
Dynamic Modulus Comparison Against RAP Content

15% RAP vs 30% RAP				
Temperature	4°C	20°C	40°C	Total
P-Value < 0.05	89%	100%	78%	89%
P-Value > 0.05	11%	0%	22%	11%

The results from the RAP comparison can conclude that RAP content greatly influences the dynamic modulus. This can be attributed to the RAP adding aged binder, which has hardened over time contributing to a stiffer AC mixture.

5. CYCLIC FATGUE TEST FOR S-VECD

5.1 Specimen Fabrication

Loose plant-produced HMA mix was obtained and short-term aged at 20°C below compaction temperature to separate the mixture that arrived at the lab in covered metal buckets. The mixture was then heated to compaction temperature and then poured into molds to be compacted in a gyrator compactor. To obtain small specimen geometry, specimens were vertically cored from the gyratory-compacted specimen with a height of 178 mm and 150 mm in diameter in accordance with AASHTO TP107. The cored specimens have 38 mm diameters and four cores are obtained from each 150 mm diameter specimen shown in Figure 5.1. The ends of the 38 mm specimens were sawed off to a height of 110 mm, as shown in Figure 5.2.

FIGURE 5.1

SGC Compacted Specimen with Four Cores Taken from the Center

FIGURE 5.2

Small Specimen Cut from 178 mm to 110 mm

The target air void of the compacted specimen was 7 ± 0.5%, and the cored specimens had an air void of 6 ± 0.5%. Four cores taken from the compacted specimen had their air voids measured, and the three with the most similar air voids were used.

5.2 Experimental Procedure

With the prepared specimens, mounting studs were glued to the specimen at a gage length of 70 mm, and the end plates were glued to the specimen as shown in Figure 5.3.

FIGURE 5.3

Small Specimen with Glued End Plates

Then, the specimen was inserted into the AMPT machine and the bottom support was tightened. The actuator applied a seating of 0.01 kN for the purpose of securing the upper loading platen with screws. Feeler gauges were used to ensure proper leveling of the specimen. The feeler gauges and the way the screws hold the test specimen in place is shown in Figure 5.4.

FIGURE 5.4

Secured Test Specimen with Feeler Gauges

The load was reduced to zero, which was the starting load for the test, and LVDTs were mounted to the specimen. The test temperature was based on LTPPBind Version 3.1 (AASHTO TP107, 2014) and used Eq. (30).

$$\text{Test Temperature (°C)} = (\text{if } \frac{T_{H+}T_L}{2} - 3 \leq 21^oC, \left(\frac{T_H+T_L}{2} - 3\right) \text{ otherwise, } 21\text{°C}) \qquad (30)$$

Where,

T_H = high-temperature PG Grade from LTPPBind (°C)

T_L = low-temperature PG Grade from LTPPBind (°C), generally a negative number

Once the specimen reached the target temperature, a dynamic modulus ($|E^*|$) fingerprint test was performed at a frequency of 10 Hz and a target strain range of 50–75 microstrains. Following the fingerprint test, the specimen rested for 20 minutes. The cyclic fatigue test was started with the peak-to-peak specimen strain amplitude of 300, 500, or

800 microstrains based on the $|E^*|_{fingerprint}$ ranges. The test was terminated when the phase angle began to drop.

5.3 Damage Characteristic Curves

C versus *S* curves were constructed with the aid of FlexMAT™ software. Three replicates were used to construct the curves and a single model was fitted via the curves. Figure 5.5(a) shows the accumulated damage between polymer-modified binder PG 76-22 and unmodified binder PG 64-22. The *C* versus *S* curves for the mixtures with polymer-modified PG 76-22 binder are higher than the curves for the mixtures with PG 64-22 binder. This outcome is expected because the modulus heavily influences these curves. The polymer-modified binder is stiffer than the unmodified binder, thus leading to a higher dynamic modulus value and a higher *C* versus *S* curve. Figure 5.5(b) shows the effect of the NMAS on the *C* versus *S* curves; the smaller 9.5 mm mixture with PG 64-22 binder has a higher curve than the 12.5 mm mixture with PG 64-22 binder.

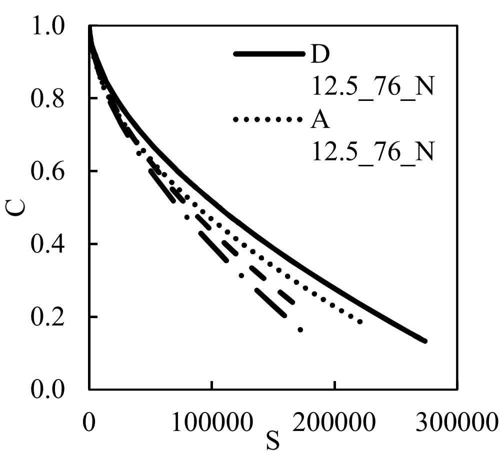

(a)

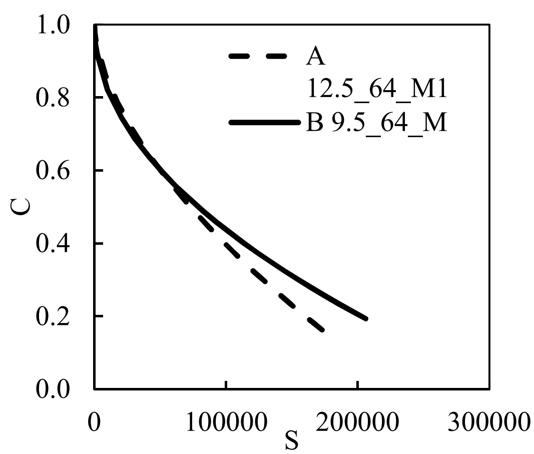

(b)

FIGURE 5.5

(a) C vs. S Curves for 12.5 mm Mixtures with PG 76-22 and PG 64-22 Binders, and
(b) C vs. S Curves for 9.5 mm and 12.5 mm Mixtures with PG 64-22 Binder and 30% RAP

5.4 D^R Failure Criterion

The following figures were arranged based on expected results of binder type and NMAS. The expected trend would be a decrease in D^R from high to low binder grade and a decrease with a larger NMAS. Figure 5.6(a) shows the trends for the mixtures with polymer-modified PG 76-22 binder that have a higher D^R value than the mixtures with unmodified PG binders. The surface mixtures also have a higher D^R value than the base mixtures. The D^R values for the 9.5 mm and 12.5 mm surface mixtures are both higher than the larger 19 mm and 25 mm mixtures, as seen in Figure 5.6(b). These mixtures contained the same PG 64-22 binder. The 9.5 mm mixtures generally have the same D^R values as the 12.5 mm mixtures with the same performance grade binder, i.e., PG 64-22. Both of these results show expected trends; i.e., the polymer-modified binder and smaller NMAS present higher D^R values that indicate better cracking resistance. Table 5.1 includes the R^2 values for D^R and the standard deviation for S_{app} for all mixtures.

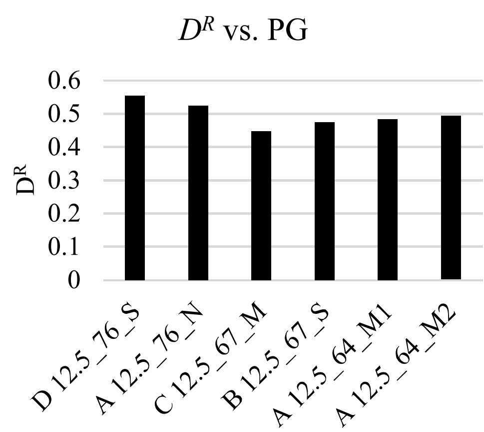

(a)

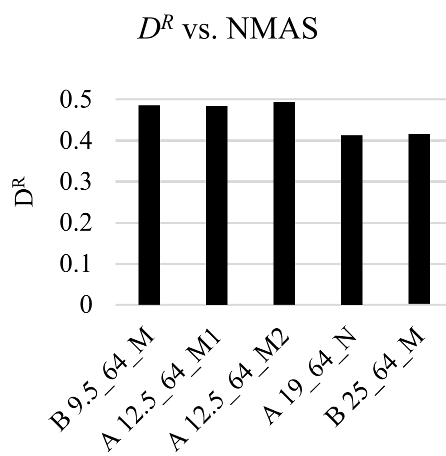

(b)

FIGURE 5.6

(a) D^R Failure Criterion Used to Compare Polymer-Modified PG 76-22 Binder with Unmodified PG 67-22 and PG 64-22 Binders, and (b) D^R Failure Criterion Used to Compare 9.5 mm, 12.5 mm, 19 mm, and 25 mm Mixtures

Table 5.1

D^R and S_{app} Values with the Corresponding R^2 and Standard Deviation Values

Specimen_ID	NMAS (mm)	Binder Grade	D^R	R^2	S_{app}	SD
B 9.5_64_M	9.5	PG 64-22	0.48	0.99	10.36	0.62
B 9.5_67_S	9.5	PG 67-22	0.50	1	9.80	1.04
A 12.5_64_M1	12.5	PG 64-22	0.48	1	9.37	0.23
A 12.5_64_M2	12.5	PG 64-22	0.49	1	8.90	0.53
B 12.5_67_S	12.5	PG 67-22	0.47	1	9.02	0.17
C 12.5_67_M	12.5	PG 67-22	0.45	1	9.94	0.61
A 12.5_76_N	12.5	PG 76-22	0.52	1	11.81	0.69
D 12.5_76_S	12.5	PG 76-22	0.55	0.99	15.40	0.49
A 19_64_S	19	PG 64-22	0.41	1	8.72	0.95
B 25_64_M	25	PG 64-22	0.42	1	8.57	0.87

5.5 S_{app} Cracking Index

Binder type is an important mixture characteristic that a fatigue index should accurately reflect. Mixtures in Georgia typically use PG 64-22 or PG 67-22 binder for normal traffic loading conditions and polymer-modified PG 76-22 binder for heavy traffic. The 12.5 mm mixtures were used to investigate the effect of binder type on S_{app}. Figure 5.7(a) shows the differences between the three binder types. The S_{app} values for PG 67-22 are slightly higher overall compared to those for PG 64-22. However, the S_{app} values for the PG 76-22 binder are significantly higher than for PG 64-22 or PG 67-22 binder. This finding implies that S_{app} can accurately rank fatigue resistance based on binder type. This finding also agrees with the results shown in Figure 5.6(a), where polymer-modified binders have higher D^R values. Mixtures with different NMAS values were investigated to determine the effects of NMAS on S_{app} and fatigue cracking resistance. Figure 5.7(b) presents the mixtures with different NMAS values. All mixtures consist of 30% RAP and PG 64-22 binder with differences in NMAS for 9.5 mm, 12.5 mm, 19 mm, and 25 mm.

This figure shows that an increase in the NMAS corresponds to a decrease in S_{app} value. This outcome again agrees with Figure 5.6(b), where D^R is shown to decrease with an increase in NMAS. D^R shows similar trends to S_{app}, but it is unable to be used by itself to rank mixtures because it only measures toughness, while S_{app} combines toughness and moduli.

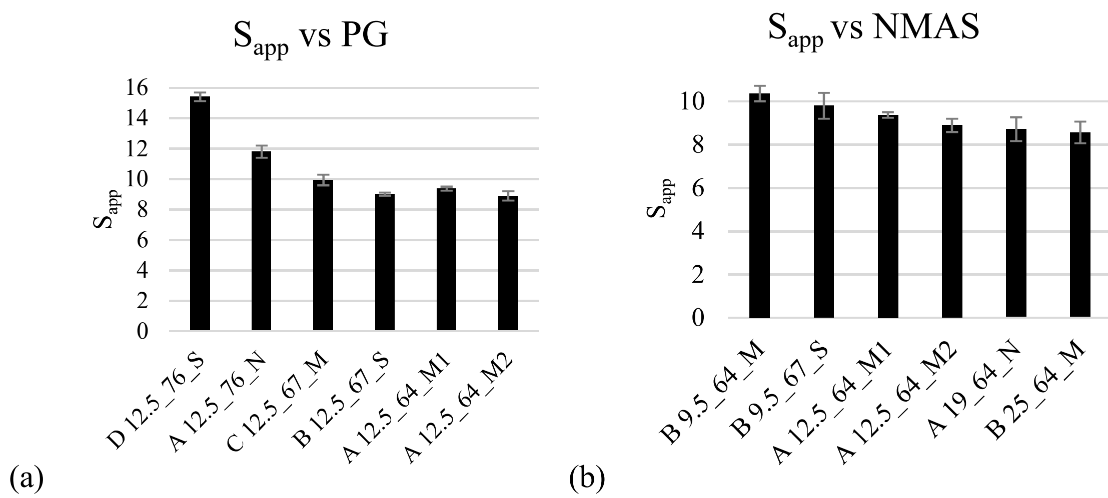

FIGURE 5.7

(a) S_{app} Values for Mixtures with Different NMAS Values, and (b) S_{app} Values for 12.5 mm Mixtures with PG 64-22, PG 67-22, and PG 76-22 Binders

The effect of binder content on fatigue cracking/resistance also was investigated by observing how different binder contents would affect S_{app} values. Mixtures with the same NMAS and binder type were chosen for comparison. Figure 5.8 compares 12.5 mm mixtures with different binder types, i.e., PG 67-22 and PG 64-22. For both PG 67-22 and PG 64-22 binders, the S_{app} value increased as the binder content increased. This result is intuitive, as an increase in the binder percentage would generally result in a softer AC mixture. No significant difference in S_{app} values due to the half-grade difference of binder was observed.

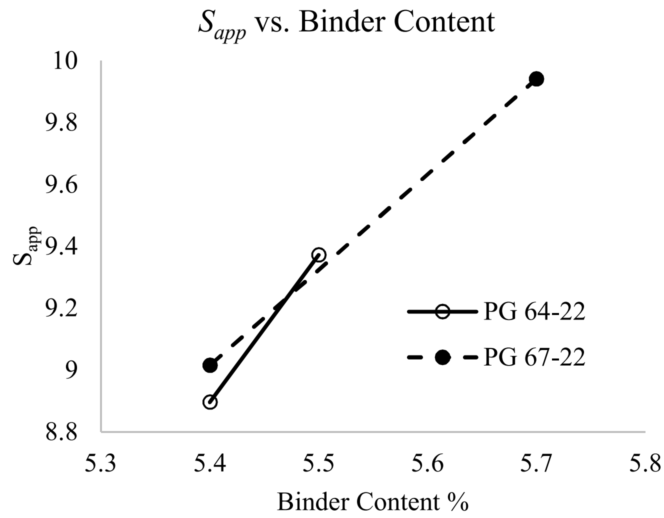

FIGURE 5.8

S_{app} Values for Mixtures with Different Binder Contents for the Same NMAS and Binder Type

Table 5.2 suggests the threshold values for S_{app} along with different traffic levels (Wang and Kim 2017). The S_{app} values from Figure 5.8 indicate that all mixes should satisfy S designation and D 12.5_76_S satisfies H designation, which has traffic level between 3 and 30 million ESALs (equivalent single axle loads).

TABLE 5.2

Recommended Threshold Values for the S_{app} Fatigue Index Parameter

Traffic Level (million ESALs)	S_{app}	Tier	Designation
≤3	≤ 8	Light	L
>3 and ≤10	>8 and ≤15	Standard	S
>10 and ≤30	>15 and ≤20	Heavy	H
>30	>20 and ≤25	Very Heavy	V
>30 and slow traffic	>25	Extremely Heavy	E

To compare the traffic level shown in Table 5.2 against one suggested by GDOT's practical guideline for specific mixtures, Table 5.3 was developed. Table 5.3 presents the calculated ESALs and measured S_{app} values for the 12.5 mm NMAS mixture in Georgia. GDOTallows 12.5 mm Superpave mixtures with PG 64 or PG 67 binders for the two-way average daily traffic (ADT) between 10,000 to 25,000 while 12.5 mm mixtures with polymer-modified binder is allowed for the two-way ADT between 25,000 and 50,000. Since GDOT uses two-way average daily traffic to select mixture type, the two-way ADT was converted into ESALs assuming 5% truck traffic, 1.17 for ESAL factor, and 1.0 for lane distribution factor.

TABLE 5.3
Recommended Threshold Values for the S_{app} Based on GDOT Mixture Selection Criteria (Assuming 5% Truck Traffic and 1.17 ESAL Factor)

Two-way ADT	Traffic Level (million ESALs)	S_{app} (from Test Results)	Mix Type	Remarks
10,000 – 25,000	>4 and ≤10	>12	12.5 mm Superpave with PG 64-22 or PG 67-22	For State Routes and for shoulders of Interstate Routes
25,000 – 50,000	>10 and ≤20	>15.5	12.5 mm Superpave with polymer modified binder	For high ADT State Routes, Interstate Routes when recommended by GDOT, all flexible pavement Interstate Ramps, and all flexible pavement roundabouts
>50,000	>20	N/A	12.5 mm Stone Matrix Asphalt	For Interstate Routes and for State Routes when recommended by GDOT

As shown in Table 5.3, all mixes used in this study are adequate for the traffic level between 4 and 20 million ESALs. Although the recommended threshold values at different traffic level in Table 5.2 and Table 5.3 show reasonable agreement, it is still based on the calculated ESALs from two-way ADT with assumption of percent truck. Therefore, it is suggested that each state agency develop their own S_{app} threshold criteria reflecting the state agency's mixture selection criteria and practical guideline.

5.6 Fatigue Performance Simulation

In this study, the goal of fatigue cracking performance simulation is to determine the practical application of available pavement evaluation programs in ranking AC mixture performance using a GDOT-approved pavement section design. This study used AASHTOWare Pavement ME (Ver. 2.3.1) and FlexPAVE™ to simulate fatigue cracking performance.

Pavement ME was originally developed under National Cooperative Highway Research Program (NCHRP) Project 1-37A and uses layered elastic theory and empirical models to determine fatigue damage and permanent deformation (Advanced Research Associates, Inc. 2004). Pavement ME has a number of global calibration factors that can be adjusted to meet local calibration factors. GDOT developed local calibration factors for rutting, bottom-up fatigue cracking, and thermal cracking.

FlexPAVE™, developed by North Carolina State University researchers, uses the finite element method to predict pavement distresses. The S-VECD model is used in FlexPAVE™ to predict fatigue damage throughout the pavement design life. Damage is calculated in FlexPAVE™ through two overlapping triangles that form the reference cross section area (Wang and Kim 2018). The top inverted triangle has a base of 170 cm, while the bottom triangle has a base of 120 cm. Each triangle calculates damage, which allows for top down cracking and bottom up cracking to be separated. Figure 5.9 shows the overlapping triangles and the separation into the top and bottom for cracking purposes. The program outputs damage contours that show the location of damage and the degree of damage. Recent research has shown that FlexPAVE™ along with D^R can reasonably predict and rank pavement performance (Wang and Kim 2018).

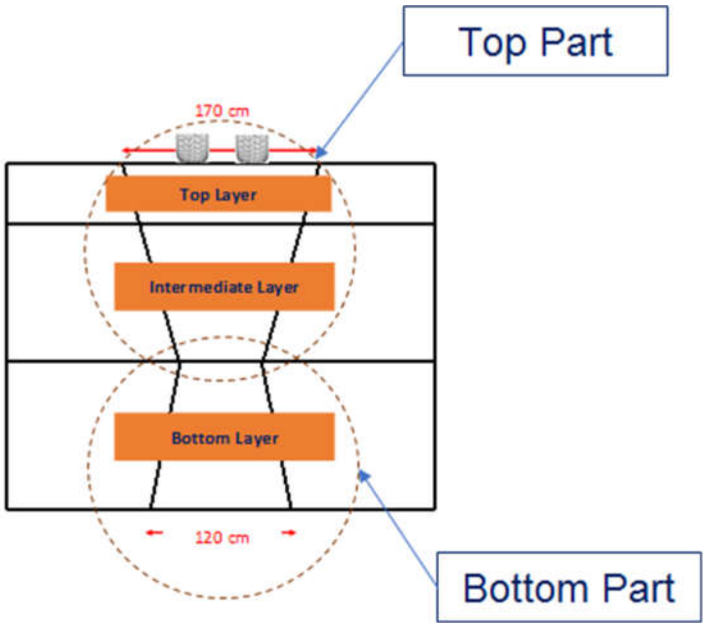

FIGURE 5.9

Damage Area Used in FlexPAVE™
Separated into Top and Bottom for Cracking Reference

5.7 Section Design

Two different pavement sections were considered in this study to determine pavement performance based on D^R and S_{app} values. The first was a single-layer pavement section 4 inch (10.16 cm) thick. A 12 inch (305 mm) unbound aggregate base was used under the asphalt layer. Underneath the aggregate base was a subgrade that was considered to be a semi-infinite layer, and modulus values were used that are specific to the typical soil in Georgia.

To investigate the effect of the surface mixtures on the fatigue cracking performance of a pavement, this single layer was changed between the various 9.5 mm and 12.5 mm

NMAS mixtures. The results from the cyclic uniaxial fatigue test and the dynamic modulus test were used in FlexPAVE™ for pavement performance evaluation. Pavement ME requires mixture dynamic modulus data along with binder complex shear modulus (G^*) data for Level 1 analysis. Traffic inputs were based on actual traffic data from an approved GDOT design. FlexPAVE™ uses the daily equivalent single-axle load from the approved design report and the vehicle speed. Pavement ME currently offers additional options for traffic inputs. A two-way average annual daily truck traffic count based on the design report was input for the number of lanes, truck percentage in the design lane, operational speed, and traffic load distribution. Climate data specific to the state of Georgia, which were available for both programs, also were used.

The second design that was used to compare the programs was a two-layer pavement section. The design consisted of a surface layer (12.5 mm NMAS) and a bottom layer (19 mm NMAS) with thicknesses of 3 inch (7.62 mm) for each, providing a total thickness of 6 inch (15.24 mm). The aggregate base and subgrade were left the same at 12 inch (305 mm) and the subgrade layer was considered to be infinite in the depth direction. The traffic conditions were applied in the programs the same way as for the single-layer section.

5.8 Results from Simulation

Figure 5.10 shows an example of the damage contours for one of the 4 inch pavement sections, to illustrate the growth of damage predicted by the FlexPAVE™ software. This figure was created using mixture A 12.5_64_M2 and shows the damage due to top down and bottom up cracking.

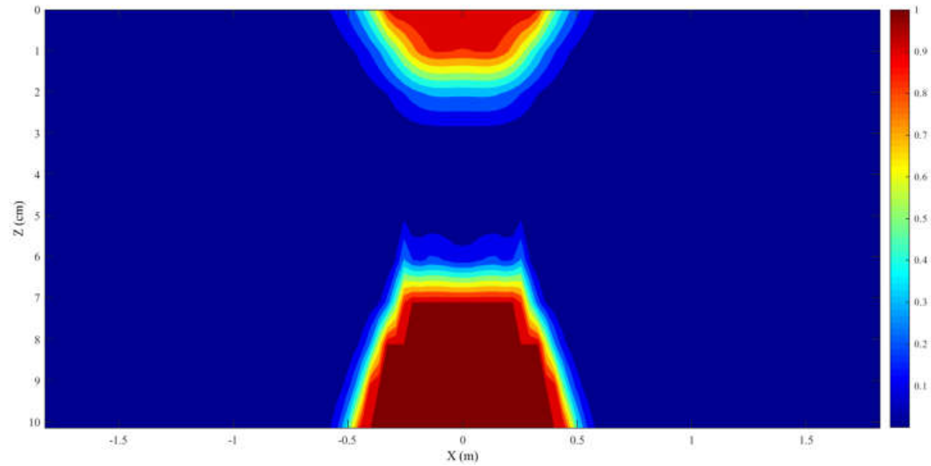

FIGURE 5.10

Damage Contours Based on Pavement Section with 12.5 mm NMAS and PG 64-22 Binder

Figure 5.11(a) through (i) show the fatigue cracking predicted by FlexPAVE™ of the 4 inch pavement section over the design life of 20 years and their correlations with S_{app} and D^R. Figure 5.12(a) through (i) show the same for the 6 inch two-layer section. Figure 5.13(a) through (d) show the top down and bottom up cracking predicted by Pavement ME over the design life of 20 years for the 4 inch section and the two 3 inch layer section. The 4 inch pavement section in FlexPAVE™ showed very good trends for a decrease in damage with an increase in binder type. It also showed that the mixtures with lowest S_{app} values had the most damage and those with the highest S_{app} values had the least. The correlation for S_{app} also shows why D^R alone is not sufficient to rank asphalt mixtures. S_{app} has a much higher R^2 value than D^R when compared against percent damage. When separated into top down and bottom up damage, it can be seen that the polymer-modified mixtures reduced cracking for both of these instances. In the case of the 6 inch two-layers, the total percent damage were very similar to each other according to FlexPAVE™; however, once separated into top down and bottom up, it is seen that the higher binder grades were able to reduce top down cracking. Pavement ME had similar results for both the 4 inch section and the 6 inch two-layer section. For both pavement sections, Pavement ME showed that the polymer-modified binders had the least amount of top down and bottom up cracking. Pavement ME shows that the most cracking would occur in the 9.5 mm NMAS mixture, while FlexPAVE™ has the 12.5 mm NMAS PG 64-22 as experiencing the most cracking.

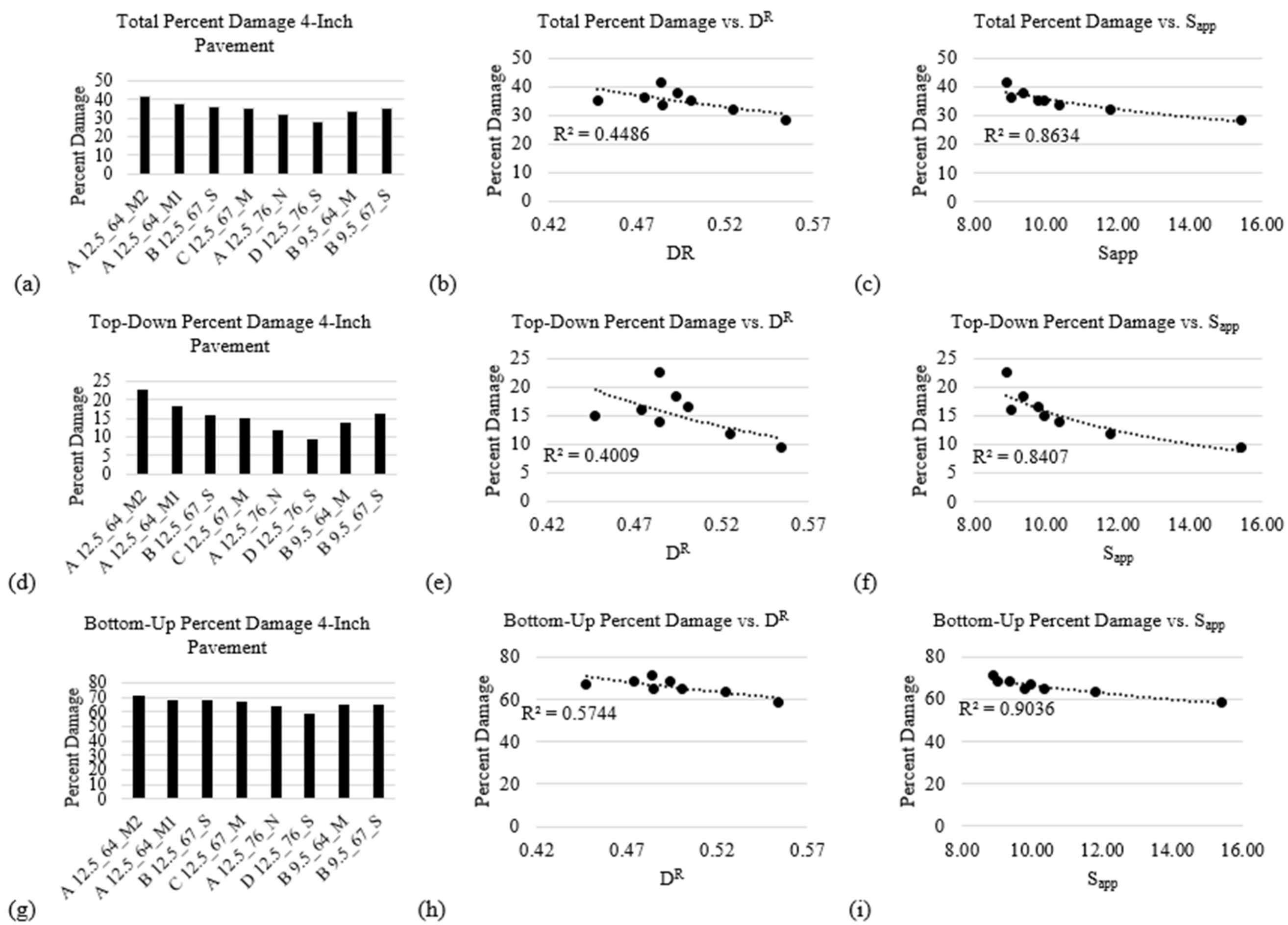

FIGURE 5.11

FlexPAVE™ Predicted Fatigue Cracking for 4 Inch Pavement Section: (a)–(c) Total Percent Damage, (d)–(f) Top Down Percent Damage, and (g)–(i) Bottom Up Percent Damage

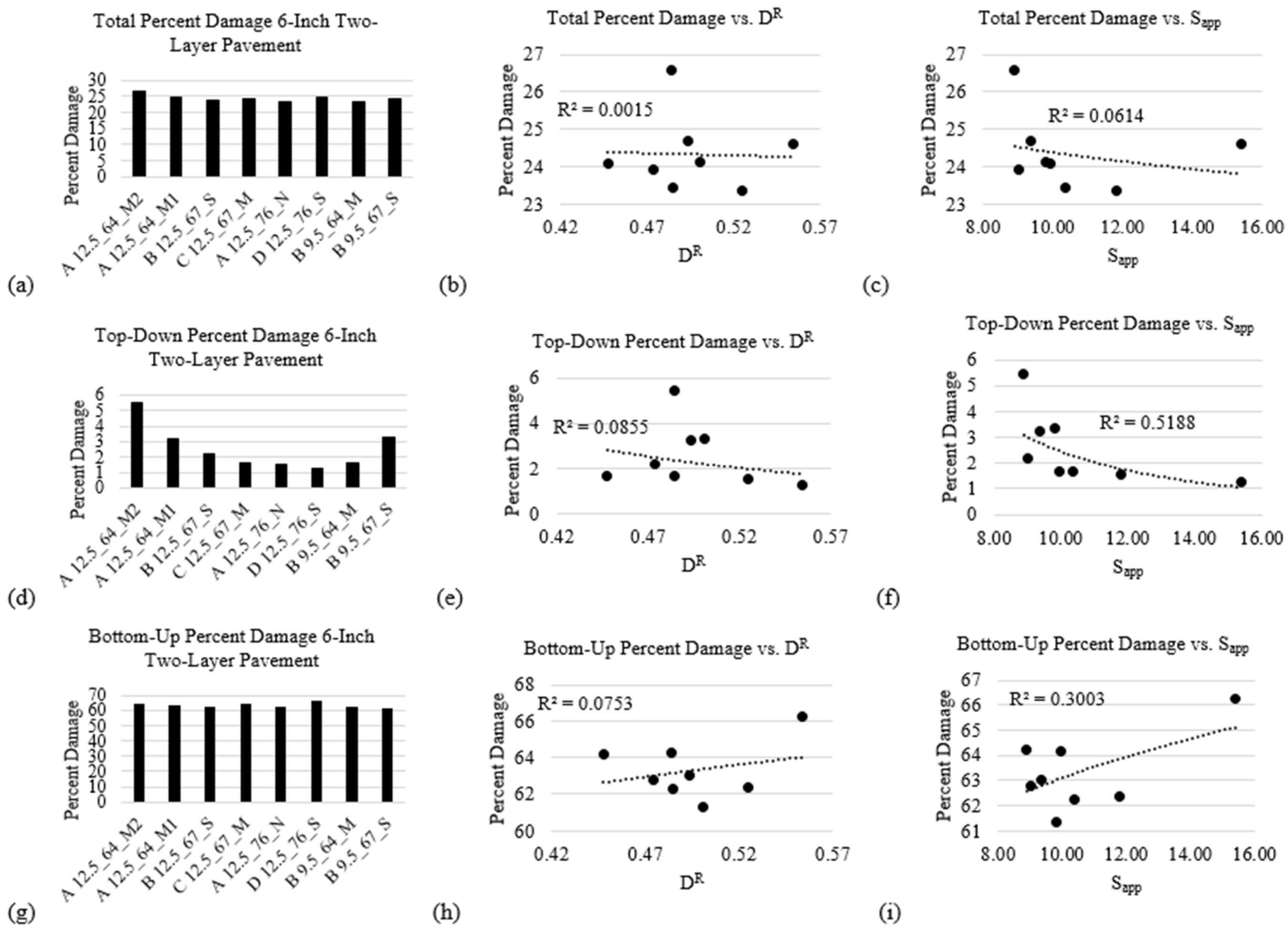

FIGURE 5.12

FlexPAVE™ Predicted Fatigue Cracking for 6 Inch Two-Layer Pavement Section: (a)–(c) Total Percent Damage, (d)–(f) Top Down Percent Damage, and (g)–(i) Bottom Up Percent Damage

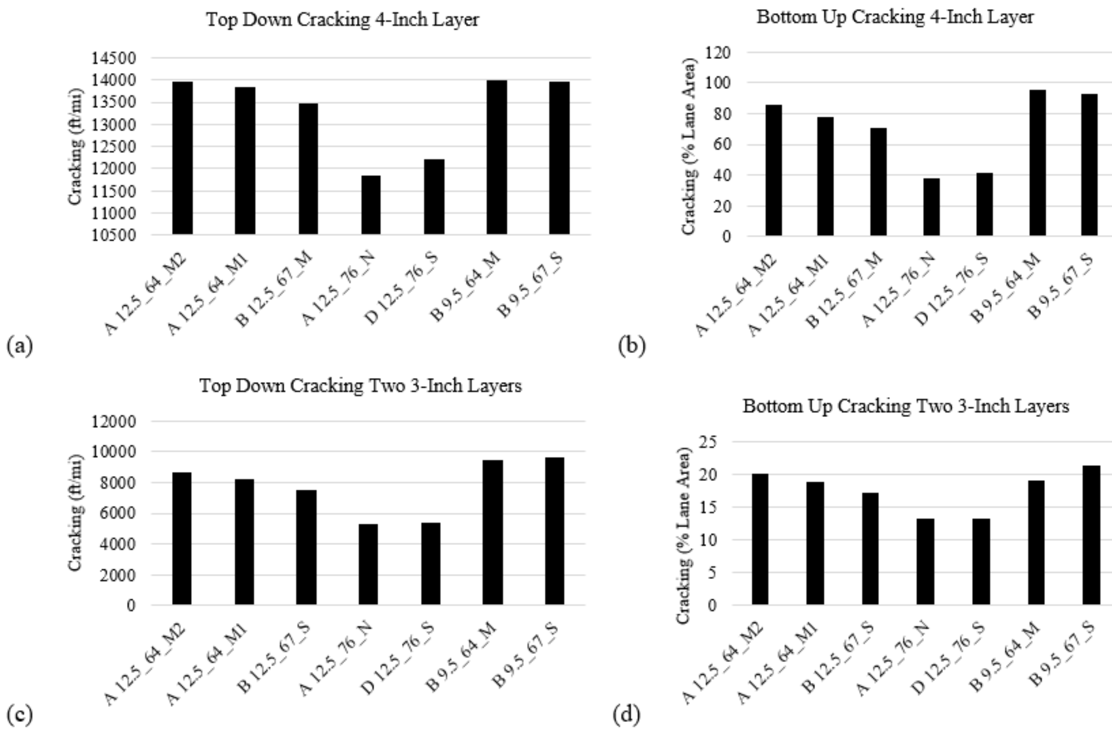

FIGURE 5.13

Pavement ME Predicted Fatigue Cracking: (a) 4 Inch Layer Top Down Cracking, (b) 4 Inch Layer Bottom Up Cracking, (c) Two 3 Inch Layers Top Down Cracking, and (d) Two 3 Inch Layers Bottom Up Cracking

6. SEMICIRCLE BEND TEST

6.1 Specimen Fabrication

Specimens were made from plant-produced loose mix asphalt in a super gyratory compactor in accordance with AASHTO T312, "Standard Method of Test for Preparing and Determining the Density of Asphalt Mixture Specimens by Means of the Superpave Gyratory Compactor (SGC)" (AASHTO T312, 2015). Specimens were made to a height of 178 mm at a target air void of 7 ± 0.5%. These SGC specimens were then cut as shown in Figure 6.1 to obtain two 50 mm thick discs from the middle of the specimen shown in Figure 6.2. Each disk was then cut in half to create four semicircle shapes, and a 15 mm notch was made at the center of the specimen as shown in Figure 6.3.

FIGURE 6.1

SGC Specimen Prepared to be Cut into Two 50 mm Disks

FIGURE 6.2

50 mm Disk Cut from an SGC Specimen

FIGURE 6.3

Semicircle with 15 mm Notch in Center

6.2 Experimental Procedure

Using the newly developed I-FIT test (AASHTO TP124), the materials were tested to determine how their mixture properties lend to their fracture resistance. The test was specifically looking at evaluating different percentages of RAP, binder types, aggregate sources, and NMAS. Prior to the I-FIT test, each mixture was subjected to quality control tests including theoretical maximum specific gravity (G_{mm}), bulk specific gravity (G_{mb}), asphalt content by ignition oven, and sieve analysis. The measurements were compared to the job mix formulas (JMFs) supplied by the producers since it is important for the state agency to understand how its approved mixes, which come from different regions of the state and are made of different binder types, perform comparative to each other. This will benefit those who create mix designs to select the optimum mix for the particular project. For this study, eight different GDOT-approved plant mixes were obtained and fabricated into specimens as shown in Table 6.1.

TABLE 6.1
Mixtures Used for SCB Testing

Specimen_ID	NMAS (mm)	Binder Grade	RAP (%)	Binder (%)	G_{mm}	Air Void (%)	VMA (%)	VFA (%)	Effective Binder (%)	Test Performed
A 12.5_76_N	12.5	PG 76-22	30	5.41	2.549	5.7	18.4	68.7	12.6	$\|E^*\|$, SVECD, SCB
C 9.5_67_M	9.5	PG 67-22	30	5.63	2.494	5.5	17.8	72.9	12.9	$\|E^*\|$, SCB, OT
A 12.5_64_M2	12.5	PG 64-22	30	5.40	2.468	5.5	17.7	68.7	12.2	$\|E^*\|$, SVECD, SCB, OT
A 12.5_64_M1	12.5	PG 64-22	30	5.50	2.459	5.5	17.7	70.7	12.5	$\|E^*\|$, SVECD, SCB
B 9.5_67_S	9.5	PG 67-22	25	5.84	2.454	5.5	18.2	70.3	12.8	$\|E^*\|$, SCB, OT
B 12.5_67_S	12.5	PG 67-22	25	5.40	2.468	6.0	18.1	66.8	12.1	$\|E^*\|$, SVECD, SCB
D 12.5_76_S	12.5	PG 76-22	25	5.37	2.483	5.5	17.4	68.6	11.9	$\|E^*\|$. SVECD, SCB OT

The test was run in an asphalt mixture performance tester (AMPT) in accordance with the I-FIT procedure at 25°C with four (4) replicates for each mix type. The test had an initial contact load of 0.1 kN and used line load displacement control at a rate of 50 mm/min. The test terminated when the load dropped below 0.1 kN.

6.3 Results and Analysis

Figure 6.4 shows the results of the I-FIT tests. As shown in Figure 6.4(a), the fracture energy values ranged from 1333 to 2521 J/m^2. The FI had values from 1.5 to 5.2, as shown in Figure 6.4(b). The coefficient of variation (CV) for FI was between 5% and 26% with an average of 15%. The fracture energy of the mixtures had a CV between 4% and 20% with an average of 11%. Interestingly, the mixtures with polymer-modified binder (PG 76-22) show lowered fracture energy and FI compared to others, which was unexpected.

The eight mixtures varied in four distinct categories: RAP content, binder type, aggregate source, and NMAS. Comparisons between mixtures needed to be appropriate in order to draw conclusions about the local fracture characteristics of plant-produced AC mixtures in Georgia. Due to the mixtures being plant-produced as opposed to laboratory-produced, the mixtures had variability in volumetric properties. Before analysis was performed on the mixture characteristics of interest, analysis of variance (ANOVA) was performed on voids in the mineral aggregate, voids filled with asphalt, and percent of air voids. The results of this analysis are presented Table 6.2.

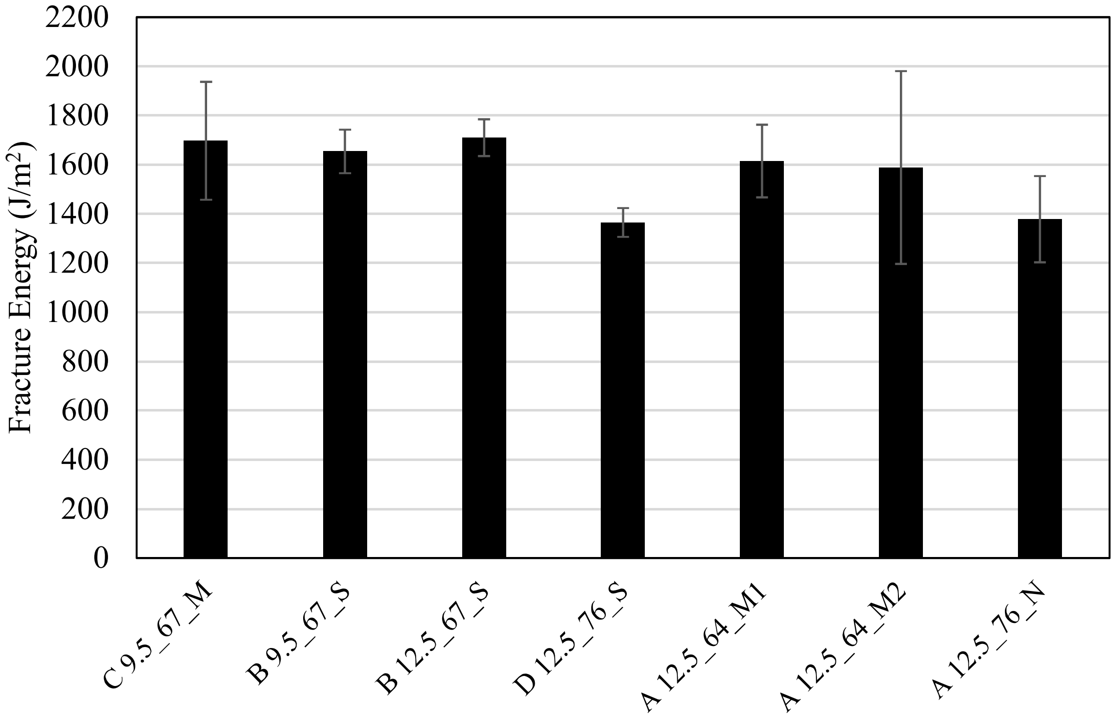

(a) Fracture Energy

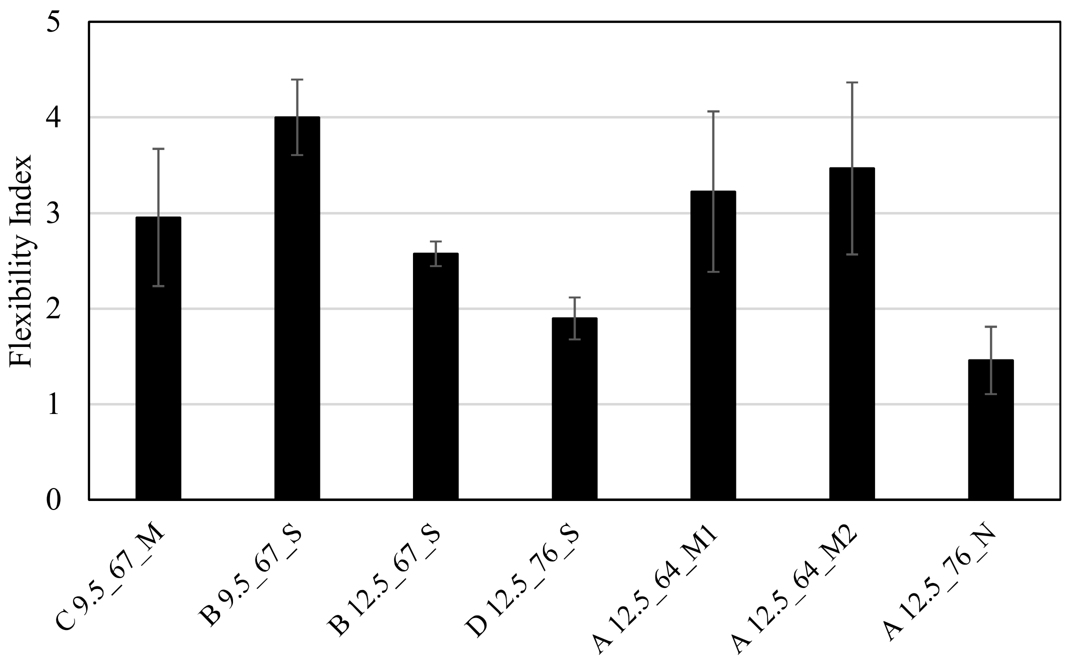

(b) Flexible Index

FIGURE 6.4

I-FIT Results for All Mixtures (a) Fracture Energy and (b) Flexible Index

TABLE 6.2
Analysis of Variance of VMA, VFA, and AV for All Mixtures at 95% Confidence Interval

Variable	**Responses**	
	FI	**Fracture Energy**
	P-Value	P-Value
VMA	0.370	0.108
VFA	0.389	0.788
AV	0.912	0.866

Based on the ANOVA of VMA, VFA, and AV, it was determined that these three volumetric properties did not have any significant influence on fracture energy or FI for this study. Knowing these three variables did not create differences within the responses, further analysis was possible on the mixture characteristics of interest. ANOVA was performed on the results from the different mixtures, presented in Table 6.3, with the variables being binder type, RAP content, aggregate source, NMAS, and the response fracture energy and FI. The order of analysis was important in this study because of the variable mixture designs. The study was limited to the material being produced by plants at the time. This led to analysis of the results in a systematic manner in order to filter out mixture characteristics that did not influence FI or fracture energy. NMAS was the first variable selected because it provided the most mixtures to analyze that had consistent variables. Aggregate source was analyzed second for similar reasons as NMAS. These two analyses provided the following findings:

- Aggregate sources had no significant difference in FI or fracture energy.
- NMAS was not found to be significant in fracture energy or FI between the 9.5 mm and 12.5 mm surface mixes.

Since these two mixture characteristics did not have any influence on FI or fracture energy, further analysis was possible on binder type and RAP content. In review of the literature, numerous researchers showed that RAP content has a significant influence on fracture energy and FI (Norouzi et al. 2017, Cascione et al. 2015, Kim, Mohammad, and Elseifi 2012). Based on those studies, RAP content was analyzed across data groups after it was determined aggregate source and NMAS were inconsequential. Binder type was then compared between mixtures that had the same RAP content. The analysis of those two mixture characteristics shows as follows:

- PG was seen to have significant impact on FI, but fracture energy failed to discriminate between mixtures.
- Mixtures with 25% and 30% RAP content are not significant for fracture energy or FI, since this was due in part to the different binder types controlling the response, as the change in RAP content was only 5%.

TABLE 6.3
Analysis of Variance of Binder Type, RAP Content, Aggregate Source, and NMAS with a 95% Confidence Interval

Variable	Responses	
	FI	**Fracture Energy**
	P-Value	P-Value
NMAS	0.312	0.911
Aggregate Source	0.075	0.087
RAP Content	0.404	0.819
Binder Type	0.004	0.110

Because ANOVA does not show where the difference in the data lies, paired *t*-tests were performed. A paired *t*-test was performed for the difference in RAP content, as well, in order to determine if the nonresponse found in the ANOVA was due to the binder variable. The results of the *t*-test are shown in Table 6.4.

TABLE 6.4
Results of Paired *t*-test with a 95% Confidence Interval

Variable	**Response**			
	FI		**Fracture**	
	T-Value	P-Value	T-Value	P-Value
RAP 25% and 30%	4.50	0.0102	0.983	0.199
PG 76-22 and PG 64-22	4.27	0.003	2.38	0.019
PG 76-22 and PG 67-22	4.21	<0.001	2.90	0.007
PG 67-22 and PG 64-22	0.367	0.359	0.237	0.408

From the *t*-test, the following observations were made:

- Fracture energy failed to discriminate the fatigue-resisting performance between 25% and 30% RAP mixes, while FI is statistically significant to differentiate fatigue-resisting performance of mixtures. This *t*-test allowed for the exclusion of binder type, which resulted in nonresponses in the ANOVA.
- FI values between mixtures with PG 64-22 and PG 76-22 had significant difference, as well as PG 67-22 and PG 76-22.
- There was no significant difference between PG 67-22 and PG 64-22 in FI or fracture energy.
- The results of lowered FI for the mixtures with polymer-modified binder (PG 76-22) compared to other mixtures with softer binders (PG 64-22 and PG 67-22) was unexpected.

7. MODIFIED OVERLAY TEST

7.1 Specimen Fabrication

Specimen fabrication for the modified overlay test was created from a super gyratory compacted specimen at a height of 178 mm and a diameter of 150 mm. Two specimens were cut from a single SGC specimen to a height of 38 mm and a diameter of 150 mm in accordance with Tex-248-F). A template was used to obtain an accurately cut specimen perpendicular to the top surface, resulting in a width of 76 mm. The specimen was glued to the base plates with weights placed on top of the specimen while the glue cured. Figure 7.1 shows the geometry of the cut specimens.

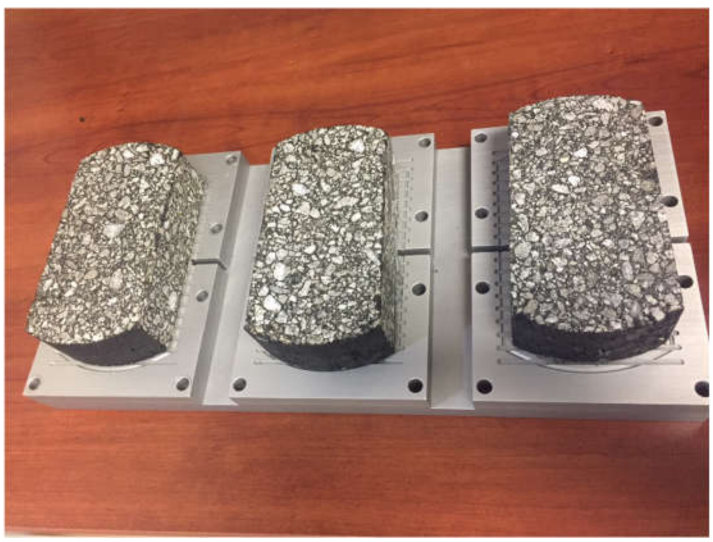

FIGURE 7.1

Test Specimens for Modified Overlay Test

7.2 Experimental Procedure

The specimen was placed into the AMPT after the glue was cured, and the target temperature of 25°C had been reached. The specimen was secured using a torque wrench by applying 1.7 Newton-meter (15 lb-in) to each bolt in a specific tightening pattern, as shown in Figure 7.2. The numbers indicate the order that the screws should the tightened. The test was started and ran until 93% reduction of the maximum load occurred or the test completed 1000 cycles.

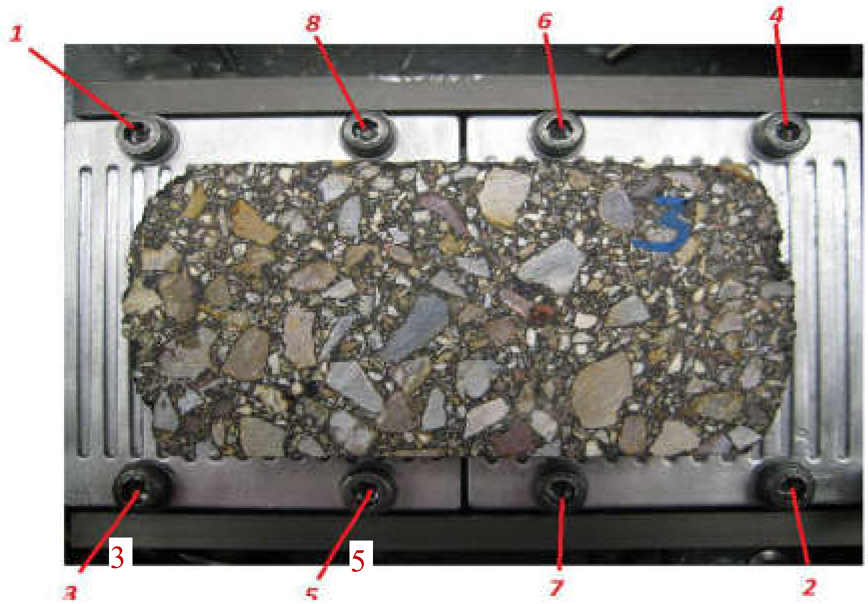

FIGURE 7.2

Tightening Pattern for Bolts Tex-248-F

7.3 Results and Analysis

The load reduction curves for each mixture were normalized by the maximum load of the first cycle shown in Figure 7.3. The power curve in Eq. (30) was fitted to the load reduction curves to obtain the value β. The value for β, or the crack progression rate, was calculated for each specimen that was tested and presented in Table 7.1, along with the cycles to failure. The crack progression rate is presented as an absolute value.

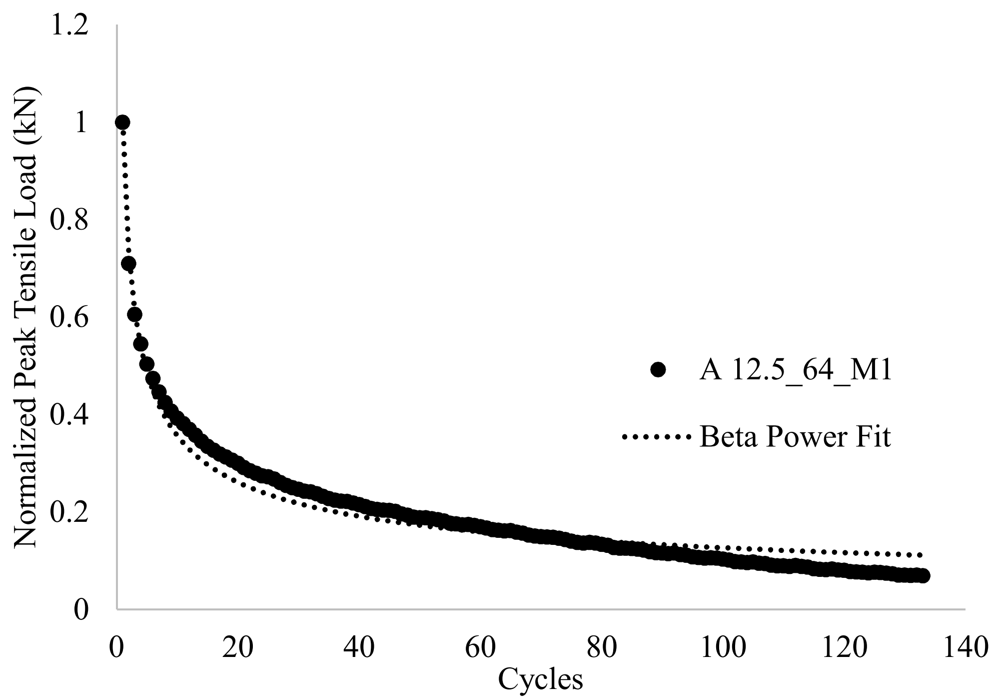

FIGURE 7.3

Normalized Load Reduction Curve with Fitted Power Curve

TABLE 7.1

Crack Progression Rate and Cycles to Failure for Various AC Mixtures

Mix ID	Crack Progression Rate			Cycles to Failure		
	Mean	SD	COV	Mean	SD	COV
B 9.5_64_M1	0.37	0.03	7%	226	10	4%
B 9.5_67_S	0.37	0.00	0%	172	12	7%
C 9.5_67_S	0.46	0.09	20%	213	29	13%
A 12.5_64_M	0.56	0.11	19%	110	23	21%
A 12.5_67_N	0.37	0.03	7%	1000	0	0%
B 12.5_67_M	0.74	0.30	41%	316	285	90%
C 12.5_67_M	0.39	0.03	8%	152	58	38%
C 12.5_76_M	0.34	0.03	7%	594	406	68%
D 12.5_76_S	0.71	0.24	34%	67	56	83%

As shown in Table 7.1, the coefficient of variation is as high as 41% for the crack progression rate and 90% for the cycles to failure. These high COVs suggest the test results are not reliable for its repeatability. Figure 7.4 and Figure 7.5 show factors influencing crack progression. There appears to be a clear trend for a lower NMAS having a lower β, which indicates better crack resistance. However, Figure 7.4 shows an opposite trend to what would be expected for different binder types. The PG 64-22 binder type performed better than the PG 67-22 and the polymer-modified PG 76-22. The large stand error bars suggest the repeatability is unreliable.

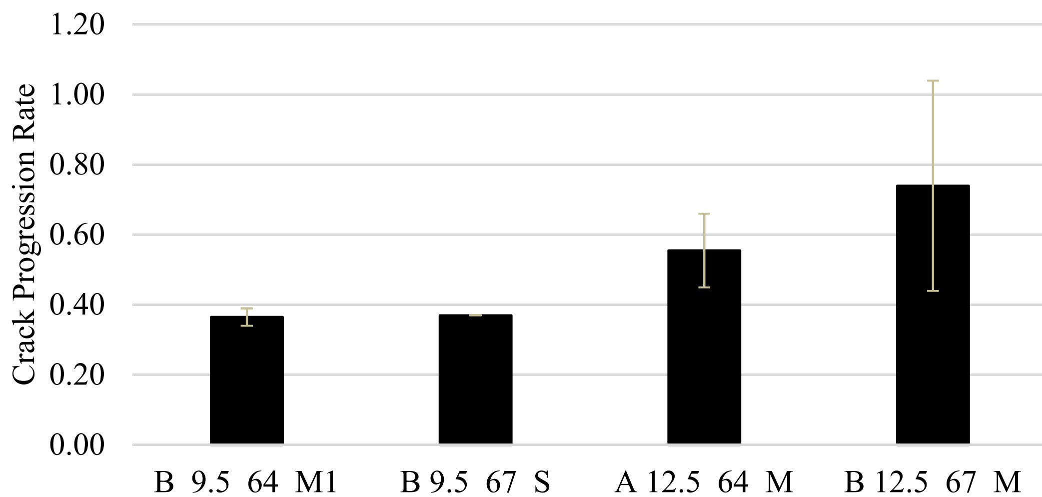

FIGURE 7.4

Crack Progression Rate Vs. NMAS

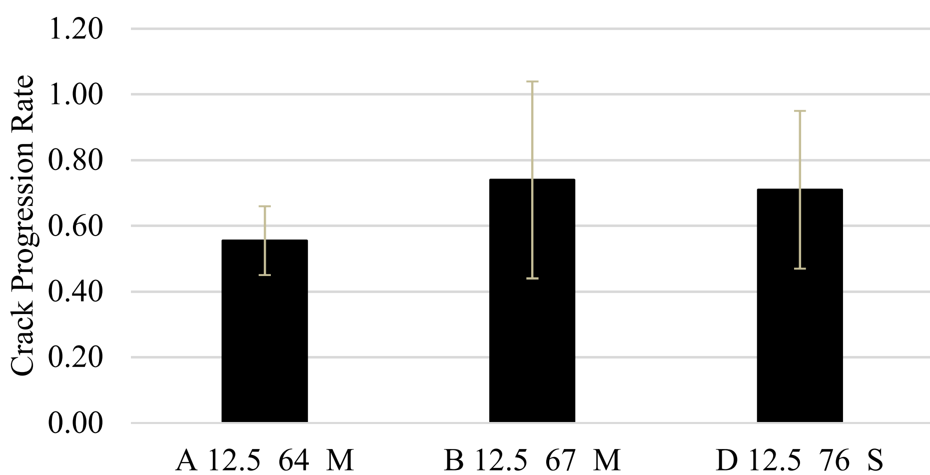

FIGURE 7.5

Crack Progression Rate Vs. Binder Type

The cycles to failure have a slight correlation to the crack progression rate, as shown in Figure 7.6. In general, as the cycles to failure increase, the crack progression rate decreases, which would be the expected trend. The crack progression rate does offer more insight to the OT, but the issues of reliability and repeatability damper the OT results from offering valuable data.

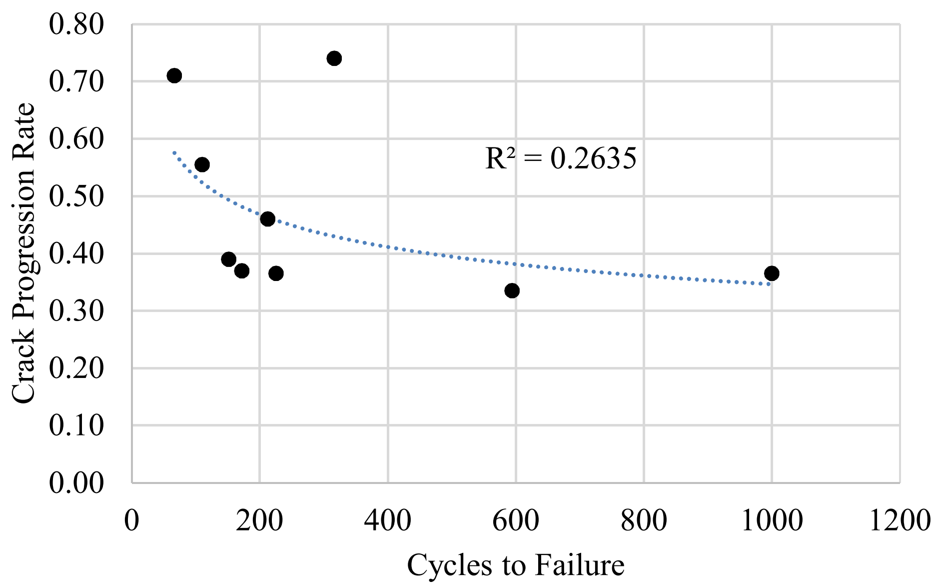

FIGURE 7.6

Cycles to Failure Vs. Crack Progression Rate

8. CONCLUSIONS

In this study, the effects of NMAS, RAP content, binder type, and binder content on mixture characteristics and fatigue cracking resistance performance were investigated. Categorical mixtures used in Georgia were fabricated and tested for dynamic modulus (|E*|) and fatigue cracking potential measurements using direct cyclic tension, semicircular bending, and modified overlay test methods. Based on laboratory tests and analyses, the following conclusions were made.

8.1 Dynamic Modulus

- Generally, Superpave mixtures with higher PG binder and increased RAP content (up to 30% RAP) result in a higher dynamic modulus master curve.
- Dynamic modulus values for NMAS between 25 mm and 19 mm were not significantly different. The same conclusion is made for 12.5 mm and 9.5 mm mixtures.
- Values for dynamic modulus were significantly different between 12.5 mm and 19 mm, as well as 12.5 mm and 25 mm, with P-values less than 0.05 for 70% of the master curves.
- Binder type influenced dynamic modulus values, with the stiffer PG 76-22 binder being significantly different with P-values less than 0.05 for 74% of the master curves from both PG 64-22 and PG 67-22. However, there was not a notable difference between PG 64-22 and PG 67-22.
- RAP content had a great effect on the dynamic modulus between 15% and 30% RAP contents with P-values less than 0.05 for 89% of the master curve.

8.2 Direct Tension Cyclic Fatigue Test Using S-VECD Model

- Controlled crosshead tension cyclic fatigue tests were performed to investigate the fatigue performance of mixtures with different mixture properties.
- Cracking parameter, S_{app}, was used to rank fatigue cracking performance of asphalt mixtures commonly used in Georgia and investigate correlations between mixture properties and fatigue cracking performances. S_{app} is a theoretically sound index parameter that can be used to predict and rank the fatigue cracking performance of asphalt mixtures. The results show that Sapp adequately reflects the effect of mixture properties on fatigue cracking performance.
- S_{app} is significantly influenced by NMAS and binder type. S_{app} values decreased with larger aggregate and increased for polymer-modified asphalt mixtures. Binder content also was shown to affect S_{app}, with a higher binder content leading to a higher S_{app} value.
- The D^R failure criterion also is influenced by NMAS and binder type. The mixtures with larger aggregate had lower D^R values, indicating that cracking resistance would be lower, too. The mixtures with modified binders showed the highest D^R values in this study.
- The trends of S_{app} as a function of binder type and NMAS are clearer than those of D^R. Therefore, S_{app} is recommended as the cracking index property.
- Both FlexPAVE™ and Pavement ME showed that the polymer-modified mixtures performed the best in terms of fatigue cracking resistance.
- Reasonable correlations were found between Pavement ME and FlexPAVE™ analyses for the top-down and bottom-up cracking predictions for a 10.2 cm (4-

inch) thick single-layer pavement, whereas the correlations were poor for a 15.2 cm (6-inch) two-layer pavement. The poor correlations for the two-layer pavement are attributable to the fact that the cracking prediction in Pavement ME depends solely on the modulus of the top layer, whereas FlexPAVE™ uses layer-specific modulus and fatigue properties throughout the asphalt layers to estimate fatigue cracking resistance.

8.3 Semicircle Bend Test

- Fracture energy alone is not enough to discriminate fatigue resisting mixture performance, while the newly developed FI is able to determine significant differences between mixture performances.
- Between two surface mixes (i.e., 9.5 mm and 12.5 mm NMAS mixtures), there was no significant difference in FI or fracture energy. AC surface mix from different locations in Georgia showed to have no significant difference between their fracture resistant properties.
- Notch width significantly affects FI. With an increased notch width from 1.5 mm to 3.5 mm, it was observed that FI was reduced up to 75%.
- The test results for mixtures with polymer-modified binder (i.e., PG 76-22) lowered FI, which was unexpected.

8.4 Modified Overlay Test

This study was conducted to determine if the OT could give reliable and repeatable results to rank AC mixtures for cracking resistance. The materials used were sourced from the state of Georgia and were composed of different mixture characteristics in order to determine if the OT accurately captures the effect on pavement performance. Based on laboratory tests and analyses, the following conclusion were made:

- The crack progression rate provided more useful information than the cycles to failure and gave a trend of a decreasing crack progression for smaller NMAS mixtures, indicating less cracking.
- With high variability of the OT results, it was challenging to identify the relationship between OT results and AC mixture properties, although the variability of the test results may be attributed to the gluing method during the test setup stage. This variability of the OT results could make this test method less favorable to predict fatigue cracking potential of AC mixtures.

8.5 Fatigue Test Method Comparisons

- For the fatigue tests, the SCB and cyclic direct tension tests with S-VECD model provide consistent test results that could be used in identifying AC cracking potential. The advantages of the SCB test over S-VECD are simple sample fabrication, ease of operation, and quick testing time. The cyclic direct tension test with S-VECD model provides more theoretically sound in-depth information to better understand AC mixture behavior. On the other hand, the cyclic direct tension test with S-VECD model requires intensive training to complete a successful test compared to the SCB test. This concern could be overcome through lab training and a workshop at the University of Georgia upon GDOT's request.

9. RECOMMENDATIONS AND FUTURE WORK

- Future study to predict AC fatigue cracking should focus on the investigation of cracking performance using field-cored specimens to compare against fatigue index rankings and pavement performance. For this task, a draft standard operating procedure (SOP) was developed to evaluate fatigue cracking resistance performance of asphalt mixture. The SOP is provided in Appendix C.
- With a larger database of dynamic modulus values created, the MEPDG can be implemented for design of flexible roadways. Its implementation would be most successful with training of staff and personnel about the inputs needed for the MEPDG. Having a firm background about these inputs and their significance will help GDOT use the MEPDG successfully in their design–build projects. For successful MEPDG implementation, Pavement ME needs accurately calibrated coefficients of AC mixtures.
- Future studies should focus on investigating cracking performance using field-cored specimens and comparing pavement condition surveys. Based on the field evaluations, index parameter criteria to select appropriate mixtures for field construction could be refined for design traffic.

10. REFERENCES

American Association of State Highway Transportation Officials (AASHTO) R83 (2018), "Preparation of Cylindrical Performance Test Specimens Using the Superpave Gyratory Compactor (SGC)." Washington, D.C.: AASHTO

AASHTO R84 (2017), "Practice For Developing Dynamic Modulus Master Curves For Asphalt Mixtures Using The Asphalt Mixture Performance Tester (AMPT)." Washington, D.C.: AASHTO.

AASHTO TP107 (2018), "Standard Method of Damage Characteristic Curve of Asphalt Concrete from Direct Tension Cyclic Fatigue Tests." Washington, D.C.: AASHTO.

AASHTO TP124 (2018). "Standard Method of Test for Determining the Fracture Potential of Asphalt Mixtures Using the Flexibility Index Test (FIT)." Washington, D.C.: AASHTO.

AASHTO T166 (2015). "Bulk Specific Gravity of Compacted Asphalt Mixtures using Saturated Surface-Dry Specimens." Washington, D.C.: AASHTO.

AASHTO T209 (2015). "Standard Method of Test for Theoretical Maximum Specific Gravity (Gmm) and Density of Hot Mix Asphalt (HMA)." Washington, D.C.:AASHTO

AASHTO, T342 (2015). "Standard Method of Test for Determining Dynamic Modulus of Hot Mix Asphalt (HMA)." Washington, D.C.: AASHTO.

Advanced Research Associates. (2004). *2002 Design Guide: Design of New and Rehabilitated Pavement Structures.* NCHRP 1-37A Project, National Cooperative Highway Research Program. National Research Council. Washington, D.C.

Bahia, H.U. (2001). *Characterization of Modified Asphalt Binders in Superpave Mix Design.* Washington, D.C.: National Academy Press.

Bari, J. (2005). *Development of a New Revised Version of the Witczak E* Predictive Models for Hot Mix Asphalt Mixtures.* Ph.D. Dissertation. Arizona State University.

Biligiri K.P., S.F. Said, H. Hakim. (2012). "Asphalt Mixtures Crack Propagation Assessment Using Semi-Circular Bending Test." *Int J Pavement Res Technol,* Vol. 5, No. 4, pp. 209−17.

Bowers, B.F., B.K. Diefenderfer, and S.D. Diefenderfer. (2015). "Evaluation of Dynamic Modulus in Asphalt Paving Mixtures Utilizing Small-Scale Specimen Geometries." *Electronic Journal of the Association of Asphalt Paving Technologists,* Vol. 84, pp. 497–526.

Cascione, A.A., R.C. Williams, and J. Yu. (2015). "Performance Testing of Asphalt Pavements with Recycled Asphalt Shingles from Multiple Field Trials." *Construction* *and Building Materials,* Vol. 101, pp. 628–642. doi:10.1016/j.conbuildmat.2015.09.027

Castorena, C., et al. (2017, September). *Development of Small Specimen Geometry for Asphalt Mixture Performance Testing*. National Cooperative Highway Research Program Innovations Deserving Exploratory Analysis Project 181. Transportation Research Board, National Research Council. Washington, D.C.

Chehab, G.R., Y.R. Kim, R.A. Schapery, M. Witczack, and R. Bonaquist. (2003). "Characterization of Asphalt Concrete in Uniaxial Tension Using a Viscoelastoplastic 23 Model." *Journal of the Association of Asphalt Paving Technology*, Vol. 72, pp. 315–355.

Christensen, Jr., D.W., T.K. Pellinen, and R.F. Bonaquist. (2003). "Hirsch Model for Estimating the Modulus of Asphalt Concrete." *Journal of the Association of Asphalt Paving Technologists* (AAPT), Vol. 72.

Chong, K.P., and Kuruppu, M.D. (1984). "New Specimen for Fracture Toughness Determination for Rock and Other Materials." *International Journal of Fracture, 26*(2). doi:10.1007/bf01157555

Clyne, T.R., X. Li, M.O. Marasteanu, and K. Engene. (2003). *Dynamic Modulus and Resilient Modulus of Mn/DOT Asphalt Mixtures.* Report: MN/RC–2003-09: Minnesota Department of Transportation, St. Paul.

Cross S.A., and Y. Jakatimath (2007). *Determination of Dynamic Modulus Master Curves for Oklahoma HMA Mixtures*. Final Report: Oklahoma Department of Transportation, Oklahoma, USA.

Daniel, J.S.. and Y.R. Kim. (2002). "Development of a Simplified Fatigue Test and Analysis Procedure Using a Viscoelastic Continuum Damage Model. *Journal of the Association of Asphalt Paving Technologists*, Vol. 71, pp. 619–650.

Epps, J.A. and C.L. Monismith. (1969). "Influences of Mixture Variables on the Flexural Fatigue Properties of Asphalt Concrete." *Proceedings* of the Association of Asphalt Paving Technologists, Vol. 38. pp. 423–464

Finn, F.N., K. Nair, and J. Hilliard. (1973, February). *Minimizing Premature Cracking of Asphalt Concrete Pavements*. National Cooperative Highway Research Program Project 9-4. Transportation Research Board, National Research Council. Washington, D.C.

Flintsch G.W., A. Loulizi, and B.K. Diefenderfer. (2007). *Asphalt Material Characterization in Support of Implementation of Mechanistic Empirical Pavement Design Guide*. Virginia Transportation Research Council: Final Report, Report No. VTRC 07-CR10

Garcia, V., et al. (2017). *Improved Overlay Tester for Fatigue Cracking Resistance of Asphalt Mixtures*. Texas Department of Transportation, Research Project 0-6815, Center for Transportation Infrastructure Systems, The University of Texas at El Paso, Tex.

Garcia, V., and A. Miramontes. (2015). "Understanding Sources of Variability of Overlay Test Procedure." *Transportation Research Record: Journal of the Transportation Research Board, No. 2507,* Transportation Research Board, Washington, D.C., pp. 1018. DOI: 10.3141/2507-02

Germann, F.P., and R.L. Lytton. (1979, March). *Methodology for Predicting the Reflection Cracking Life of Asphalt Concrete Overlays*. Research Report FHWA/TX-79/09+207-5, College Station, Texas.

Im, S., H. Ban, and Y.-R. Kim. (2014). "Mode-Dependent Fracture Behavior of Asphalt Mixtures with Semicircular Bend Test." *Transportation Research Record: Journal of the Transportation Research Board, No. 2447*, pp. 23–31.

Irwin, G.R. (1948). "Fracture Dynamics," *Trans. Am. Soc. Met*. Vol. 40A, pp. 147–166.

Kennedy, T.W., F.L. Roberts, and R.B. McGennis. (1984). "Effects of Compaction Temperature and Effort on the Engineering Properties of Asphalt Concrete Mixtures." *Placement and Compaction of Asphalt Mixtures*, F.T. Wagner, Ed. ASTM Special Technical Publication 829. American Society for Testing and Materials, Philadelphia, Penn. pp. 48–66.

Khalid, H.A., and O.K. Monney. (2009). "Moisture Damage Potential of Cold Asphalt," *International Journal of Pavement Engineering*, Vol. 10, No. 5, pp. 311–318. http://dx.doi.org/10.1080/10298430802169838

Kim, Y.R., and D.N. Little. "One-dimensional Constitutive Modeling of Asphalt Concrete." *ASCE Journal of Engineering Mechanics*, Vol. 116, No. 4, 1990, pp. 751–772.

Kim, M., L. Mohammad, and M. Elseifi. (2012). "Characterization of Fracture Properties of Asphalt Mixtures as Measured by Semicircular Bend Test and Indirect Tension Test." *Transportation Research Record: Journal of the Transportation Research Board, 2296*, pp. 115–124. doi:10.3141/2296-12

Kim, Y.R., Y. Seo, M. King, and M. Momen. (2004). "Dynamic Modulus Testing of Asphalt Concrete in Indirect Tension Mode." *Transportation Research Record: Journal of the Transportation Research Board, No. 1891*, pp. 163–173. http://dx.doi.org/10.3141/1891-19

Kutay, M.E., N. Gibson, J. Youtcheff, and R. Dongre. "Use of Small Samples to Predict Fatigue Lives of Field Cores: Newly Developed Formulation Based on Viscoelastic Continuum Damage Theory." *Transportation Research Record: Journal of the Transportation Research Board, No. 2127*, 2009, pp. 90–97. http://dx.doi.org/10.3141/2127-11

Lee, K., S. Pape, C. Castorena, and Y.-R. Kim. (2017). "Evaluation of Small Specimen Geometries for Asphalt Mixture Performance Testing and Pavement Performance Prediction." *Transportation Research Record: Journal of the Transportation Research Board, No. 2631*, pp. 74–82. http://dx.doi.org/10.3141/2631-09

Li, X.J., and M.O. Marasteanu (2009). "Using Semi Circular Bending Test to Evaluate Low Temperature Fracture Resistance for Asphalt Concrete." *Experimental Mechanics*, Vol. 50, No. 7, pp. 867–876.

Li, X., and N.H. Gibson. (2013). "Using Small Scale Specimens for AMPT Dynamic Modulus and Fatigue Tests." *Electronic Journal of the Association of Asphalt Paving Technologists*, Vol. 82, pp. 579–616.

Lim, I.L., I.W. Johnson, and S.K. Choi. (1993). "Stress Intensity Factors for Semi-circular Specimens Under Three-Point Bending." *Engineering Fracture Mechanics* Vol. 44, No. 3, pp. 363–382.

Linden, R.N., J.P. Mahoney, and N.C. Jackson. (1989). *The Effect of Compaction on Asphalt Concrete Performance*. 1989 Annual Meeting of the Transportation Research Board, Washington, D.C.

Ling, C., D. Swiertz, T. Mandal, P. Teymourpour, and H. Bahia. (2017). "Sensitivity of the Illinois Flexibility Index Test to Mixture Design Factors." *Transportation Research Record: Journal of the Transportation Research Board, 2631*, pp. 153–159. doi:10.3141/2631-17

Marasteanu, M.O., et al. (2004). "Low Temperature Cracking of Asphalt Concrete Pavement."

Norouzi, A., Y.-R. Kim, S. S. Kim, and J. Yang. (2017). "Effect of Reclaimed Asphalt Pavement Content and Binder Grade on Fatigue-Resisting Performance of Asphalt Mixtures in Georgia." *Journal of Materials in Civil Engineering,* Vol. 29, No. 9, pp. 04017115. doi:10.1061/(asce)mt.1943-5533.0001960

Nsengiyumva, G., T. You, and Y. Kim. (2016). "Experimental-Statistical Investigation of Testing Variables of a Semicircular Bending (SCB) Fracture Test Repeatability for Bituminous Mixtures." *Journal of Testing and Evaluation*, Vol. 45, No. 5, 20160103. doi:10.1520/jte20160103

Ozer, H., I.L. Al-Qadi, J. Lambros, A. El-Khatib, P. Singhvi, and B. Doll. (2016). "Development of the Fracture-based Flexibility Index for Asphalt Concrete Cracking Potential Using Modified Semi-circle Bending Test Parameters. *Construction and Building Materials,* Vol. 115, pp. 390–401. doi:10.1016/j.conbuildmat.2016.03.144

Ozer, H., I.L. Al-Qadi, P. Singhvi, T. Khan, J. Rivera-Perez, and A. El-Khatib. (2016). "Fracture Characterization of Asphalt Mixtures with High Recycled Content Using Illinois Semicircular Bending Test Method and Flexibility Index." *Transportation Research Record: Journal of the Transportation Research Board, No. 2575*, pp. 130–137. doi:10.3141/2575-14

Pell, P.S., and I.F. Taylor. (1969). "Asphalt Road Materials in Fatigue." *Proceedings* of the Association of Asphalt Paving Technologists, Vol. 38. pp. 371–464.

PI (Pavement Interactive). (2011). "Bulk Specific Gravity." http://www.pavementinteractive.org/article/bulk-specific-gravity/

PI (Pavement Interactive). (2011). "Theoretical Maximum Specific Gravity." http://www.pavementinteractive.org/theoretical-maximum-specific-gravity/

PI (Pavement Interactive). (2011). "Binder Content." http://www.pavementinteractive.org/binder-content/

Roberts, F.L., P.S. Kandhal, E.R. Brown, D.Y. Lee, and T.W. Kennedy. (1996). "Hot Mix Asphalt Materials, Mixture Design, and Construction." National Asphalt Paving Association Education Foundation. Lanham, MD.

Sabouri, M., T. Bennert, J.S. Daniel and Y.R. Kim (2015). "A Comprehensive Evaluation of the Fatigue Behaviour of Plant-produced RAP Mixtures." *Road Materials and Pavement Design*, Vol. 16, Sup. 2, pp. 29–54, DOI: 10.1080/14680629.2015.1076997

Sargand, S.M. and S.S. Kim. (2001). "Performance Evaluation of Polymer Modified and Unmodified Superpave Mixes. *Second International Symposium on Maintenance and Rehabilitation of Pavements and Technological Control*, Auburn, AL.

Schapery, R.A. (1984). "Correspondence Principles and a Generalized J-integral for Large Deformation and Fracture Analysis of Viscoelastic Media." *Int. J. Fract.,* Vol. 25, pp: 195–

Shu, X., and B. Huang. (2008). "Micromechanics-based Dynamic Modulus Prediction of Polymeric Asphalt Concrete Mixtures." *Composites B*,Vol. 39, No. 44. pp. 704–713.

Underwood, B.S. Y.R. Kim, and M.N. Guddati. (2010). "Improved Calculation Method of Damage Parameter in Viscoelastic Continuum Damage Model." *Inter. J. Pave. Eng.*, Vol.. 11, No. 6, pp. 459–476.

Wagoner, M.P., W.G. Buttlar, and G.H. Paulino. (2005). "Development of a Single-edge Notched Beam Test for Asphalt Concrete Mixtures." *Journal of Testing and Evaluation*, Vol. 33, No. 6, pp. 452–460.

Walubita, L.F., A.N.M. Faruk, G. Das, H.A. Tanvir, J. Zhang, and T. Scullion. (2012). *The Overlay Tester: A Sensitivity Study to Improve OT Repeatability and Minimize Variability in the OT Test Results.* Report FHWA/TX-12/0-6607-1. Texas A&M Transportation Institute, Texas A&M University System, College Station.

Walubita, L.F., A.N.M. Faruk, Y. Koohi, R. Luo, T. Scullion, and R.L. Lytton. (2013). *The Overlay Tester (OT): Comparison with Other Crack Test Methods and Recommendations for Surrogate Crack Test.* Report FHWA/ TX-13/0-6607-2. Texas A&M Transportation Institute, Texas A&M University System, College Station.

Wang, Y. and Y.R. Kim (2017). "Development of a Pseudo Strain Energy-based Fatigue Failure Criterion for Asphalt Mixtures." *International Journal of Pavement Engineering*, 2017, DOI: 10.1080/10298436.2017.1394100.

Wang, Y. and Y.R. Kim. (2018). "Development of a Simple Fatigue Index Parameter for Asphalt Concrete based on the Viscoelastic Continuum Damage Theory." *Journal of Association of Asphalt Paving Technologies*, accepted, 2018.

Wu, Z., et al. (2005). "Fracture Resistance Characterization of Superpave Mixtures Using the Semi-circular Bending Test." *Journal of ASTM International*, Vol. 2, No. 3, pp. 1–15.

Zeiada, W.A., K.E. Kaloush, B.S. Underwood, and M.S. Mamlouk. (2013). "Effect of Air Voids and Asphalt Content on Fatigue Damage Using the Viscoelastic Continuum Damage Analysis." *Airfield and Highway Pavement 2013*. doi:10.1061/9780784413005.094

Zhou, F., and T. Scullion. Overlay Tester: *A Rapid Performance Related Crack Resistance Test*. FHWA/TX-05/0-4467-2. Texas Transportation Institute, College Station, 2005.

Zhu, H., Sun, L., Yang, J., Z. Chen, and W. Gu. (2011). "Developing Master Curves and Predicting Dynamic Modulus of Polymer-modified Asphalt Mixtures. *J Mater Civ Eng*, Vol. 23 No. 2, pp. 131–137.

APPENDIX A

Catalog of MEPDG Design Inputs for Asphalt Mixtures

TABLE A.1

Mixture ID A_12.5_67_N

Mixture Type: A 12.5_67_N

Level 1

Asphalt Mix: Dynamic Modulus Table

Temperature (°F)	Mixture |E*|, psi					
	0.1 Hz	**0.5 Hz**	**1 Hz**	**5 Hz**	**10 Hz**	**25 Hz**
39.2	1196709	1468848	1600929	1911746	2046825	2218405
68	368348	546358	635750	895078	1022953	1200915
104	72843	120391	147741	254010	318939	426653

Asphalt Binder: Superpave Binder Test Data

Temperature (°F)	Angular Freq. = 10 rad/sec	
	G* (Pa)	Delta (degree)
See Appendix B		

Asphalt General: Volumetric Properties as Built

Effective Binder Content (%)	11.8
Air Voids (%)	6.3
Total Unit Weight (pcf)	145

Level 2

Asphalt Mix: Aggregate Gradation

Cumulative % Retained on 3/4 Inch Sieve	0
Cumulative % Retained on 3/8 Inch Sieve	13
Cumulative % Retained on #4 Sieve	25
% Passing #200 Sieve	6.3

Asphalt Binder: Superpave Binder Test Data

Temperature (°F)	Angular Freq. = 10 rad/sec	
	G* (Pa)	Delta (degree)
See Appendix B		

Asphalt General: Volumetric Properties as Built

Effective Binder Content (%)	11.8
Air Voids (%)	6.3
Total Unit Weight (pcf)	145

Level 3

Asphalt Mix: Aggregate Gradation

Cumulative % Retained on 3/4 Inch Sieve	0
Cumulative % Retained on 3/8 Inch Sieve	13
Cumulative % Retained on #4 Sieve	25
% Passing #200 Sieve	6.3
Asphalt Binder: Superpave Binder Grading:	PG 67-22

Asphalt General: Volumetric Properties as Built

Effective Binder Content (%)	11.8
Air Voids (%)	6.3
Total Unit Weight (pcf)	145

Note: The table summarizes the test data using extracted asphalt binder from asphalt plant mix.

TABLE A.2
Mixture ID A _12.5_76_N

Mixture Type: A 12.5_76_N

Level 1

Asphalt Mix: Dynamic Modulus Table

Temperature (°F)	Mixture |E*|, psi					
	0.1 Hz	**0.5 Hz**	**1 Hz**	**5 Hz**	**10 Hz**	**25 Hz**
39.2	1236304	1525751	1657929	1981267	2122679	2303977
68	356213	535287	624437	887874	1013864	1199077
104	68424	107193	129408	227033	288819	420707

Asphalt Binder: Superpave Binder Test Data

Temperature (°F)	Angular Freq. = 10 rad/sec	
	G* (Pa)	Delta (degree)
See Appendix B		

Asphalt General: Volumetric Properties as Built

Effective Binder Content (%)	12.6
Air Voids (%)	5.7
Total Unit Weight (pcf)	145

Level 2

Asphalt Mix: Aggregate Gradation

Cumulative % Retained on 3/4 Inch Sieve	0
Cumulative % Retained on 3/8 Inch Sieve	10
Cumulative % Retained on #4 Sieve	27
% Passing #200 Sieve	6.3

Asphalt Binder: Superpave Binder Test Data

Temperature (°F)	Angular Freq. = 10 rad/sec	
	G* (Pa)	Delta (degree)
See Appendix B		

Asphalt General: Volumetric Properties as Built

Effective Binder Content (%)	12.6
Air Voids (%)	5.7
Total Unit Weight (pcf)	145

Level 3

Asphalt Mix: Aggregate Gradation

Cumulative % Retained on 3/4 Inch Sieve	0
Cumulative % Retained on 3/8 Inch Sieve	10
Cumulative % Retained on #4 Sieve	27
% Passing #200 Sieve	6.3
Asphalt Binder: Superpave Binder Grading:	PG 76-22

Asphalt General: Volumetric Properties as Built

Effective Binder Content (%)	12.6
Air Voids (%)	5.7
Total Unit Weight (pcf)	145

Note: The table summarizes the test data using extracted asphalt binder from asphalt plant mix.

TABLE A.3
Mixture ID A 19_64_N1

Mixture Type: A 19_64_N1

Level 1

Asphalt Mix: Dynamic Modulus Table

Temperature (°F)	Mixture |E*|, psi					
	0.1 Hz	**0.5 Hz**	**1 Hz**	**5 Hz**	**10 Hz**	**25 Hz**
39.2	1470782	1766998	1902608	2232473	2373885	2555425
68	495643	703531	805154	1093393	1229197	1418133
104	97615	162491	198267	333056	410506	537414

Asphalt Binder: Superpave Binder Test Data

Temperature (°F)	Angular Freq. = 10 rad/sec	
	G* (Pa)	Delta (degree)
See Appendix B		

Asphalt General: Volumetric Properties as Built

Effective Binder Content (%)	11.6
Air Voids (%)	5.5
Total Unit Weight (pcf)	145

Level 2

Asphalt Mix: Aggregate Gradation

Cumulative % Retained on 3/4 Inch Sieve	5
Cumulative % Retained on 3/8 Inch Sieve	11
Cumulative % Retained on #4 Sieve	27
% Passing #200 Sieve	5.8

Asphalt Binder: Superpave Binder Test Data

Temperature (°F)	Angular Freq. = 10 rad/sec	
	G* (Pa)	Delta (degree)
See Appendix B		

Asphalt General: Volumetric Properties as Built

Effective Binder Content (%)	11.6
Air Voids (%)	5.5
Total Unit Weight (pcf)	145

Level 3

Asphalt Mix: Aggregate Gradation

Cumulative % Retained on 3/4 Inch Sieve	5
Cumulative % Retained on 3/8 Inch Sieve	11
Cumulative % Retained on #4 Sieve	27
% Passing #200 Sieve	5.8
Asphalt Binder: Superpave Binder Grading:	PG 64-22

Asphalt General: Volumetric Properties as Built

Effective Binder Content (%)	11.6
Air Voids (%)	5.5
Total Unit Weight (pcf)	145

Note: The table summarizes the test data using extracted asphalt binder from asphalt plant mix.

TABLE A.4
Mixture ID A 25_64_N1

Mixture Type: A 25 64 N1

Level 1

Asphalt Mix: Dynamic Modulus Table

Temperature (°F)	Mixture |E*|, psi					
	0.1 Hz	**0.5 Hz**	**1 Hz**	**5 Hz**	**10 Hz**	**25 Hz**
39.2	1491958	1756555	1875438	2161550	2283430	2438814
68	518414	718035	814243	1085754	1212228	1390576
104	112825	181733	218814	359743	438885	573577

Asphalt Binder: Superpave Binder Test Data

Temperature (°F)	Angular Freq. = 10 rad/sec	
	G* (Pa)	Delta (degree)
See Appendix B		

Asphalt General: Volumetric Properties as Built

Effective Binder Content (%)	11.2
Air Voids (%)	5.5
Total Unit Weight (pcf)	145

Level 2

Asphalt Mix: Aggregate Gradation

Cumulative % Retained on 3/4 Inch Sieve	12
Cumulative % Retained on 3/8 Inch Sieve	9
Cumulative % Retained on #4 Sieve	20
% Passing #200 Sieve	5.7

Asphalt Binder: Superpave Binder Test Data

Temperature (°F)	Angular Freq. = 10 rad/sec	
	G* (Pa)	Delta (degree)
See Appendix B		

Asphalt General: Volumetric Properties as Built

Effective Binder Content (%)	11.2
Air Voids (%)	5.5
Total Unit Weight (pcf)	145

Level 3

Asphalt Mix: Aggregate Gradation

Cumulative % Retained on 3/4 Inch Sieve	12
Cumulative % Retained on 3/8 Inch Sieve	9
Cumulative % Retained on #4 Sieve	20
% Passing #200 Sieve	5.7
Asphalt Binder: Superpave Binder Grading:	PG 64-22

Asphalt General: Volumetric Properties as Built

Effective Binder Content (%)	11.2
Air Voids (%)	5.5
Total Unit Weight (pcf)	145

Notes: The table summarizes the test data using extracted asphalt binder from asphalt plant mix.

TABLE A.5
Mixture ID B 9.5_64_M1

Mixture Type: B 9.5_64_M1

Level 1

Asphalt Mix: Dynamic Modulus Table

Temperature (°F)	Mixture |E*|, psi					
	0.1 Hz	**0.5 Hz**	**1 Hz**	**5 Hz**	**10 Hz**	**25 Hz**
39.2	1112490	1419100	1557998	1895453	2039379	2221354
68	294717	466152	555012	829472	963391	1161368
104	51861	87236	109857	205132	267015	376422

Asphalt Binder: Superpave Binder Test Data

Temperature (°F)	Angular Freq. = 10 rad/sec	
	G* (Pa)	Delta (degree)
See Appendix B		

Asphalt General: Volumetric Properties as Built

Effective Binder Content (%)	12.6
Air Voids (%)	6.5
Total Unit Weight (pcf)	145

Level 2

Asphalt Mix: Aggregate Gradation

Cumulative % Retained on 3/4 Inch Sieve	0
Cumulative % Retained on 3/8 Inch Sieve	1
Cumulative % Retained on #4 Sieve	28
% Passing #200 Sieve	6

Asphalt Binder: Superpave Binder Test Data

Temperature (°F)	Angular Freq. = 10 rad/sec	
	G* (Pa)	Delta (degree)
See Appendix B		

Asphalt General: Volumetric Properties as Built

Effective Binder Content (%)	12.6
Air Voids (%)	6.5
Total Unit Weight (pcf)	145

Level 3

Asphalt Mix: Aggregate Gradation

Cumulative % Retained on 3/4 Inch Sieve	0
Cumulative % Retained on 3/8 Inch Sieve	1
Cumulative % Retained on #4 Sieve	28
% Passing #200 Sieve	6
Asphalt Binder: Superpave Binder Grading:	PG 64-22

Asphalt General: Volumetric Properties as Built

Effective Binder Content (%)	12.6
Air Voids (%)	6.5
Total Unit Weight (pcf)	145

Notes: The table summarizes the test data using extracted asphalt binder from asphalt plant mix.

TABLE A.6
Mixture ID B 9.5_64_M2

Mixture Type: B 9.5_64_M2

Level 1

Asphalt Mix: Dynamic Modulus Table

Temperature (°F)	Mixture |E*|, psi					
	0.1 Hz	**0.5 Hz**	**1 Hz**	**5 Hz**	**10 Hz**	**25 Hz**
39.2	1144592	1448011	1586619	1929102	2077428	2269265
68	320631	484185	569129	840592	972480	1161706
104	55898	95773	121218	221715	286305	401223

Asphalt Binder: Superpave Binder Test Data

Temperature (°F)	Angular Freq. = 10 rad/sec	
	G* (Pa)	Delta (degree)
See Appendix B		

Asphalt General: Volumetric Properties as Built

Effective Binder Content (%)	11.6
Air Voids (%)	6.5
Total Unit Weight (pcf)	145

Level 2

Asphalt Mix: Aggregate Gradation

Cumulative % Retained on 3/4 Inch Sieve	0
Cumulative % Retained on 3/8 Inch Sieve	6
Cumulative % Retained on #4 Sieve	27
% Passing #200 Sieve	6.5

Asphalt Binder: Superpave Binder Test Data

Temperature (°F)	Angular Freq. = 10 rad/sec	
	G* (Pa)	Delta (degree)
See Appendix B		

Asphalt General: Volumetric Properties as Built

Effective Binder Content (%)	11.6
Air Voids (%)	6.5
Total Unit Weight (pcf)	145

Level 3

Asphalt Mix: Aggregate Gradation

Cumulative % Retained on 3/4 Inch Sieve	0
Cumulative % Retained on 3/8 Inch Sieve	6
Cumulative % Retained on #4 Sieve	27
% Passing #200 Sieve	6.5
Asphalt Binder: Superpave Binder Grading:	PG 64-22

Asphalt General: Volumetric Properties as Built

Effective Binder Content (%)	11.6
Air Voids (%)	6.5
Total Unit Weight (pcf)	145

Notes: The table summarizes the test data using extracted asphalt binder from asphalt plant mix.

TABLE A.7
Mixture ID C 9.5_67_M

Mixture Type: C 9.5_67_M

Level 1

Asphalt Mix: Dynamic Modulus Table

Temperature (°F)	Mixture |E*|, psi					
	0.1 Hz	**0.5 Hz**	**1 Hz**	**5 Hz**	**10 Hz**	**25 Hz**
39.2	1463361	1726339	1852135	2156522	2288071	2452061
68	476933	676989	773053	1053556	1184912	1368772
104	93071	138676	172015	292107	362692	482300

Asphalt Binder: Superpave Binder Test Data

Temperature (°F)	Angular Freq. = 10 rad/sec	
	G* (Pa)	Delta (degree)
See Appendix B		

Asphalt General: Volumetric Properties as Built

Effective Binder Content (%)	12.9
Air Voids (%)	5
Total Unit Weight (pcf)	145

Level 2

Asphalt Mix: Aggregate Gradation

Cumulative % Retained on 3/4 Inch Sieve	0
Cumulative % Retained on 3/8 Inch Sieve	5
Cumulative % Retained on #4 Sieve	32
% Passing #200 Sieve	5.5

Asphalt Binder: Superpave Binder Test Data

Temperature (°F)	Angular Freq. = 10 rad/sec	
	G* (Pa)	Delta (degree)
See Appendix B		

Asphalt General: Volumetric Properties as Built

Effective Binder Content (%)	12.9
Air Voids (%)	5
Total Unit Weight (pcf)	145

Level 3

Asphalt Mix: Aggregate Gradation

Cumulative % Retained on 3/4 Inch Sieve	0
Cumulative % Retained on 3/8 Inch Sieve	5
Cumulative % Retained on #4 Sieve	32
% Passing #200 Sieve	5.5
Asphalt Binder: Superpave Binder Grading:	PG 67-22

Asphalt General: Volumetric Properties as Built

Effective Binder Content (%)	12.9
Air Voids (%)	5
Total Unit Weight (pcf)	145

Notes: The table summarizes the test data using extracted asphalt binder from asphalt plant mix.

TABLE A.8

Mixture ID A 12_64_M2

Mixture Type: A 12.5_64_M2

Level 1

Asphalt Mix: Dynamic Modulus Table

Temperature (°F)	Mixture |E*|, psi					
	0.1 Hz	**0.5 Hz**	**1 Hz**	**5 Hz**	**10 Hz**	**25 Hz**
39.2	1323423	1568103	1683069	1996206	2129448	2302478
68	406687	590256	681679	962279	1097889	1284602
104	73500	139754	178784	316715	396631	528228

Asphalt Binder: Superpave Binder Test Data

Temperature (°F)	Angular Freq. = 10 rad/sec	
	G* (Pa)	Delta (degree)
See Appendix B		

Asphalt General: Volumetric Properties as Built

Effective Binder Content (%)	12.2
Air Voids (%)	5.5
Total Unit Weight (pcf)	145

Level 2

Asphalt Mix: Aggregate Gradation

Cumulative % Retained on 3/4 Inch Sieve	0
Cumulative % Retained on 3/8 Inch Sieve	12
Cumulative % Retained on #4 Sieve	27
% Passing #200 Sieve	5.9

Asphalt Binder: Superpave Binder Test Data

Temperature (°F)	Angular Freq. = 10 rad/sec	
	G* (Pa)	Delta (degree)
See Appendix B		

Asphalt General: Volumetric Properties as Built

Effective Binder Content (%)	12.2
Air Voids (%)	5.5
Total Unit Weight (pcf)	145

Level 3

Asphalt Mix: Aggregate Gradation

Cumulative % Retained on 3/4 Inch Sieve	0
Cumulative % Retained on 3/8 Inch Sieve	12
Cumulative % Retained on #4 Sieve	27
% Passing #200 Sieve	5.9
Asphalt Binder: Superpave Binder Grading:	PG 64-22

Asphalt General: Volumetric Properties as Built

Effective Binder Content (%)	12.2
Air Voids (%)	5.5
Total Unit Weight (pcf)	145

Notes: The table summarizes the test data using extracted asphalt binder from asphalt plant mix.

TABLE A.9
Mixture ID A 12.5_64_M1

Mixture Type: A 12.5_64_M1

Level 1

Asphalt Mix: Dynamic Modulus Table

Temperature (°F)	Mixture |E*|, psi					
	0.1 Hz	**0.5 Hz**	**1 Hz**	**5 Hz**	**10 Hz**	**25 Hz**
39.2	1179401	1480935	1618672	1977206	2130270	2327183
68	346061	545004	644597	941345	1085126	1296881
104	47684	84325	114638	225679	299020	452422

Asphalt Binder: Superpave Binder Test Data

Temperature (°F)	Angular Freq. = 10 rad/sec	
	G* (Pa)	Delta (degree)
See Appendix B		

Asphalt General: Volumetric Properties as Built

Effective Binder Content (%)	12.5
Air Voids (%)	5.5
Total Unit Weight (pcf)	145

Level 2

Asphalt Mix: Aggregate Gradation

Cumulative % Retained on 3/4 Inch Sieve	0
Cumulative % Retained on 3/8 Inch Sieve	14
Cumulative % Retained on #4 Sieve	26
% Passing #200 Sieve	5.8

Asphalt Binder: Superpave Binder Test Data

Temperature (°F)	Angular Freq. = 10 rad/sec	
	G* (Pa)	Delta (degree)
See Appendix B		

Asphalt General: Volumetric Properties as Built

Effective Binder Content (%)	12.5
Air Voids (%)	5.5
Total Unit Weight (pcf)	145

Level 3

Asphalt Mix: Aggregate Gradation

Cumulative % Retained on 3/4 Inch Sieve	0
Cumulative % Retained on 3/8 Inch Sieve	14
Cumulative % Retained on #4 Sieve	26
% Passing #200 Sieve	5.8
Asphalt Binder: Superpave Binder Grading:	PG 64-22

Asphalt General: Volumetric Properties as Built

Effective Binder Content (%)	12.5
Air Voids (%)	5.5
Total Unit Weight (pcf)	145

Notes: The table summarizes the test data using extracted asphalt binder from asphalt plant mix.

TABLE A.10
Mixture ID B 12.5_64_M

Mixture Type: B 12.5_64_M

Level 1

Asphalt Mix: Dynamic Modulus Table

Temperature (°F)	Mixture |E*|, psi					
	0.1 Hz	**0.5 Hz**	**1 Hz**	**5 Hz**	**10 Hz**	**25 Hz**
39.2	1210826	1490991	1616013	1923010	2057219	2298901
68	357905	536254	625984	890388	1017006	1194050
104	82169	139865	172499	295732	368928	485152

Asphalt Binder: Superpave Binder Test Data

Temperature (°F)	Angular Freq. = 10 rad/sec	
	G* (Pa)	Delta (degree)
See Appendix B		

Asphalt General: Volumetric Properties as Built

Effective Binder Content (%)	12.5
Air Voids (%)	5.6
Total Unit Weight (pcf)	145

Level 2

Asphalt Mix: Aggregate Gradation

Cumulative % Retained on 3/4 Inch Sieve	0
Cumulative % Retained on 3/8 Inch Sieve	13
Cumulative % Retained on #4 Sieve	25
% Passing #200 Sieve	6

Asphalt Binder: Superpave Binder Test Data

Temperature (°F)	Angular Freq. = 10 rad/sec	
	G* (Pa)	Delta (degree)
See Appendix B		

Asphalt General: Volumetric Properties as Built

Effective Binder Content (%)	12.5
Air Voids (%)	5.6
Total Unit Weight (pcf)	145

Level 3

Asphalt Mix: Aggregate Gradation

Cumulative % Retained on 3/4 Inch Sieve	0
Cumulative % Retained on 3/8 Inch Sieve	13
Cumulative % Retained on #4 Sieve	25
% Passing #200 Sieve	6
Asphalt Binder: Superpave Binder Grading:	PG 64-22

Asphalt General: Volumetric Properties as Built

Effective Binder Content (%)	12.5
Air Voids (%)	5.6
Total Unit Weight (pcf)	145

Notes: The table summarizes the test data using extracted asphalt binder from asphalt plant mix.

TABLE A.11
Mixture ID B 25_64_M

Mixture Type: B 25_64_M

Level 1

Asphalt Mix: Dynamic Modulus Table

Temperature (°F)	Mixture |E*|, psi					
	0.1 Hz	**0.5 Hz**	**1 Hz**	**5 Hz**	**10 Hz**	**25 Hz**
39.2	1633901	1958448	2101746	2442295	2582160	2761910
68	603116	861767	982874	1334978	1492103	1710868
104	133923	224422	274267	466104	571788	736406

Asphalt Binder: Superpave Binder Test Data

Temperature (°F)	Angular Freq. = 10 rad/sec	
	G* (Pa)	Delta (degree)
See Appendix B		

Asphalt General: Volumetric Properties as Built

Effective Binder Content (%)	9.4
Air Voids (%)	5.9
Total Unit Weight (pcf)	145

Level 2

Asphalt Mix: Aggregate Gradation

Cumulative % Retained on 3/4 Inch Sieve	10
Cumulative % Retained on 3/8 Inch Sieve	8
Cumulative % Retained on #4 Sieve	17
% Passing #200 Sieve	5

Asphalt Binder: Superpave Binder Test Data

Temperature (°F)	Angular Freq. = 10 rad/sec	
	G* (Pa)	Delta (degree)
See Appendix B		

Asphalt General: Volumetric Properties as Built

Effective Binder Content (%)	9.4
Air Voids (%)	5.9
Total Unit Weight (pcf)	145

Level 3

Asphalt Mix: Aggregate Gradation

Cumulative % Retained on 3/4 Inch Sieve	10
Cumulative % Retained on 3/8 Inch Sieve	8
Cumulative % Retained on #4 Sieve	17
% Passing #200 Sieve	5
Asphalt Binder: Superpave Binder Grading:	PG 64-22

Asphalt General: Volumetric Properties as Built

Effective Binder Content (%)	9.4
Air Voids (%)	5.9
Total Unit Weight (pcf)	145

Notes: The table summarizes the test data using extracted asphalt binder from asphalt plant mix.

TABLE A.12
Mixture ID B 9.5_67_S

Mixture Type: B 9.5_67_S

Level 1

Asphalt Mix: Dynamic Modulus Table

Temperature (°F)	Mixture |E*|, psi					
	0.1 Hz	**0.5 Hz**	**1 Hz**	**5 Hz**	**10 Hz**	**25 Hz**
39.2	1168813	1443853	1568731	1874955	2005150	2167254
68	321549	489407	574060	834984	959330	1146235
104	56396	96736	121416	227903	290221	383335

Asphalt Binder: Superpave Binder Test Data

Temperature (°F)	Angular Freq. = 10 rad/sec	
	G* (Pa)	Delta (degree)
See Appendix B		

Asphalt General: Volumetric Properties as Built

Effective Binder Content (%)	12.8
Air Voids (%)	5.5
Total Unit Weight (pcf)	145

Level 2

Asphalt Mix: Aggregate Gradation

Cumulative % Retained on 3/4 Inch Sieve	0
Cumulative % Retained on 3/8 Inch Sieve	3
Cumulative % Retained on #4 Sieve	28
% Passing #200 Sieve	5.3

Asphalt Binder: Superpave Binder Test Data

Temperature (°F)	Angular Freq. = 10 rad/sec	
	G* (Pa)	Delta (degree)
See Appendix B		

Asphalt General: Volumetric Properties as Built

Effective Binder Content (%)	12.8
Air Voids (%)	5.5
Total Unit Weight (pcf)	145

Level 3

Asphalt Mix: Aggregate Gradation

Cumulative % Retained on 3/4 Inch Sieve	0
Cumulative % Retained on 3/8 Inch Sieve	3
Cumulative % Retained on #4 Sieve	28
% Passing #200 Sieve	5.3
Asphalt Binder: Superpave Binder Grading:	PG 67-22

Asphalt General: Volumetric Properties as Built

Effective Binder Content (%)	12.8
Air Voids (%)	5.5
Total Unit Weight (pcf)	145

Notes: The table summarizes the test data using extracted asphalt binder from asphalt plant mix.

TABLE A.13
Mixture ID B 12.5_67_S

Mixture Type: B 12.5_67_S

Level 1

Asphalt Mix: Dynamic Modulus Table

Temperature (°F)	Mixture |E*|, psi					
	0.1 Hz	**0.5 Hz**	**1 Hz**	**5 Hz**	**10 Hz**	**25 Hz**
39.2	1210826	1490991	1616013	1923010	2057219	2298901
68	357905	536254	625984	890388	1017006	1194050
104	82169	139865	172499	295732	368928	485152

Asphalt Binder: Superpave Binder Test Data

Temperature (°F)	Angular Freq. = 10 rad/sec	
	G* (Pa)	Delta (degree)
See Appendix B		

Asphalt General: Volumetric Properties as Built

Effective Binder Content (%)	12.1
Air Voids (%)	6
Total Unit Weight (pcf)	145

Level 2

Asphalt Mix: Aggregate Gradation

Cumulative % Retained on 3/4 Inch Sieve	0
Cumulative % Retained on 3/8 Inch Sieve	14
Cumulative % Retained on #4 Sieve	25
% Passing #200 Sieve	5

Asphalt Binder: Superpave Binder Test Data

Temperature (°F)	Angular Freq. = 10 rad/sec	
	G* (Pa)	Delta (degree)
See Appendix B		

Asphalt General: Volumetric Properties as Built

Effective Binder Content (%)	12.1
Air Voids (%)	6
Total Unit Weight (pcf)	145

Level 3

Asphalt Mix: Aggregate Gradation

Cumulative % Retained on 3/4 Inch Sieve	0
Cumulative % Retained on 3/8 Inch Sieve	14
Cumulative % Retained on #4 Sieve	25
% Passing #200 Sieve	5
Asphalt Binder: Superpave Binder Grading:	PG 67-22

Asphalt General: Volumetric Properties as Built

Effective Binder Content (%)	12.1
Air Voids (%)	6
Total Unit Weight (pcf)	145

Notes: The table summarizes the test data using extracted asphalt binder from asphalt plant mix.

TABLE A.14

Mixture ID D 12.5_76_S

Mixture Type: D 12.5_76_S

Level 1

Asphalt Mix: Dynamic Modulus Table

Temperature (°F)	Mixture |E*|, psi					
	0.1 Hz	**0.5 Hz**	**1 Hz**	**5 Hz**	**10 Hz**	**25 Hz**
39.2	1389174	1643619	1759069	2039331	2166433	2309682
68	519574	721854	811778	1080291	1209569	1381294
104	105805	173756	210257	343160	417564	537994

Asphalt Binder: Superpave Binder Test Data

Temperature (°F)	Angular Freq. = 10 rad/sec	
	G* (Pa)	Delta (degree)
See Appendix B		

Asphalt General: Volumetric Properties as Built

Effective Binder Content (%)	11.9
Air Voids (%)	5.5
Total Unit Weight (pcf)	145

Level 2

Asphalt Mix: Aggregate Gradation

Cumulative % Retained on 3/4 Inch Sieve	0
Cumulative % Retained on 3/8 Inch Sieve	12
Cumulative % Retained on #4 Sieve	28
% Passing #200 Sieve	4.9

Asphalt Binder: Superpave Binder Test Data

Temperature (°F)	Angular Freq. = 10 rad/sec	
	G* (Pa)	Delta (degree)
See Appendix B		

Asphalt General: Volumetric Properties as Built

Effective Binder Content (%)	11.9
Air Voids (%)	5.5
Total Unit Weight (pcf)	145

Level 3

Asphalt Mix: Aggregate Gradation

Cumulative % Retained on 3/4 Inch Sieve	0
Cumulative % Retained on 3/8 Inch Sieve	12
Cumulative % Retained on #4 Sieve	28
% Passing #200 Sieve	4.9

Asphalt Binder: Superpave Binder Grading: PG 76-22

Asphalt General: Volumetric Properties as Built

Effective Binder Content (%)	11.9
Air Voids (%)	5.5
Total Unit Weight (pcf)	145

Notes: The table summarizes the test data using extracted asphalt binder from asphalt plant mix.

TABLE A.15
Mixture ID A_19_64_N2

Mixture Type: A 19_64_N2

Level 1

Asphalt Mix: Dynamic Modulus Table

Temperature (°F)	Mixture |E*|, psi					
	0.1 Hz	**0.5 Hz**	**1 Hz**	**5 Hz**	**10 Hz**	**25 Hz**
39.2	1930214	2251667	2390420	2712936	2844002	3043236
68	755068	1051187	1146139	1477986	1610840	1825110
104	168897	280358	343208	597073	702661	882556

Asphalt Binder: Superpave Binder Test Data

Temperature (°F)	Angular Freq. = 10 rad/sec	
	G* (Pa)	Delta (degree)
		See Appendix B

Asphalt General: Volumetric Properties as Built

Effective Binder Content (%)	10.1
Air Voids (%)	5
Total Unit Weight (pcf)	145

Level 2

Asphalt Mix: Aggregate Gradation

Cumulative % Retained on 3/4 Inch Sieve	1
Cumulative % Retained on 3/8 Inch Sieve	9
Cumulative % Retained on #4 Sieve	19
% Passing #200 Sieve	5.3

Asphalt Binder: Superpave Binder Test Data

Temperature (°F)	Angular Freq. = 10 rad/sec	
	G* (Pa)	Delta (degree)
		See Appendix B

Asphalt General: Volumetric Properties as Built

Effective Binder Content (%)	10.1
Air Voids (%)	5
Total Unit Weight (pcf)	145

Level 3

Asphalt Mix: Aggregate Gradation

Cumulative % Retained on 3/4 Inch Sieve	1
Cumulative % Retained on 3/8 Inch Sieve	9
Cumulative % Retained on #4 Sieve	19
% Passing #200 Sieve	5.3
Asphalt Binder: Superpave Binder Grading:	PG 64-22

Asphalt General: Volumetric Properties as Built

Effective Binder Content (%)	10.1
Air Voids (%)	5
Total Unit Weight (pcf)	145

TABLE A.16
Mixture ID A_25_64_N2

Mixture Type: A 25_64_N2

Level 1

Asphalt Mix: Dynamic Modulus Table

Temperature (°F)	Mixture |E*|, psi					
	0.1 Hz	**0.5 Hz**	**1 Hz**	**5 Hz**	**10 Hz**	**25 Hz**
39.2	1956490	2270932	2411402	2723306	2852245	3012222
68	727075	1000134	1128444	1479194	1631436	1842418
104	139570	208758	265661	451310	557671	718615

Asphalt Binder: Superpave Binder Test Data

Temperature (°F)	Angular Freq. = 10 rad/sec	
	G* (Pa)	Delta (degree)
		See Appendix B

Asphalt General: Volumetric Properties as Built

Effective Binder Content (%)	9.8
Air Voids (%)	5.2
Total Unit Weight (pcf)	145

Level 2

Asphalt Mix: Aggregate Gradation

Cumulative % Retained on 3/4 Inch Sieve	9
Cumulative % Retained on 3/8 Inch Sieve	7
Cumulative % Retained on #4 Sieve	15
% Passing #200 Sieve	5.5

Asphalt Binder: Superpave Binder Test Data

Temperature (°F)	Angular Freq. = 10 rad/sec	
	G* (Pa)	Delta (degree)
		See Appendix B

Asphalt General: Volumetric Properties as Built

Effective Binder Content (%)	9.8
Air Voids (%)	5.2
Total Unit Weight (pcf)	145

Level 3

Asphalt Mix: Aggregate Gradation

Cumulative % Retained on 3/4 Inch Sieve	9
Cumulative % Retained on 3/8 Inch Sieve	7
Cumulative % Retained on #4 Sieve	15
% Passing #200 Sieve	5.5
Asphalt Binder: Superpave Binder Grading:	PG 64-22

Asphalt General: Volumetric Properties as Built

Effective Binder Content (%)	9.8
Air Voids (%)	5.2
Total Unit Weight (pcf)	145

TABLE A.17
Mixture ID C_12.5_67_M

Mixture Type: C 12.5 67 M

Level 1

Asphalt Mix: Dynamic Modulus Table

Temperature (°F)	Mixture |E*|, psi					
	0.1 Hz	**0.5 Hz**	**1 Hz**	**5 Hz**	**10 Hz**	**25 Hz**
39.2	1279574	1578594	1720199	2067855	2214972	2402313
68	384399	572417	664709	940910	1071976	1265166
104	68453	116446	147049	265903	339389	451552

Asphalt Binder: Superpave Binder Test Data

Temperature (°F)	Angular Freq. = 10 rad/sec	
	G* (Pa)	Delta (degree)
		See Appendix B

Asphalt General: Volumetric Properties as Built

Effective Binder Content (%)	11.5
Air Voids (%)	5.8
Total Unit Weight (pcf)	145

Level 2

Asphalt Mix: Aggregate Gradation

Cumulative % Retained on 3/4 Inch Sieve	0
Cumulative % Retained on 3/8 Inch Sieve	12
Cumulative % Retained on #4 Sieve	27
% Passing #200 Sieve	6.1

Asphalt Binder: Superpave Binder Test Data

Temperature (°F)	Angular Freq. = 10 rad/sec	
	G* (Pa)	Delta (degree)
		See Appendix B

Asphalt General: Volumetric Properties as Built

Effective Binder Content (%)	11.5
Air Voids (%)	5.8
Total Unit Weight (pcf)	145

Level 3

Asphalt Mix: Aggregate Gradation

Cumulative % Retained on 3/4 Inch Sieve	0
Cumulative % Retained on 3/8 Inch Sieve	12
Cumulative % Retained on #4 Sieve	27
% Passing #200 Sieve	6.1
Asphalt Binder: Superpave Binder Grading:	PG 67-22

Asphalt General: Volumetric Properties as Built

Effective Binder Content (%)	11.5
Air Voids (%)	5.8
Total Unit Weight (pcf)	145

TABLE A.18
Mixture ID C_12.5_76_M

Mixture Type: C 12.5_76_M

Level 1

Asphalt Mix: Dynamic Modulus Table

Temperature (°F)	Mixture |E*|, psi					
	0.1 Hz	**0.5 Hz**	**1 Hz**	**5 Hz**	**10 Hz**	**25 Hz**
39.2	958049	1208384	1337299	1634965	1766756	1937031
68	273203	424236	502073	743997	859882	1030978
104	55376	87076	107410	193819	250529	351234

Asphalt Binder: Superpave Binder Test Data

Temperature (°F)	Angular Freq. = 10 rad/sec	
	G* (Pa)	Delta (degree)
		See Appendix B

Asphalt General: Volumetric Properties as Built

Effective Binder Content (%)	11.5
Air Voids (%)	5.8
Total Unit Weight (pcf)	145

Level 2

Asphalt Mix: Aggregate Gradation

Cumulative % Retained on 3/4 Inch Sieve	0
Cumulative % Retained on 3/8 Inch Sieve	12
Cumulative % Retained on #4 Sieve	27
% Passing #200 Sieve	6.1

Asphalt Binder: Superpave Binder Test Data

Temperature (°F)	Angular Freq. = 10 rad/sec	
	G* (Pa)	Delta (degree)
		See Appendix B

Asphalt General: Volumetric Properties as Built

Effective Binder Content (%)	11.5
Air Voids (%)	5.8
Total Unit Weight (pcf)	145

Level 3

Asphalt Mix: Aggregate Gradation

Cumulative % Retained on 3/4 Inch Sieve	0
Cumulative % Retained on 3/8 Inch Sieve	12
Cumulative % Retained on #4 Sieve	27
% Passing #200 Sieve	6.1
Asphalt Binder: Superpave Binder Grading:	PG 76-22

Asphalt General: Volumetric Properties as Built

Effective Binder Content (%)	11.5
Air Voids (%)	5.8
Total Unit Weight (pcf)	145

TABLE A.19
Mixture ID B_19_67_M

Mixture Type: B 19_64_M

Level 1

Asphalt Mix: Dynamic Modulus Table

Temperature (°F)	Mixture |E*|, psi					
	0.1 Hz	**0.5 Hz**	**1 Hz**	**5 Hz**	**10 Hz**	**25 Hz**
39.2	1404621	1732479	1884914	2249032	2401467	2601329
68	410167	619119	720307	1036345	1186508	1403871
104	58218	114875	149650	283163	369557	539590

Asphalt Binder: Superpave Binder Test Data

Temperature (°F)	Angular Freq. = 10 rad/sec	
	G* (Pa)	Delta (degree)
		See Appendix B

Asphalt General: Volumetric Properties as Built

Effective Binder Content (%)	10.5
Air Voids (%)	5.5
Total Unit Weight (pcf)	145

Level 2

Asphalt Mix: Aggregate Gradation

Cumulative % Retained on 3/4 Inch Sieve	1
Cumulative % Retained on 3/8 Inch Sieve	14
Cumulative % Retained on #4 Sieve	25
% Passing #200 Sieve	6

Asphalt Binder: Superpave Binder Test Data

Temperature (°F)	Angular Freq. = 10 rad/sec	
	G* (Pa)	Delta (degree)
		See Appendix B

Asphalt General: Volumetric Properties as Built

Effective Binder Content (%)	10.5
Air Voids (%)	5.5
Total Unit Weight (pcf)	145

Level 3

Asphalt Mix: Aggregate Gradation

Cumulative % Retained on 3/4 Inch Sieve	1
Cumulative % Retained on 3/8 Inch Sieve	14
Cumulative % Retained on #4 Sieve	25
% Passing #200 Sieve	6
Asphalt Binder: Superpave Binder Grading:	PG 64-22

Asphalt General: Volumetric Properties as Built

Effective Binder Content (%)	10.5
Air Voids (%)	5.5
Total Unit Weight (pcf)	145

APPENDIX B

Aging and DSR Testing of Georgia Binders

INTRODUCTION

The accurate characterization of in situ aging of asphalt pavement materials over the service life of the pavement is of utmost importance to the implementation of mechanistic–empirical (ME) pavement design and analysis methods. The key product of NCHRP 09-54 is a laboratory aging procedure that prescribes a set of laboratory aging conditions to represent the long-term aged state of asphalt mixtures in a pavement as a function of climate and depth. The results of this project will also yield a pavement aging model that can serve as a basis for the future development of a methodology that integrates the effects of long-term aging in Pavement ME Design.

The development of the pavement aging model is ongoing. This model will predict the evolution of asphalt mixture performance with long-term aging. Implementation of the model will require quantifying asphalt binder kinetics using relatively simple and efficient test methods. The universal simple aging test (USAT) or the rolling thin film oven (RTFO) and pressure aging vessel (PAV) can be used to obtain various levels of binder aging, which can then be characterized using the dynamic shear rheometer (DSR) to obtain the binder kinetics.

The binder kinetics and properties can then be coupled with the mixture properties at short-term aged condition to predict the aged mixture properties at any duration and depth in the field using the pavement aging model that will be developed under NCHRP 09-54.

In this report, both USAT and RTFO/PAV aging methods were used to age two different asphalt binder sources obtained from Georgia. The kinetics, linear viscoelastic properties, as well as damage properties of both these binder sources were characterized at various age levels using the DSR. When the NCHRP 9-54 pavement aging model is complete and implemented in the Pavement ME Design and FlexPAVE™ programs, the experimental data obtained from this project can be used to evaluate the pavement performance with long-term aging.

MATERIALS AND TEST METHODS

The two asphalt binder sources obtained from Georgia are PG64-22 and PG76-22 binders.

Aging Methods

Universal Simple Aging Test (USAT)
Farrar et al. (2014) proposed the USAT for the efficient simulation of asphalt binder aging in the laboratory. The USAT uses thin binder films to induce a kinetics-controlled reaction. The binder is placed in grooved plates to achieve a film thickness of 300 micrometers. The USAT plates are placed in an oven at 135°C for four hours to simulate short-term aging and best mimic the short-term aging of loose mixtures. After this binder short-term aging

process, the USAT plates are placed in an oven at 95°C for 2 days, 4 days, and 8 days to simulate various levels of long-term aging.

Rolling Thin Film Oven (RTFO)
RTFO aging was conducted using selected original asphalt binder samples according to AASHTO T240 to simulate short-term aging.

Pressure Aging Vessel (PAV)
Asphalt binder residue obtained from the RTFO aging was subjected to PAV aging based on AASHTO R28 at 100°C for 20 hours and 40 hours to simulate two levels of long-term aging.

Testing Method: Dynamic Shear Rheometer (DSR)

Temperature–Frequency Sweep Test
Temperature–frequency sweep testing is conducted at frequencies ranging from 0.1 Hz to 30 Hz and multiple temperatures (i.e., 5°C, 20°C, 35°C, 50°C, and 64°C) using asphalt binders in the DSR with 8 mm parallel plate geometry. The strain amplitude used is chosen such that the linear viscoelastic limit is maintained. The rheological properties obtained are the dynamic shear modulus (G*) and phase angle.

Linear Amplitude Sweep (LAS) Test
The LAS test (AASHTO TP101) consists of oscillatory shear in strain-controlled mode in the DSR using an 8 mm parallel plate geometry at a frequency of 10 Hz. The strain amplitude is increased linearly from 0.1% to 30% to induce fatigue damage at an accelerated rate. The simplified viscoelastic continuum damage (S-VECD) modeling can be applied to LAS test results to predict the fatigue life at any loading history of interest.

RESULTS

Both binders were tested after short-term aging (STA), and after 2 days, 4 days, and 8 days of long-term aging (LTA). Figure B.1 and Figure B.2 show the evolution of |G*| with aging using USAT and RTFO/PAV, respectively. Figure B.3 and Figure B.4

show the evolution of the phase angle for both binders with aging using USAT and RTFO/PAV, respectively.

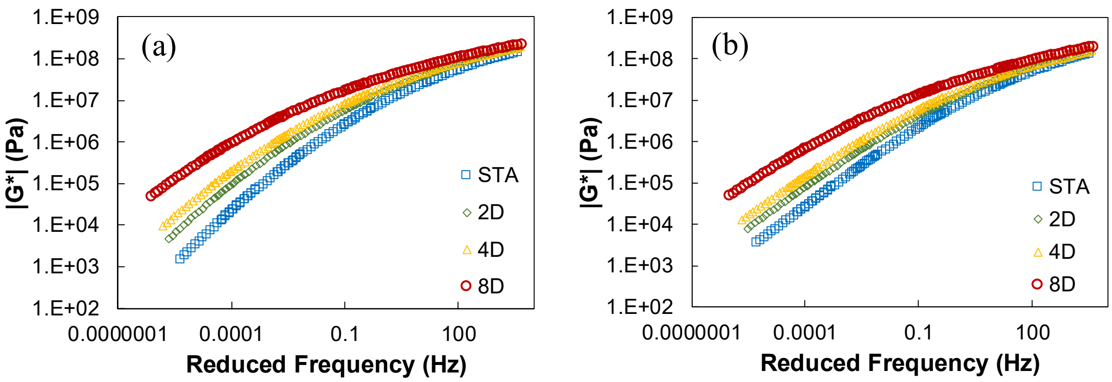

FIGURE B.1

Evolution of the Dynamic Shear Modulus as Aging Advances Using USAT for:
(a) PG 64-22, and (b) PG 76-22

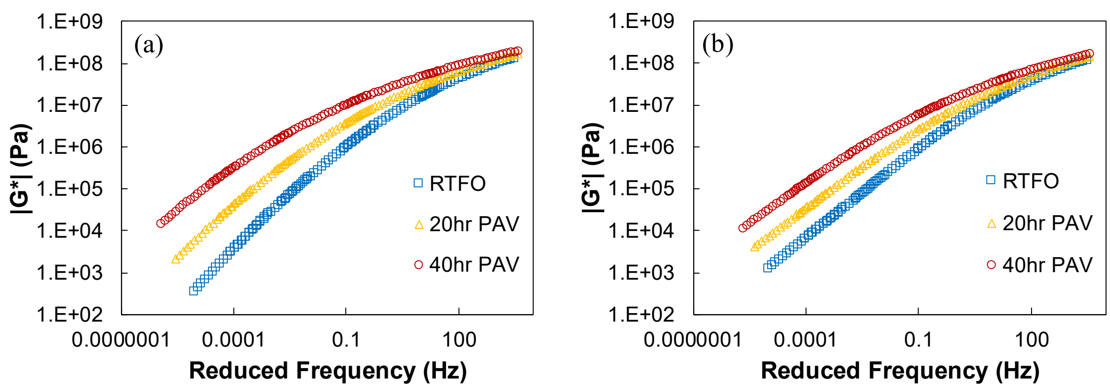

FIGURE B.2

Evolution of the Dynamic Shear Modulus as Aging Advances Using RTFO/PAV for:
(a) PG 64-22, and (b) PG 76-22

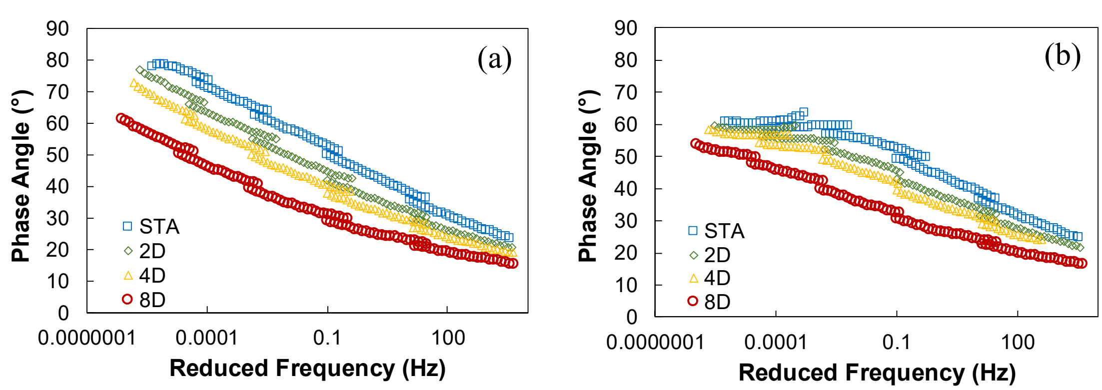

FIGURE B.3

Evolution of Phase Angle as Aging Advances Using USAT for:
(a) PG 64-22, and (b) PG 76-22

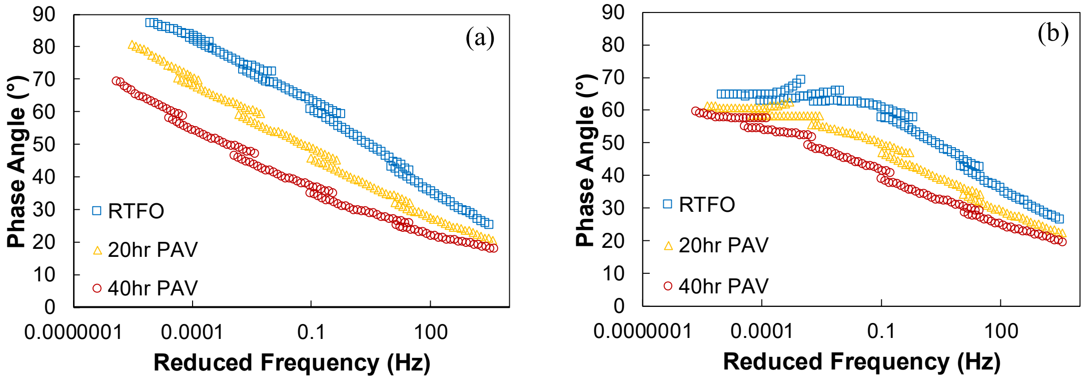

FIGURE B.4

Evolution of Phase Angle as Aging Advances Using RTFO/PAV for:
(a) PG 64-22, and (b) PG 76-22

A significant increase is evident in the dynamic shear modulus values when the aging duration is increased. The phase angle, on the other hand, drops when age level increases. Both of these trends are expected since the binder is stiffened with aging. Table B.1 and Table B.2 show the values of |G*| at 10 rad/s and the phase angle at different temperatures for both binders aged using both USAT and RTFO/PAV.

TABLE B.1

|G*| at 10 rad/s and Phase Angle as a Function of Temperature (USAT Aging)

Temperature (°F)	|G*| (Pa)	Phase Angle (°)	Temperature (°F)	|G*| (Pa)	Phase Angle (°)
PG 64-22 – STA			**PG 76-22 – STA**		
147.2	15,136.4	70.64	**147.2**	23,305.8	67.39
158.0	7,455.4	72.39	**158.0**	11,916.7	69.27
168.8	3,963.9	73.80	**168.8**	6,526.4	70.82
179.6	2,289.2	74.92	**179.6**	3,853.2	72.09
190.4	1,442.9	75.80	**190.4**	2,465.0	73.09
PG 64-22 – 2D			**PG 76-22 – 2D**		
147.2	43,059.3	64.28	**147.2**	48,644.9	63.06
158.0	20,327.6	66.48	**158.0**	23,767.8	65.38
168.8	10,129.8	68.33	**168.8**	12,209.7	67.37
179.6	5,369.4	69.88	**179.6**	6,645.0	69.06
190.4	3,046.2	71.16	**190.4**	3,855.9	70.47
PG 64-22 – 4D			**PG 76-22 – 4D**		
147.2	76,013.9	60.41	**147.2**	77,727.2	59.87
158.0	35,750.7	62.82	**158.0**	37,750.4	62.36
168.8	17,541.1	64.90	**168.8**	19,097.8	64.53
179.6	9,051.7	66.67	**179.6**	10,144.4	66.41
190.4	4,946.2	68.17	**190.4**	5,696.4	68.01
PG 64-22 – 8D			**PG 76-22 – 8D**		
147.2	293,245.2	50.72	**147.2**	253,791.8	51.33
158.0	140,595.3	53.51	**158.0**	123,718.0	54.13
168.8	68,221.4	56.05	**168.8**	61,163.5	56.70
179.6	33,768.0	58.35	**179.6**	30,904.1	59.02
190.4	17,172.9	60.40	**190.4**	16,072.2	61.10

TABLE B.2

|G*| at 10 rad/s and Phase Angle as a Function of Temperature (RTFO/PAV Aging)

Temperature (°F)	|G*| (Pa)	Phase Angle (°)	Temperature (°F)	|G*| (Pa)	Phase Angle (°)
PG 64-22 – RTFO			**PG 76-22 – RTFO**		
147.2	4,711.0	79.82	**147.2**	9,309.8	73.71
158.0	2,418.1	81.16	**158.0**	4,994.6	75.13
168.8	1,376.7	82.19	**168.8**	2,935.1	76.25
179.6	873.6	82.96	**179.6**	1,898.7	77.10
190.4	620.0	83.50	**190.4**	1,357.3	77.72
PG 64-22 – 20hr PAV			**PG 76-22 – 20hr PAV**		
147.2	22,717.5	68.63	**147.2**	28,113.1	66.86
158.0	10,716.1	70.63	**158.0**	13,920.4	68.96
168.8	5,398.0	72.29	**168.8**	7,340.9	70.72
179.6	2,924.4	73.64	**179.6**	4,152.5	72.17
190.4	1,713.6	74.73	**190.4**	2,534.2	73.35
PG 64-22 – 40hr PAV			**PG 76-22 – 40hr PAV**		
147.2	100,935.9	57.74	**147.2**	67,055.8	60.53
158.0	47,170.8	60.30	**158.0**	32,275.0	63.02
168.8	22,745.9	62.54	**168.8**	16,176.6	65.19
179.6	11,409.2	64.49	**179.6**	8,510.1	67.07
190.4	5,994.7	66.18	**190.4**	4,730.9	68.67

The damage characteristic curves, which indicate the level of accumulated damage under fatigue loading, show an upward shift with aging as shown in Figure B.5 and Figure B.6 for USAT and RTFO/PAV aging, respectively. For the same value of C (pseudo stiffness or material integrity), the STA curve shows lower accumulated damage values than the LTA curves. These trends are expected since the damage characteristic curves of stiffer materials are generally higher than the curves of softer materials. The fatigue resistance is expected to decrease with prolonged aging due to the embrittlement imposed by oxidation.

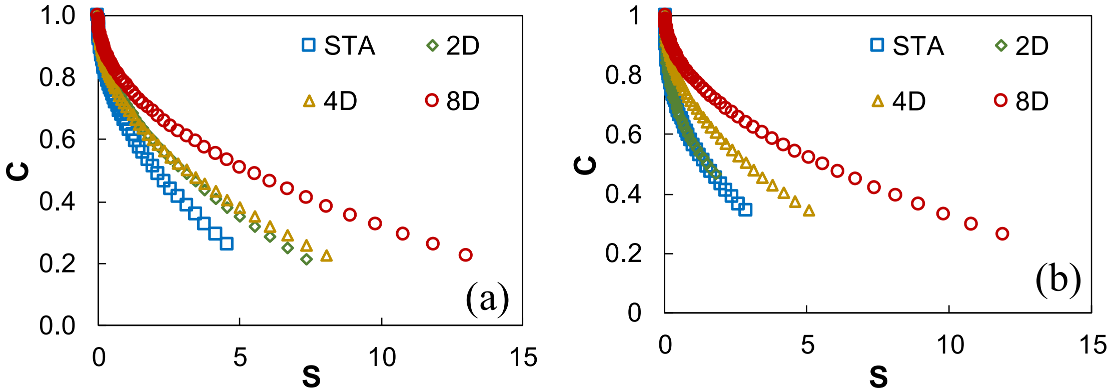

FIGURE B.5

Damage Characteristic Curves as Aging Advances Using USAT for:
(a) PG 64-22, and (b) PG 76-22

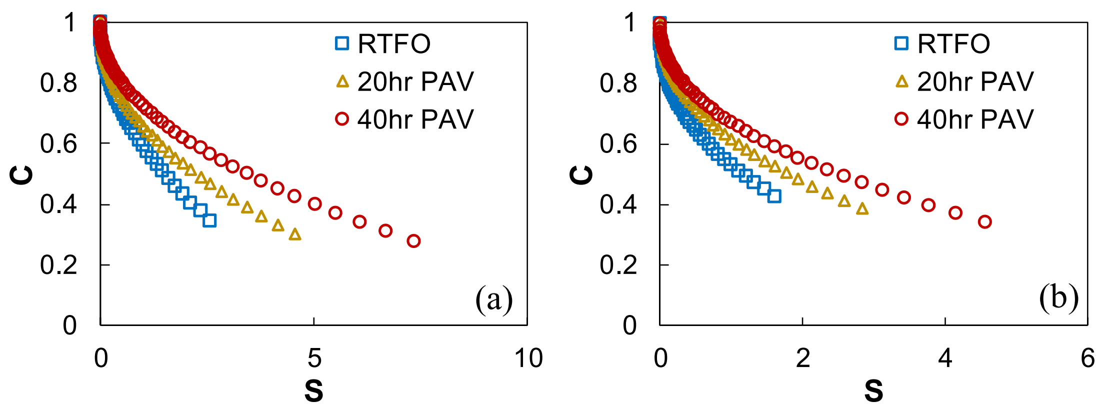

FIGURE B.6

Damage Characteristic Curves as Aging Advances Using RTFO/PAV for:
(a) PG 64-22, and (b) PG 76-22

REFERENCES

Farrar, M.J., J.P. Planche, R.W. Grimes, and Q. Qin. (2014). "The Universal Simple Aging Test (USAT): Simulating Short- and Long-Term Hot and Warm Mix Oxidative Aging in the Laboratory." *Asphalt Pavements,* Kim, Y.R., Ed., London: CRC Press, Taylor & Francis Group. pp. 79–87.

APPENDIX C

Proposed Standard Operating Procedure (SOP)

Georgia Department of Transportation
Office of Materials and Testing

Proposed Standard Operating Procedure (SOP) – DRAFT
Measurements of Dynamic Modulus (|E*|) and Development of Mastercurve of Asphalt Concrete Mixture

---

I. General

The purpose of this Standard Operating Procedure is to outline the methodology for measuring Dynamic Modulus (|E*|) of Asphaltic Concrete Mixture. This test is designed to be performed with an asphalt mixture performance tester (AMPT) in accordance with AASHTO TP107 for small specimen (1.5-in. diameter). The measurements of dynamic modulus of asphaltic concrete mixtures is a very technical process requiring highly skilled testing personnel, precision testing equipment, and close adherence to design guidelines and test procedures to assure high quality mix designs. It is a requirement for lab certification that the design equipment must meet all requirements and tolerances stated in the test procedures. Equipment calibration records shall be furnished to OMAT for review prior to initial certification and shall be available for inspection at all times. In case commercial laboratories that satisfy the requirements, research universities in Georgia that have extensive experience to measure dynamic modulus with small specimen (38 mm diameter) of asphaltic concrete mix should conduct this test with plant mix or field cores.

II. Specimen Fabrication

This procedure governs the sampling procedure to fabricate hot mix asphaltic concrete for dynamic modulus and fatigue cracking tests.

A. Sampling

Randomly select plant mix (verification mix) is collected in accordance with below references. The sampling testing, and inspection duties are to be performed by a GDOT Certified Contractor QCT and/or University of Georgia (UGA) Pavement Research Lab:

References: GDOT Specifications

- GSP 15 (Sampling Procedures For Asphalt Concrete Mixtures)
- GDT 73 (Method of Random Selection And Acceptance Testing of Asphaltic Concrete).
- DOT 162 (Asphaltic Concrete Plant Sampling Report).

This procedure also utilize 6-inch diameter field cores to run dynamic modulus test. The 6-inch diameter field cores will be used to prepare 38-mm-diameter by 110-mm-height for dynamic modulus test utilizing small cylindrical performance test specimens. This practice is intended for dense-graded asphalt mixtures with nominal maximum aggregate sizes up to 25.0 mm.

B. Procedure for Specimen Fabrication from Gyratory Specimens

1. Asphalt Mixture Preparation:
    a. Prepare asphalt mixture for each Superpave Gyratory Compactor (SGC) specimen in accordance with T312 and prepare a companion test specimen for maximum specific gravity (Gmm) in accordance with T 209.
    b. The mass of asphalt mixture needed for each specimen will depend on the SGC specimen height, the Gmm of the mixture, the nominal maximum aggregate size, gradation (coarse or fine), and target air void content of the test specimens.
    c. Perform conditioning on the asphalt mixture for the test specimens and companion Gmm sample in accordance with SOP 2.
    d. SGC Specimen Compaction:
        i. Compact the SGC specimens to a height of 180 mm or higher, in accordance with T312, carefully following the exceptions noted.
        ii. Pour the mixture into the center of the mold to minimize air void variation between samples. Pouring material down the sides of the mold will result in lower air voids on that side of the mold.
        iii. Charge the mold in two equal lifts, and rod the sample 20 times after each lift, to minimize vertical air void variance.
2. SGC Specimen Density and Air Voids:
    a. Determine the Gmm of the asphalt mixture in accordance with SOP 2 and Section 828.
    b. Determine Gmb of the SGC specimen in accordance with SOP 2 and Section 828. Record the Gmb of the SGC specimen.
    c. Compute the air void content of the SGC specimen in accordance with SOP 2 and Section 828. Record the air void content of the SGC specimen.
3. Test Specimen Preparation:
    a. Prepare the gyratory specimen by marking the location(s) where the cores will be taken. All cores must be taken within the inner 100 mm of the gyratory specimen. As many as four 38-mm diameter cores can be extracted from one gyratory specimen, as shown by the gray circles in Figure 1. The optimal lines to mark to extract four gyratory specimens are shown in white in Figure 1.
    b. Drill a core of nominal diameter of 38 mm from the SGC specimen. Both the SGC specimen and the drill shall be adequately supported to ensure

that the resulting core is cylindrical with sides that are smooth, parallel, and meet the tolerances on specimen diameter given in Table 1.

c. Saw the ends of the core to obtain a test specimen of a nominal height of 110 mm. Both the core and the saw shall be adequately supported to ensure that the resulting test specimen meets the tolerances given in Table 1 for height, end flatness, and end perpendicularity.

d. With most equipment, it is better to perform the coring before the sawing. However, these operations may be performed in either order as long as the dimensional tolerances in Table 1 are satisfied.

e. Test specimens shall meet the dimensional tolerances given in Table 1.

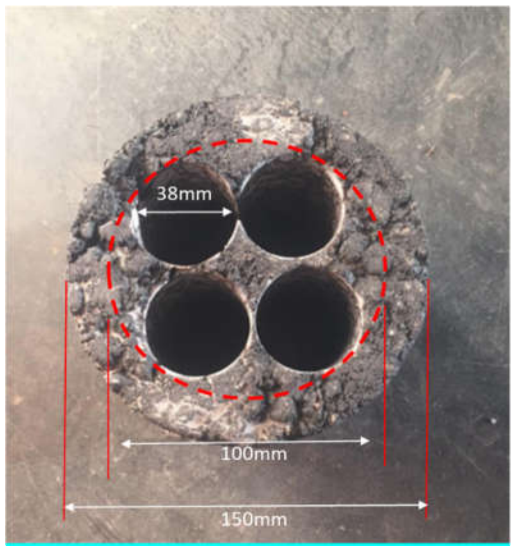

Figure 1-Graphic of a marked gyratory specimen

Table 1— Test Specimen Dimensional Tolerances

Item	Specification
Average diameter	36 to 40 mm
Standard deviation of diameter	≤0.5 mm
Height	107.5 to 112.5 mm
End flatness	≤0.5 mm
End perpendicularity	≤1.0 mm

4. Test Specimen Density and Air Voids:

   a. Determine the Gmm of the asphalt mixture in accordance with SOP 2.

   b. Determine Gmb of the test specimen in accordance with SOP 2. Record the Gmb of the SGC specimen.

   c. Compute the air void content of the SGC specimen in accordance with T 269. Record the air void content of the SGC specimen.

References:

AASHTO Standards:

- R 30, Mixture Conditioning of Hot Mix Asphalt
- T 166, Bulk Specific Gravity (G_{mb}) of Compacted Hot Mix Asphalt (HMA) Using Saturated Surface Dry Specimens
- T 209, Theoretical Maximum Specific Gravity (G_{mm}) and Density of Hot Mix Asphalt (HMA)
- T 269, Percent Air Voids in Compacted Dense and Open Asphalt Mixtures
- T 312, Preparing and Determining the Density of Asphalt Mixture Specimens by Means of the Superpave Gyratory Compactor
- T 342, Determining the Dynamic Modulus of Hot Mix Asphalt (HMA)
- TP 107, Determining the Damage Characteristic Curve and Analysis Parameters Using Small Specimens in the Asphalt Mixture Performance Tester (AMPT) Cyclic Fatigue Test

ASTM Standard:

- D3549/D3549M, Standard Test Method for Thickness or Height of Compacted Bituminous Paving Mixture Specimens

III. Test Procedure

Dynamic Modulus (|E*|) is the absolute value of the complex modulus calculated by dividing the peak-to-peak stress by the peak-to-peak strain for a material subjected to a sinusoidal loading.

Phase Angle (δ) is the angle in degrees between a sinusoidally applied stress and the resulting strain in a controlled stress test.

1. Dynamic Modulus Test

   This test method describes the procedure for measuring the dynamic modulus of asphaltic concrete mixture using 38-mm diameter small specimen. A test specimen at a specific test temperature is subjected to a controlled sinusoidal (haversine) compressive stress of various frequencies. The applied stresses and resulting axial strains are measured as a function of time and used to calculate the dynamic modulus and phase angle.

   a. Place the specimens to be tested in the environmental chamber with the "dummy" specimen and monitor the temperature of the "dummy" specimen to determine when testing can begin.
   b. Place platens and friction reducers inside the testing chamber. Turn on the AMPT, set the temperature control to the desired testing temperature, and

allow the testing chamber to equilibrate at the testing temperature for at least 1 h.

c. When the "dummy" specimen and the testing chamber reach the target temperature, open the testing chamber. Remove a test specimen from the conditioning chamber and quickly place it in the testing chamber.

d. Assemble the specimen to be tested with platens in the following order from bottom to top: bottom loading platen, bottom friction reducer, specimen, top friction reducer, and top loading platen.

e. Install the specimen-mounted deformation-measuring system on the gauge points per the manufacturer's instructions. Ensure that the deformation-measuring system is within its calibrated range. Ensure that the top loading platen is free to rotate during loading.

f. Close the testing chamber and allow the chamber temperature to return to the testing temperature.

g. Procedures in Step (c) through Step (i), including the return of the test chamber to the target temperature, shall be completed in 5 min.

h. Enter the required identification and control information into the dynamic modulus software.

i. Follow the software prompts to begin the test. The AMPT will automatically unload when the test is complete and will display the test data and data quality indicators.

j. Review the data quality indicators as discussed in Step (e). Retest specimens with data quality indicators above the values specified in Step (e).

k. Once acceptable data have been collected, open the test chamber and remove the tested specimen. Repeat procedures in Step (c) through Step (k) for the remaining test specimens.

2. Computations and Data Quality

a. The calculation of dynamic modulus, phase angle, and the data quality indicators is performed automatically by the AMPT software.

b. Accept only test data meeting the data quality statistics given in Table 2. Table 3 summarizes actions that can be taken to improve the data quality statistic. Repeat tests as necessary to obtain test data meeting the data quality statistics requirements.

Table 2—Data Quality Statistics Requirements

Data Quality Statistic	Limit
Deformation drift	In direction of applied load

Peak-to-peak strain	50 to 75 μstrain
Load standard error	10%
Deformation standard error	10%
Deformation uniformity	30%
Phase uniformity	3°

Table 3—Data Quality Statistics Requirements

Item	Cause	Possible Solutions
Deformation drift not in direction of applied load	Gauge points are moving apart	Reduce LVDT spring force. Add compensation springs. Reduce test temperature.
Peak-to-peak strain too high	Load level too high	Reduce load level.
Peak-to-peak strain too low	Load level too low	Increase load level.
Load standard error >10%	Applied load not sinusoidal	Adjust tuning of hydraulics.
Deformation standard error >10%	1. Deformation not sinusoidal 2. Loose gauge point 3. Excessive noise on deformation signals 4. Damaged LVDT	1. Adjust tuning of hydraulics. 2. Check gauge points. Reinstall if loose. 3. Check wiring of deformation sensors. 4. Replace LVDT.
Deformation uniformity >30%	1. Eccentric loading 2. Loose gauge point 3. Sample ends not parallel 4. Poor gauge point placement 5. Non-uniform air void distribution	1. Ensure specimen is properly aligned. 2. Check gauge points. Reinstall if loose. 3. Check parallelism of sample ends. Mill ends if out of tolerance. 4. Check for specimen non-uniformity (segregation, air voids). Move gauge points. 5. Ensure test specimens are cored from the middle of the gyratory specimen.
Phase uniformity >3°	1. Eccentric loading 2. Loose gauge point 3. Poor gauge point placement 4. Damaged LVDT	1. Ensure specimen is properly aligned. 2. Check gauge points. Reinstall if loose. 3. Check for specimen non-uniformity (segregation, air voids). Move gauge points. 4. Replace LVDT.

3. Development of Mastercurve

Using Excel spreadsheet, mastercurve of dynamic modulus is generated in accordance with AASHTO R84.

Step 1: Copy and paste frequency, dynamic modulus, phase angle, and test temperature data into the pink cells within the measured data table. Each block of test data should correspond to a single replicate and temperature of testing. Include data for each test specimen. Do not average data prior to entry into the spreadsheet.

Step 2: Enter the desired reference temperature into the Tref cell of the shift factor table.

Step 3: Run Solver

IV. Maintenance

This list should serve as a guideline for when the dynamic modulus test should be conducted re re-evaluated.

1. Per GDOT SOP 2, all mix designs shall be subjected to one or more field verifications during production at the discretion of the State Bituminous Construction Engineer. When field verification tests are conducted in accordance with SOP 2, dynamic modulus test should be conducted.
2. Field cores taken for performance evaluation and remaining design life prediction.
3. Asphalt mixtures with binder grades outside of PG 76-22, PG 67-22, and PG 64-22.
4. Asphalt mixtures with a reclaimed asphalt pavement (RAP) above 30% or below 25%.
5. Asphalt mixtures that use limestone as an aggregate source.
6. Asphalt mixtures in pavements that failed to reach the design life.
7. The dynamic modulus test is conducted in accordance with AASHTO T342 (4-in. diameter specimen) or TP107 (1.5-in. diameter specimen) at the standard test temperatures and frequencies from the dynamic modulus mastercurve of each replicate specimen. This SOP introduce to use small specimen to measure dynamic modulus. The dynamic modulus test results of the small and large specimens generally differ significantly at 54°C whereas the majority of the mixtures evaluated demonstrated statistically equivalent dynamic modulus results at low and intermediate temperatures. Additionally, at low and intermediate temperatures, COV values are less than 15%, indicating that specimen-to-specimen variability is within the generally accepted range. Therefore, it is recommended to limit small specimen testing to the temperatures outlined in AASHTO PP61, which specifies three test temperatures with the highest temperature selected as a function of the Performance Grade (PG). The highest temperature specified by AASHTO PP61 ranges between 35°C and 45°C for different asphalt binder PG grades. In Georgia, the recommended three temperatures for dynamic modulus test are 4ºC, 20ºC, and 40ºC. The observed difference in the mastercurve at high temperature does not significantly affect pavement fatigue performance predictions (Castorena et al., 2017).

Georgia Department of Transportation

Office of Materials and Testing

Proposed Standard Operating Procedure (SOP) – DRAFT
Asphalt Mixture Test to Evaluate Fatigue Cracking Resistance Performance

---

I. General

The purpose of this Standard Operating Procedure is to outline the methodology for maintaining, managing, and updating the materials library as it relates to the Asphalt Mixture Database. All tests are designed to be performed with an asphalt mixture performance tester (AMPT).

II. Specimen Fabrication

A. Semicircular Bend (SCB)

This test procedure is for asphaltic concrete mixtures composed of aggregates with an NMAS of 19 mm or less. The following instructions detail how to prepare a specimen for testing.

1. Compact an asphalt mixture into a cylinder with a height of 178 mm, a diameter of 150 mm, and a target air void percentage of 7 ± 0.5 %, per AASHTO T 312.
2. Cut two 50 mm thick disks from the compacted cylinder.
3. Cut each of the two disks in half, creating a total of four semicircle shapes with a thickness of 50 mm.
4. Cut a notch in the middle of the semicircle perpendicular to the flat surface with a length of 15 ± 1 mm.
5. Measure the bulk specific gravity of each cut specimen according to AASHTO T 166 to determine the air voids of the specimens.
6. Condition the test specimens in the environmental chamber at a temperature of 25 ± 0.5 °C for 2 ± 0.5 hr.

B. Direct Tension Test for S-VECD

This test procedure is for asphaltic concrete mixtures composed of aggregates with an NMAS of 25 mm or less. The following instructions detail how to prepare a specimen for testing.

1. Compact an asphalt mixture into a cylinder with a height of 178 mm, a diameter of 150 mm, and a target air void percentage of 7 ± 0.5 % per AASHTO T 312.
2. Core vertically, from the inner 100 mm diameter, four cylindrical specimens with a diameter of 38 mm.

3. Cut the top and bottom of the 100 mm specimens to form a cylinder with a height of 110 ± 1 mm.
4. Measure the bulk specific gravity of each cut specimen according to AASHTO T 166 to determine the air voids of the specimens.
5. Glue the mounting studs to the 100 mm cylindrical specimen using a gage length of 70 ± 1 mm center to center. Note: For gluing, use Devcon 10240 plastic steel putty, or another putty with equivalent properties and a spacing fixture to ensure an accurate gage length.
6. Clean the end plates to ensure the grooves are free of any debris or old glue by heating them in an oven or by soaking in acetone.
7. Glue the end plates to the cylindrical specimen using approximately 7 grams of Devcon 10240 plastic steel putty.
8. Divide the glue into quarters using each to spread over the four contact areas, ensuring the glue fills all the grooves in the end plates.
9. Use a gluing jig to center the specimen on top of the plates to ensure when the load is not eccentrically applied and that screw holes align with the AMPT.
10. Lower the gluing jig's weight onto the specimen and allow for initial set to occur before moving the specimen.
11. Move the specimen after initial set to an environmental chamber for conditioning. Note: Hold the specimen from the bottom so that tension is not applied to the adhesive.
12. Condition the specimens at one of the following temperatures based on the asphalt binder grade:
    a. PG 64-22: 18°C
    b. PG 67-22: 19.5°C
    c. PG 76-22: 21°C
13. Allow the glue to fully cure based on the manufacturer's curing time before testing.

III. Test Procedure

A. Semicircular Bend (SCB)

This method covers the determination of fracture energy (G_f) and the post-peak slope, using semicircular asphalt specimens at 25°C. These parameters are used to calculate the flexibility index (FI), which ranks asphalt mixtures based on their resistance to asphalt cracking. A mixture with a higher FI indicates better pavement performance than a mixture with a lower FI.

1. Place the SCB testing apparatus inside the AMPT test chamber.
2. Turn on the AMPT and set the climate-controlled chamber to the test temperature of 25°C.
3. Allow the chamber to reach the test temperature before proceeding.
4. Remove one of the cut specimens from its conditioning chamber and quickly place it inside the AMPT to keep the specimen temperature constant.
5. Place the specimen with the flat side on the rollers of the testing apparatus and the loading head centered above the notch.

6. Ensure that the specimen is centered in both the x and y directions on the testing apparatus.
7. Place the steel ball bearing on top of the loading head.
8. Lower the AMPT chamber. Note: Steps 4–8 should be completed in less than 5 minutes to help maintain testing temperature.
9. Apply an initial contact load of 0.1 ± 0.01 kN at a loading rate of 0.05 kN/s.
10. Set the linear load displacement (LLD) control to a rate of 50 mm/min.
11. Set the test termination to when load drops below 0.1 kN and start the test.

Fracture Energy (G_f) – Calculate by dividing the work of fracture (W_f), which is the total area under the load line displacement curve in Figure C.1, by the ligament of the area (A_{lig}) using Eq. (C.1) and Eq. (C.2)

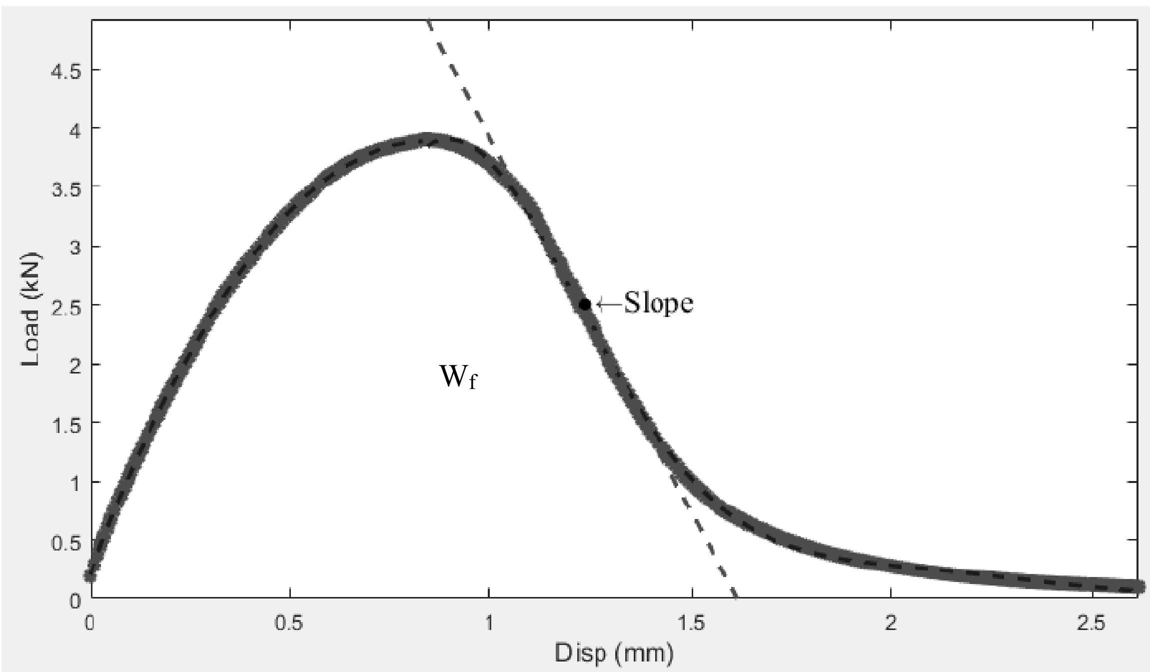

FIGURE C.1

Load vs Load Line Displacement Curve

$$G_f = \frac{W_f}{A_{lig}} \tag{C.1}$$

$$A_{lig} = t(r-a) \tag{C.2}$$

Where,

t =thickness of specimen (mm)
r = radius of specimen (mm)
a = notch length of specimen (mm)

Determine the inflection point of the curve after the peak load. Calculate the slope of the tangential line passing through the inflection point. Designate this slope as m. Calculate FI using Eq. (C.3).

$$\mathrm{FI} = \frac{G_f}{|m|}\ x\ A \tag{C.3}$$

Where,

A = 0.01 (unit-less conversion factor)

B. Direct Tension for S-VECD

This test method covers the procedure for testing asphalt concrete mixtures to determine the damage characteristic curve and fatigue analysis parameters (i.e., D^R, S_{app}) via the direct tension cyclic fatigue test using the AMPT. The failure criterion D^R when used with the mixture's modulus can determine the mixture's S_{app} value. A higher S_{app} value indicates better pavement performance than a lower value.

1. Turn on the AMPT and set the climate-controlled chamber to the correct testing temperature based on the asphalt binder grade.
2. Attach spacers to the machine to compensate for the reduced height of the specimen.
3. Remove the specimen from the conditioning chamber and insert it into the AMPT.
4. Tighten the bottom platen to the bottom support. Note: A torque wrench is useful to use here with the torque set to 12 N*m.
5. Raise the actuator by applying a seating load of 0.01 kN.
6. Check the top platen to determine if it is level.
7. Proceed to Step 10 if the top platen is level; otherwise, continue with Step 8.
8. Loosen the screws on the bottom spacer until the top platen sits level with the machine surface.
9. Insert feeler gauges as needed under the bottom spacer and retighten the screws, ensuring the top platen does not move.
10. Insert screws through the top platen into the ring at the top of the machine, but do not tighten the screws.
11. Use feeler gauges on each side of the screws to fill all the gaps before tightening the screws.
12. Tighten the top platen to the ring using the torque wrench in increments starting at 4 N*m of torque and going up to 12 N*m. Note: This increased incremental tightening is to ensure that the specimen does not break.
13. Reduce the load to 0 kN after the top platen has been filly secured.
14. Attach the three strain gauges to the specimen and adjust the stain gauges so that the displacement during testing will not exceed the gauges' limits.
15. Lower the cell and allow for adequate time for the specimen to reach its testing temperature.
16. Input a test frequency of 10 Hz with a target strain range of 50–75 microstrain in the tension compression mode of loading for the dynamic modulus fingerprint test.

17. Start the fingerprint test and ensure the strain does not exceed 150 microstrain and reaches a minimum of 50 data points per cycle.
18. Allow the specimen to rest for 20 minutes after the fingerprint test.
19. Set the cyclic fatigue test to run a pull-pull actuator displacement.
20. Set the target peak to peak on-strain amplitude for the first test specimen to 300, 500, or 800 microstrain (ε_{os1}) based on the $|E^*|_{\text{fingerprint}}$ ranges in Table C.1. Note: These are suggested values, but after running numerous tests, operators may have a more educated guess of the expected cycle count for an asphalt mixture at a strain level. A good test is a cycle count above 2000.

TABLE C.1

Target on Specimen Strain Levels for the First Specimen

Case (units in MPa)	ε_{os1}
$\lvert E^*\rvert_{\text{fingerprint} > 8,800}$	300
$4,400 < \lvert E^*\rvert_{\text{fingerprint}} < 8,800$	500
$\lvert E^*\rvert_{\text{fingerprint}} < 4,400$	800

21. Manually terminate the test when the phase angle beings to drop.
22. Export the test results to FlexMAT for analysis.
23. Repeat the necessary steps to complete a total of three tests.
24. Adjust the cyclic fatigue test target strain level so that each test uses a different target strain level. Note: It is important to try to have tests with at least one cycle count above 10,000. The lower the target strain, the more likely a test will have higher cycle counts.

Figure C.2 shows the results from a successful test. The test was terminated as soon as the phase angle began to drop.

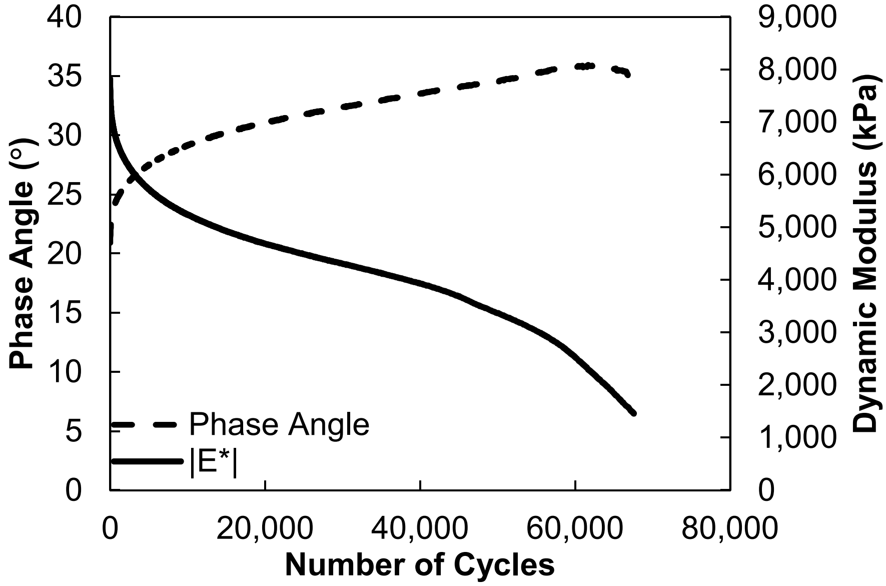

FIGURE C.2

Expected Results of a Cyclic Fatigue Test

IV. Maintenance

This list should serve as a guideline for when the asphalt mixtures should be added and re-evaluated.

1. Field cores taken for performance evaluation.
2. Asphalt mixtures with binder grades outside of PG 76-22, PG 67-22, and PG 64-22.
3. Asphalt mixtures with a reclaimed asphalt pavement (RAP) above 30% or below 25%.
4. Asphalt mixtures that use limestone as an aggregate source.
5. Asphalt mixtures in pavements that failed to reach the design life.